Zero-Dimensional Carbon Nanomaterials: Synthesis, Characterisations and Applications

Thesis submitted to
the University of Calicut in partial fulfilment of
the requirements for the degree of

DOCTOR OF PHILOSOPHY IN CHEMISTRY
in the Faculty of Science

By

SREEJA K.

Under the guidance of
Dr. Resmi M.R.

Research and Post Graduate Department of Chemistry
Sree Neelakanta Government Sanskrit College, Pattambi
(Affiliated to the University of Calicut, Kerala, India)
December 2022

Sree Neelakanta Govt. Sanskrit College
Pattambi, Palakkad Dt, Kerala - 679 306
(Accredited by NAAC with A+ Grade)
Ph: 0466-2212223
e-mail: sngscollege@gmail.com
website: www.sngscollege.org

Date: 30. 12. 2022

CERTIFICATE

Certified that the thesis entitled **"Zero-dimensional Carbon Nanomaterials: Synthesis, Characterisations and Applications"**, is an authentic record of research work carried out by **Ms. Sreeja K**. under my supervision at the Research and Post Graduate Department of Chemistry, SNGS College, Pattambi in partial fulfillment of the requirements for the award of the degree of Doctor of Philosophy in Chemistry of the University of Calicut, and has not been included in any other thesis submitted previously for the award of any other degree.

Pattambi

Dr. Resmi M.R
(Supervising Guide)
Professor
Research and Post Graduate
Department of Chemistry
S. N. G. S. College, Pattambi

Sree Neelakanta Govt. Sanskrit College
Pattambi, Palakkad Dt, Kerala - 679 306
(Accredited by NAAC with A+ Grade)
Ph: 0466-2212223
e-mail: sngscollege@gmail.com
website: www.sngscollege.org

Date: 20. 09. 2023

CERTIFICATE

This is to certify that the thesis entitled “**Zero-Dimensional Carbon Nanomaterials: Synthesis, Characterisations and Applications”**, bound herewith is a bonafide research work done by Ms. Sreeja K. under my supervision at the Research and Post Graduate Department of Chemistry, SNGS College, Pattambi in partial fulfilment of the requirements for the award of the degree of Doctor of Philosophy in Chemistry of the University of Calicut. I also certify that the corrections/suggestions from the adjudicators have been incorporated into the revised thesis and the contents in the thesis and the soft copy are one and the same.

Pattambi

Dr. Resmi M.R.
(Supervising Guide)
Professor
Research and Post Graduate
Department of Chemistry
SNGS College, Pattambi

DECLARATION

I hereby declare that the present work entitled **"Zero-Dimensional Carbon Nanomaterials: Synthesis, Characterisations and Applications"** is an authentic record of the original work done by me under the supervision of **Dr. Resmi M. R**., Professor, Research and Post Graduate Department of Chemistry, SNGS College, Pattambi in partial fulfilment of the requirement for the award of the degree of Doctor of Philosophy in Chemistry of the University of Calicut, and has not been included in any other thesis submitted previously for the award of any other degree.

Pattambi **Sreeja. K**
30. 12. 2022

Dedicated to

My Family & My Teachers

ACKNOWLEDGEMENTS

Each endeavour we make in the course of our life is accomplished successfully only if we are inspired and supported by our teachers, family and friends.

First and foremost, I wish to record my deep sense of gratitude and sincere thanks to my research guide, my beloved teacher, Dr. Resmi M. R. for the scholarly advice, unstinting support and inspiration extended to me throughout my research work. I am much indebted to her for the fruitful suggestions, meticulous instructions and valuable guidance without which it would have been difficult to complete my work. I reserve my gratitude to her.

I owe my sincere gratitude to my teachers Dr. Femina K. S. and Dr. Binitha N. N. who encouraged me to enter the fascinating field of research.

I would like to thank Dr. P. Raveendran, Professor, Department of Chemistry, for his valuable advice during the communication of articles. I extend my heartfelt gratitude to doctoral committee members Prof. Dr.V. Anilkumar, Prof. Dr. P. Raveendran, Dr. H. K. Santhosh. I also acknowledge Prof. Dr. V. V. Radhakrishnan, Dean of the Faculty of Science, University of Calicut.

I thankfully acknowledge the Council of Scientific & Industrial Research New Delhi, India for the CSIR-JRF & SRF. I should thank Sree Neelakanta Government Sanskrit College, Pattambi, and the

University of Calicut for providing all the facilities for carrying out the research.

I am forever indebted to all my beloved teachers- Dr. Raveendran, Dr. Jacob Jose, Dr. P. Venugopalan, Dr. Manoj T. P., Dr. Anjaly Mathew, Mrs. Usha M, Dr. Remani K. C., Dr. Vinod Raphael, Dr. Jincy E. M., who through their immense knowledge and teaching opened the door to the fascinating world of Chemistry.

I extend my gratitude to all teachers in the Chemistry Department- Dr. Surendran P., Mr. Roy K. B., Mrs. Ramlath K. T. and all non-teaching staff- Surettan, Raghuvettan, Vijayalakshmi Chechi, Pramodettan, Usha Chechi for their huge support and affection.

It is a pleasure to acknowledge my sincere thanks to the Principal, of SNGS College, Pattambi. I thank all the administrative staff, and all the teaching & non-teaching staff of SNGS college, Pattambi.

I extend my profound gratitude to SAIF Kochi, IIT Kanpur, IIT Madras, IISER Trivandrum, PSG Coimbatore, CSIF- Calicut university, SAIF –MG University for analysis. I also thank Dr. Vimala. K, Women scientist, Periyar University, for her support in biological studies.

I owe a great deal to my friends and seniors who have supported me in this venture. I take this opportunity to convey my gratitude to Dr. Rajeena, Dr. Sudha, Dr. Sowmya, Dr. Divya, Dr. Vijayasree, Dr. Silija, Dr. Vinu, Dr. Deepthi, Dr. Shaniba, Akbar, *Shameena, Suvarna, Haritha, Suchitra miss, Chandini, Vidya. My deepest and heartiest thanks to all.*

Last but not least, I express my love and affection towards my family. I am always grateful to my parents and my husband, my daughter, my brother, and my sister-in-law for their unconditional love and diligent support which led to the completion of my research. Thank you, Pappa, Amma, Unni and Chinnu for always being there for me. Love you all.

Words are not enough to express my gratitude and endless love towards my husband and my daughter. I thank my better half, Sandeep for his constant support, care and encouragement. My little angel, Ameya, my world, I thank her for perking up my weary spirit with her innocent smile and bundle of love.

Above all, it has never been on my merit but on the grace and benevolence of God Almighty that my endeavour has become a reality. Thank you, God, for Everything.

Sreeja K.

PREFACE

In the current era, nanomaterial-based technology has turned out to be an inevitable part of life. Reduction of the size of materials through confinement in all three dimensions to nanoscale results in zero-dimensional nanomaterials which exhibit novel and tunable properties. 0-D nanomaterials, considered next-generation materials, are generally spherical or quasi-spherical nanoparticles with a diameter of less than 100 nm with exciting properties such as high surface-to-volume ratio, tunable band gap, optical stability, strong and excitation-dependent photoluminescence and cell permeability.

Among various classes of nanomaterials, carbon-based nanomaterial synthesis and applications is a hot topic in research mainly owing to their low toxicity and unique properties. 0-D carbon nanomaterials include mainly graphene quantum dots (GQDs), carbon dots (CDs), fullerene, carbon nano onions (CNOs) and nano horns.

This Ph.D. dissertation focus on the synthesis of zero-dimensional nanomaterials – GQDs (graphene quantum dots), NGQDs (nitrogen-doped graphene quantum dots), FGQDs (fluorine-rich graphene quantum dots) and CNOs (carbon nano onions). The facile and cost-effective hydrothermal synthesis of these fascinating nanomaterials, their characterisations using various analytical techniques are demonstrated. Further their potential applications in the field of photocatalysis, fluorescent sensing of metal ions, and biological applications including anti-cancer, anti-oxidant and cell imaging are explored.

The thesis is structured into eight chapters.

Chapter 1: Chapter 1 provides a brief introduction to the 0-D nanomaterials under investigation, their properties, applications and finally the specific objectives of the present work.

Chapter 2: In chapter 2**,** the chemicals used, and methodologies adopted for the synthesis of nanomaterials are discussed in detail. The various analytical techniques employed for the characterisation of the prepared 0-D nanomaterials and for their applications investigated are also provided in the chapter.

Chapter 3: Chapter 3 presents the exciting future of GQDs and N-GQDs as green sensitizers in various semiconductor-based catalytic systems. Here, GQDs and NGQDs are prepared using the hydrothermal method and are successfully loaded onto the TiO_2 semiconductor photocatalyst. The material characterisation is carried out by FTIR, XRD and UV-DRS spectroscopy. Employing the developed hybrid TiO_2/NGQD catalyst, a photocatalytic water-splitting reaction is carried out. The NGQD-sensitized TiO_2 photocatalyst was found to be superior to the bare sol-gel titania catalyst in its performance.

Chapter 4: In chapter 4, the synthesis of small-sized GQDs by increasing the hydrothermal reaction time is reported. The prepared GQDs are characterised using TEM, FTIR, Raman and PL analysis.

Anti-cancer, anti-oxidant and cell imaging using the synthesised GQDs having excellent water-solubility, small size, and strong and excitation-dependent fluorescence are also discussed here.

Chapter 5: In chapter 5, an alternative route for the Hummers method for the synthesis of fluorine-rich graphene quantum dots is discussed. The nucleophilic substitution with less reductive defluorination in fluorographite is investigated and the mechanism for the formation of FGQDs from the precursor hydroxy fluorographene is also provided in detail. FGQDs as fluorescent turn-off metal sensor is also highlighted.

Chapter 6: Chapter 6 includes the synthesis of both spherical and hollow carbon nano onions (CNOs) from graphene oxide by varying the reaction time and temperature. The morphology and functionalisation of highly water-soluble CNOs using TEM, SEM, FTIR, Raman and PL analysis are also discussed. An investigation of highly fluorescent hollow CNOs towards metal sensing and biological applications such as anti-cancer and antioxidant activities are also discussed.

Chapter 7: The entire work done for this PhD project is summarised in Chapter 7.

Chapter 8: Chapter 8 provides a note on the future outlook of the research carried out.

CONTENTS

Page No.

CHAPTER 1 **1-36**

INTRODUCTION AND LITERATURE REVIEW

1.1 Zero-dimensional carbon nanomaterials 1

1.2 From graphene-to-graphene quantum dots 2

1.3 Graphene Quantum Dots (GQDs) 3

1.4 Nitrogen-doped graphene quantum dots (N-GQDs) 5

1.5 Titanium dioxide (TiO_2) 5

1.6 Titania/graphene quantum dot & titania/N-doped graphene quantum dot nanocomposites 6

1.7 Fluorine-rich graphene quantum dots 7

1.8 Carbon nano onions 9

1.9 Photocatalytic water splitting 10

1.10 Fluorescent sensing of metal ions 12

1.11 Anti-cancer and anti-oxidant properties 14

1.12 Objectives of the thesis 16

References 17

CHAPTER 2 **37-57**

EXPERIMENTAL METHODS AND CHARACTERISATION TECHNIQUES

2.1 Experimental Procedures 37

2.2 Experimental section 38

- 2.2.1 Preparation of Graphene oxide 38
- 2.2.2 Preparation of Graphene quantum dots 39
  - 2.2.2.1 Preparation of GQDs of sizes (10-20 nm) used in photocatalytic water splitting studies 39

            2.2.2.2 Preparation of GQDs of sizes (1-3 nm) used in biological studies 40
        2.2.3 Preparation of nitrogen-doped graphene quantum dots (N -GQDs) 40
        2.2.4 Preparation of titania 41
            2.2.4.1 Preparation of TiO_2/GQD and TiO_2/N-GQD nanocomposites 42
            2.2.4.2 Preparation of P25 TiO_2/N-GQD nanocomposites 42
        2.2.5 Preparation of CNOs 42
        2.2.6 Preparation of FGQDs 43
2.3 Hydrogen production by photocatalytic water splitting 44
2.4 Fluorescent sensing of metal ions 44
        2.4.1 Detection of Fe^{2+} ions 44
        2.4.2 Detection of Fe^{3+} ions 45
2.5 Biological applications 46
        2.5.1 Cell culture 46
        2.5.2 Evaluation of cytotoxicity (MTT Assay) 46
        2.5.3 Morphological analysis 47
        2.5.4 In vitro antioxidant assays 47
            2.5.4.1 Hydrogen peroxide scavenging assay 48
        2.5.5 Cell incubation and Bio-imaging 48
2.6 Characterisation techniques 49
        2.6.1 Transmission Electron microscopy (TEM) 49
        2.6.2 Scanning electron microscopy (SEM) 50
        2.6.3 FTIR (Fourier Transform Infra-Red) Spectroscopy 50
        2.6.4 Raman spectroscopy 51
        2.6.5 X-ray diffraction (XRD) 51
        2.6.6 X-ray photoelectron spectroscopy (XPS) 52
        2.6.7 Ultraviolet-Visible absorption spectroscopy 53
        2.6.8 Fluorescence spectroscopy 53

2.6.9 Lifetime (Fluorescence decay) measurement 54
2.6.10 Quantum yield measurements 54
2.6.11 Zeta potential analyser 55
References 56
CHAPTER 3 **59-79**

PHOTOCATALYTIC WATER SPLITTING USING TiO_2-NGQD NANOCOMPOSITES

3.1 Introduction 59
3.2 Experimental methods 61
3.3 Results and Discussion 62
3.3.1 TEM analysis 62
3.3.2 PL spectral analysis 65
3.3.3 XRD analysis 67
3.3.4 FTIR spectral analysis 68
3.3.5 UV-Visible diffuse reflectance spectroscopy 69
3.3.6 Kubelka- Munk plot 70
3.3.7 PL spectral analysis 71
3.3.8 Photocatalytic water splitting studies 72
3.4 Conclusions 74
References 76
CHAPTER 4 **81-99**

PREPARATION, CHARACTERISATION AND BIOLOGICAL APPLICATIONS OF SMALL-SIZED FLUORESCENT GRAPHENE QUANTUM DOTS

4.1 Introduction 81
4.2 Experimental methods 84
4.3 Results and discussion 84
4.3.1TEM analysis 84
4.3.2 FTIR analysis 85
4.3.3 Raman spectroscopic analysis 86
4.3.4 Fluorescence spectral analysis 87
4.3.5 Anti-cancer activity of GQDs 88

4.3.5.1 Cell viability analysis 88
4.3.5.2 Possible mechanism for the anti-cancer activity of GQDs 89
4.3.6 Anti-Oxidant property of GQDs 90
4.3.7 Morphology study of GQDs treated MCF-7 cells 91
4.3.8 Cell imaging of HBL-100 cells 91
4.4 Conclusions 92
References 94
CHAPTER 5 **101-127**
FLUORINE-RICH GRAPHENE QUANTUM DOTS FROM HYDROXY FLUOROGRAPHENE AND THEIR APPLICATION FOR SENSING OF Fe (III) IONS
5.1 Introduction 101
5.2 Experimental methods 104
5.3 Result and discussion 104
5.3.1 TEM analysis 104
5.3.2 FTIR analysis 105
5.3.3 AFM analysis 107
5.3.4 Raman analysis 107
5.3.5 XPS analysis 108
5.3.6 Schematic representation of the formation of FGQDs 112
5.3.7 Analysing optical properties of FGQDs 112
5.3.8 FGQDs as a turn-off sensor for Fe^{3+} 113
5.3.9 Mechanism for fluorescence quenching 116
5.3.9(a) Zeta potential measurement 116
5.3.9(b) Lifetime measurement 117
5.4 Conclusions 118
References 120

CHAPTER 6 **129-153**

HYDROTHERMAL CONVERSION OF GRAPHENE OXIDE TO CARBON NANO ONIONS FOR METAL SENSING AND BIOLOGICAL APPLICATIONS

6.1 Introduction 129

6.2 Experimental methods 132

6.3 Results and discussion 132

- 6.3.1 TEM images 132
- 6.3.2 FTIR and Raman Analysis 134
- 6.3.3 Curling and closure- CNO formation 136
- 6.3.4 PL spectroscopic analysis 137
- 6.3.5 Exploring the optical properties of hollow CNOs 137
- 6.3.6 Fluorescent detection of Fe^{2+} ions 138
- 6.3.7 Investigating the anti-cancer activity of CNOs on MCF-7 cell line 140
  - 6.3.7.1 MTT assay 140
  - 6.3.7.2 MCF-7 cell morphology analysis 141
  - 6.3.7.3 DAPI staining-to study nuclear morphology 142

6.4 Conclusions 143

References 145

7. SUMMARY AND CONCLUSIONS **155-158**

7.1 Overall conclusions 155

8. FUTURE OUTLOOK **159-160**

8.1 Future outlook 159

PUBLICATIONS

PAPERS PRESENTED IN SEMINARS /CONFERENCE

LIST OF ABBREVIATIONS

0D - Zero dimensional
1D - One dimensional
2D - Two dimensional
3D - Three dimensional
CDs - Carbon dots
SWCNT - Single-walled carbon nanotube
MWCNT - Multi-walled carbon nanotube
GO - Graphene oxide
GQDs - Graphene quantum dots
NGQDs - Nitrogen doped graphene quantum dots
HOMO - Highest occupied molecular orbital
LUMO - Lowest unoccupied molecular orbital
VB - Valence band
CB - Conduction band
FGQDs - Fluorine rich graphene quantum dots
$(CF)_n$ - Fluorographite
CNOs - Carbon nano onions
OLC - Onion like carbon
NDs - Nanodiamonds
PEC - Photoelectrochemical reaction
ECL - Electrochemiluminescence
PL - Photoluminescence
SPR - Surface plasmon resonance
PET - Photoelectron transfer
FRET - Fluorescence resonance energy transfer
IFE - Inner filter effect

DET - Dexter energy transfer
CEE - Crosslink-enhanced emission
AIEE - Aggregation-induced emission enhancement
LOD - Limit of detection
WHO - World health organisation
MCF-7 - Michigan cancer foundation-7
ROS - Reactive oxygen species
H_2O_2 - Hydrogen peroxide
HFG - Hydroxy fluorographene
LED - Light emitting diode
GC - Gas chromatography
TCD - Thermal conductivity detector
UV - Ultra-violet
OD - Optical density
MTT - 3-(4,5-dimethylthiazol-2yl)-2,5-diphenyltetrazolium bromide
BSS - Balanced salt solution
DMEM - Dulbecco’s modified eagles’ medium
HEPES - 4-(2-hydroxyethyl)-1-piperazineethane sulfonic acid
DAPI - 4, 6-diamidino-2-phenylindole
DPPH - 1,1-diphenyl-2-picryl hydrazyl
IC_{50} - Half maximal inhibitory concentration
DMSO - Dimethyl sulfoxide
PBS - Phosphate buffer solution
PL - Photoluminescence
PLE - Photoluminescence excitation
FL - Fluorescence
TCSPC - Time-correlated single photon counting

ABSTRACT

Reduction in the size of materials in all three dimensions to nanoscale results in zero-dimensional (0-D) nanomaterials which exhibit novel and tunable properties. 0-D carbon nanomaterials include many interesting materials such as fullerenes, graphene quantum dots, carbon dots, carbon nano onions and nanodiamonds.

Graphene quantum dots (GQDs) are nanometre-sized fragments of graphene which have attracted considerable interest recently because of their band gap tunability, strong photoluminescence, higher water solubility, better chemical stability, low toxicity, excellent biocompatibility. The doping of nitrogen into GQDs (NGQDs) gives rise to much more attractive properties, such as electrocatalytic activity, photocatalytic activity, broad tunable photoluminescence. The exciting future of GQDs and N-GQDs as green sensitizers in various titanium dioxide based photocatalytic systems are investigated here by means of an important reaction, the photocatalytic generation of hydrogen via water splitting. The splitting water using solar energy for hydrogen generation have attracted much attention because of its cost-effectiveness, simplicity and the massive potential for further development.

In addition, the hydrothermal synthesis, characterisation and biological applications of small-sized GQDs including anti-cancer, anti-oxidant, cell imaging are also presented here. The prepared GQDs exhibited concentration-dependent cytotoxicity towards MCF-7 cells. On the other hand, negligible toxicity was shown towards normal

breast cells. The unique excitation-dependent emission property of GQDs was utilised in cellular labelling.

Fluorination is an efficient method to modify the properties of carbon materials. F doping can intensively modulate the chemical, structural, and electronic features of GQDs due to the electronegativity difference between carbon and fluorine. The investigations leading to the development of fluorine-rich graphene quantum dots (FGQDs) from hydroxy fluorographene and its application for fluorescence sensing of ferric ions are discussed here.

Carbon nano onions (CNOs) or multi-layered fullerenes are fascinating carbon nano-allotropes consisting of multiple shells of sp^2 hybridised carbon with spherical or polyhedral shape, possessing high surface to volume ratio, thermal stability and electrical conductivity. This Ph.D dissertation focus on the facile and cost-effective synthesis of spherical and dense CNOs as well as hollow, polyhedral CNOs. The biological applications of hollow, polyhedral CNOs are demonstrated here - including anti-cancer, anti-oxidant, cell imaging applications.

സംഗ്രഹം

നാനോ സ്കെയിലിലേക്ക് ത്രിമാന പദാർത്ഥങ്ങളുടെ വലിപ്പം കുറക്കുന്നത് പൂജ്യം-മാനം (0-D)ഉള്ള നാനോ മെറ്റീരിയലുകൾക്ക് കാരണമാകുന്നു, അത് പുതിയതും ട്യൂൺ ചെയ്യാവുന്നതുമായ ഗുണങ്ങൾ പ്രദർശിപ്പിക്കുന്നു. 0-D കാർബൺ നാനോ മെറ്റീരിയലുകളിൽ ഫുള്ളറീനുകൾ, ഗ്രാഫീൻ ക്വാണ്ടം ഡോട്ടുകൾ, കാർബൺ ഡോട്ടുകൾ, കാർബൺ നാനോ ഉള്ളി, നാനോഡയമണ്ട്സ് തുടങ്ങിയ രസകരമായ നിരവധി വസ്തുക്കൾ ഉൾപ്പെടുന്നു.

ഗ്രാഫീൻ ക്വാണ്ടം ഡോട്ടുകൾ (GQDs) ഗ്രാഫീനിന്റെ നാനോമീറ്റർ വലിപ്പമുള്ള ശകലങ്ങളാണ്. അവയുടെ ബാൻഡ് ഗ്യാപ്പ് ട്യൂണബിലിറ്റി, ശക്തമായ ഫോട്ടോലൂമിനെസെൻസ്, ജലത്തിൽ ലയിക്കാനുള്ള ഉയർന്ന കഴിവ് , മികച്ച രാസ സ്ഥിരത, കുറഞ്ഞ വിഷാംശം, മികച്ച ജൈവ അനുയോജ്യത, എന്നിവ കാരണം അടുത്തിടെ ഗണ്യമായ താൽപ്പര്യം ആകർഷിച്ചു. നൈട്രജനെ GQD-കളിലേക്ക് (NGQDs) ഡോപ്പിംഗ് ചെയ്യുന്നത് ഇലക്ട്രോകാറ്റലിറ്റിക് ആക്റ്റിവിറ്റി, ഫോട്ടോകാറ്റലിറ്റിക് ആക്റ്റിവിറ്റി, ബ്രോഡ് ട്യൂണബിൾ ഫോട്ടോലൂമിനെസെൻസ് എന്നിങ്ങനെയുള്ള കൂടുതൽ ആകർഷകമായ ഗുണങ്ങൾക്ക് കാരണമാകുന്നു. വിവിധ ടൈറ്റാനിയം ഡയോക്സൈഡ് അധിഷ്ഠിത ഫോട്ടോകാറ്റലിറ്റിക് സിസ്റ്റങ്ങളിലെ ഗ്രീൻ സെൻസിറ്റൈസറുകളായി ജിക്യൂഡികളുടെയും എൻ-ജിക്യൂഡികളുടെയും ആവേശകരമായ ഭാവി, ജലവിഭജനത്തിലൂടെ ഹൈഡ്രജന്റെ ഫോട്ടോകാറ്റലിറ്റിക് ഉൽപാദനം പഠിച്ചുകൊണ്ട് ഈ പഠനത്തിൽ അന്വേഷിക്കപ്പെടുന്നു. ഹൈഡ്രജൻ ഉൽപാദനത്തിനായി സൗരോർജ്ജം ഉപയോഗിച്ച് ജലം വിഭജിക്കുന്നത്, അതിന്റെ ചുരുങ്ങിയ ചെലവ്, ലാളിത്യം, കൂടുതൽ വികസനത്തിനുള്ള വൻ സാധ്യത എന്നിവ കാരണം വളരെയധികം ശ്രദ്ധ ആകർഷിക്കുന്നുണ്ട്.

കൂടാതെ, ചെറിയ വലിപ്പത്തിലുള്ള GQD-കളുടെ ഹൈഡ്രോതെർമൽ സിന്തസിസ്, സ്വഭാവപഠനം, ആന്റി കാൻസർ , ആന്റി ഓക്സിഡന്റ് സ്വഭാവഗുണങ്ങൾ , സെൽ ഇമേജിംഗ് എന്നിവയുൾപ്പെടെയുള്ള ജൈവിക ഉപയോഗങ്ങൾ എന്നിവയും ഇവിടെ അവതരിപ്പിക്കുന്നു. തയ്യാറാക്കിയ GQD-കൾ MCF-7 എന്ന സ്തനാർബുദ സെല്ലുകളിലേക്ക് ഗാഢത -ആശ്രിത സൈറ്റോടോക്സിസിറ്റി പ്രദർശിപ്പിച്ചു. മറുവശത്ത്, സാധാരണ ബ്രെസ്റ്റ്

കോശങ്ങളോട് നിസ്സാരമായ വിഷാംശം കാണിക്കുന്നു. സെല്ലുലാർ ലേബലിംഗിനായി, GQD-കളുടെ തനതായ എക്സ്ഐറ്റേഷൻ ആശ്രയിച്ചുള്ള എമിഷൻ പ്രോപ്പർട്ടി ഉപയോഗിച്ചിരിക്കുന്നു.

കാർബൺ വസ്തുക്കളുടെ ഗുണങ്ങൾ പരിഷ്കരിക്കുന്നതിനുള്ള കാര്യക്ഷമമായ മാർഗ്ഗമാണ് ഫ്ലൂറിനേഷൻ. കാർബണും ഫ്ലൂറിനും തമ്മിലുള്ള ഇലക്ട്രോനെഗറ്റിവിറ്റി വ്യത്യാസം കാരണം F ഡോപ്പിംഗിന് GQD-കളുടെ രാസ, ഘടനാപരമായ, ഇലക്ട്രോണിക് സവിശേഷതകൾ തീവ്രമായി മോഡുലേറ്റ് ചെയ്യാൻ കഴിയും. ഹൈഡ്രോക്സി ഫ്ലൂറോഗ്രാഫീനിൽ നിന്നുള്ള ഫ്ലൂറിൻ സമ്പുഷ്ടമായ ഗ്രാഫീൻ ക്വാണ്ടം ഡോട്ടുകൾ (എഫ്ജിക്യുഡി) വികസിപ്പിക്കുന്നതിലേക്ക് നയിക്കുന്ന അന്വേഷണങ്ങളും ഫെറിക് അയോണുകളുടെ ഫ്ലൂറസെൻസ് സെൻസിംഗിനായുള്ള അതിന്റെ പ്രയോഗവും ഇവിടെ ചർച്ചചെയ്യുന്നു.

കാർബൺ നാനോ ഉള്ളി (CNOs) അല്ലെങ്കിൽ മൾട്ടി-ലേയേർഡ് ഫുള്ളെറിനുകൾ സ്ഫെറിക്കൽ അല്ലെങ്കിൽ പോളിഹെഡ്രൽ ആകൃതിയിലുള്ള sp2 ഹൈബ്രിഡൈസ്ഡ് കാർബണിന്റെ ഒന്നിലധികം ഷെല്ലുകൾ അടങ്ങുന്ന ആകർഷകമായ കാർബൺ നാനോ-അലോട്രോപ്പുകളാണ്. ഉയർന്ന പ്രതല /വ്യാപ്ത അനുപാതം, താപ സ്ഥിരത, വൈദ്യുത ചാലകത എന്നിവ ഇവയുടെ പ്രത്യേകതകളാണ്. ഈ പിഎച്ച്.ഡി പ്രബന്ധം ഗോളാകൃതിയിലുള്ളതും ഇടതൂർന്നതുമായ സിഎൻഒകളുടെയും പൊള്ളയായ, പോളിഹെഡ്രൽ സിഎൻഒകളുടെയും ലളിതവും ചെലവ് കുറഞ്ഞതുമായ ഉത്പാദനത്തിൽ ശ്രദ്ധ കേന്ദ്രീകരിക്കുന്നു. പൊള്ളയായ, പോളിഹെഡ്രൽ CNO-കളുടെ ജൈവ ഉപയോഗങ്ങൾ - കാൻസർ വിരുദ്ധ, ആന്റി ഓക്സിഡന്റ്, സെൽ ഇമേജിംഗ് ആപ്ലിക്കേഷനുകൾ ഉൾപ്പെടെ ഇവിടെ പഠനവിധേയമാക്കിയിരിക്കുന്നു.

CHAPTER 1

INTRODUCTION AND LITERATURE SURVEY

1.1. Zero-dimensional carbon nanomaterials

Materials with at least one dimension in nano-scale (1-100 nm) are called nanomaterials. In this size regime, size determines the material properties. The idea of nanotechnology formally started with the historical talk entitled “There’s plenty of room at the bottom” by Richard P. Feynman [1], who is regarded as the father of nanotechnology. According to Siegel, nanomaterials are classified as zero-dimensional (0-D), one-dimensional (1-D), two-dimensional (2-D), and three-dimensional (3-D). 0-D nanomaterials possess nano-dimensions in all three directions which include metal nanoparticles and quantum dots [2]. In 1-D nanomaterials, the dimensions in two directions are within the nanoscale, and nanowires, nanorods, and nanotubes can be included in this category. The dimension in only one direction is within the nanoscale for 2-D nanomaterials. Nanofilms and nanosheets comes in this category. In 3-D nanomaterials, none of the three dimensions comes within nanoscale, however the material will be nano-structured [3] .

Carbon, one of the most abundant elements on the earth, plays a vital role in our lives as it is the base element of all organic materials. Due to its unique ability to form allotropes, it exists in different crystalline forms - diamond, graphite, and many nanocarbon forms like fullerenes and carbon nanotubes. It also exists in an amorphous state in charcoal, amorphous carbon, soot and glassy carbon. The nature of hybridization of carbon in its allotropic form determines its physical and chemical properties. Among carbon nanomaterials, graphene quantum dots (GQDs), carbon dots (CDs), fullerene, carbon nano onions (CNOs), and nanodiamond are 0-D, while single-walled carbon nanotube (SWCNT), multi-walled carbon nanotube (MWCNT), carbon nanohorns are 1-D nano forms. On the other hand, graphene is a 2-D nanomaterial.

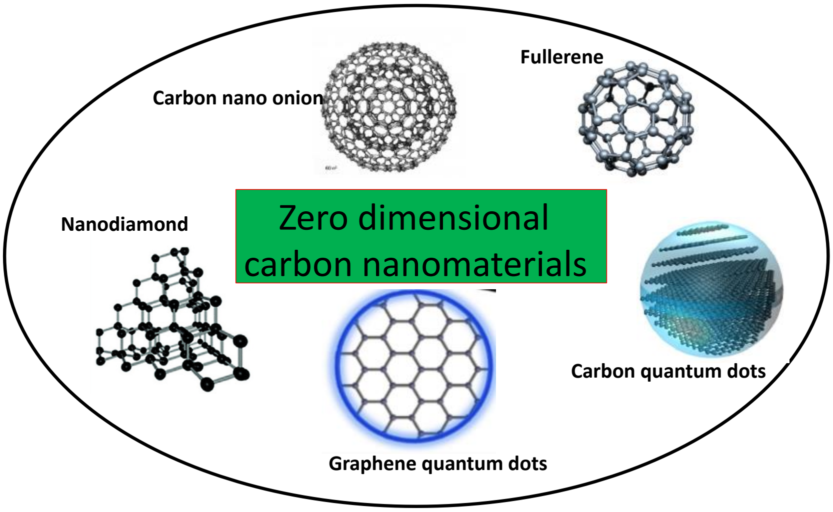

Figure 1.1 Various zero-dimensional carbon nanomaterials.

1.2. From graphene to graphene quantum dots

Among carbon nanomaterials, graphene is a zero- band -gap, 2D sheet of 1-10 layers of sp^2-hybridised carbons arranged in a honeycomb lattice with excellent thermal, mechanical, electrical, and optical properties, and also with high specific surface area and high carrier mobility [4]–[6]. Historically, R.Wallace was the person who first investigated the properties of graphene in 1947 [7], followed by Mcclure in 1956 [8], and Semenoff in 1984 [9]. However, the initial discoveries on graphene were mostly unnoticed until the Nobel prize for Physics in 2010 was awarded to Andre Geim and Kostya Novoselov for the ground breaking experiment – the exfoliation of graphite using a scotch tape method resulting in graphene [4]. Since then, this wonder material has been ruling the field of material chemistry with its unique physical and chemical properties. But the zero-band gap of graphene limits its application as a semiconductor in the field of optoelectronics. The research to overcome this challenge led to the cutting of graphene into nanosized fragments called graphene quantum dots (GQDs).

1.3. Graphene Quantum Dots (GQDs)

Graphene quantum dots (GQDs), a new rising carbon nanomaterial, are nanometer-sized sp^2 fragments of graphene with exciton confinement and a quantum size effect [10]. The average size of GQDs is below 20 nm. The characteristic quantum confinement and edge effect offer noble and novel properties to GQDs, such as non-zero and tunable band gap, strong photoluminescence (PL), excellent water solubility and ease of functionalization [11]–[18]. In addition to this, GQDs also possess excellent biocompatibility, lower toxicity, have molecular characters which make them easier to handle than colloidal semiconductor QDs [10], [19], [20]. Because of these interesting, unique properties, GQDs find potential applications in many fields, such as bioimaging [21], drug delivery [22], sensing [23]–[32], photodetectors [33], [34], LEDs [27, 28], solar cells [35] and so on.

The spectroscopic properties of GQDs vary depending on the preparation method and edge functional groups [13], [36], [37]. The absorption spectra of GQDs in the UV region show a prominent peak at 230-270 nm due to π-π * transition of core graphitic structure, while the peak at 320-370 nm belongs to the n-π * transition of functional groups. i.e. functional groups on GQDs can host absorption features and mark the fluorescence emission [15], [38]. Thus, in general, the PL emission of GQDs is determined by its size, edge structure (zig-zag or armchair) and surface chemical functionalities. GQDs exhibit emission peaks varying from blue to red region of visible light when excited with UV radiation. Furthermore, GQDs exhibit excitation-dependent PL emission as poly-dispersed GQDs with different energy levels can be photo-selected by excitation photon energy. Thus, controlled synthesis of GQDs with energetically uniform PL is highly desirable to advance its applications.

GQDs were first fabricated by Ponomarenko et al.[39]. The synthesis methods for GQDs can be classified as top-down and bottom-up approaches. The top-down methods include cleavage or exfoliation of bulk graphene-based material under harsh conditions like hydrothermal/solvothermal cutting, microwave-assisted cutting, electrochemical cutting and nanolithography [13], [15], [40], [19], [39]. Even though top-down methods are of low cost, they require harsh conditions, involve multi-steps and lack morphological control. In the bottom-up method, GQDs are prepared from polycyclic aromatic compounds by pyrolysis or cage opening of fullerenes [41], [42]. Precise control of morphology, size and shape are the advantages of bottom-up. However, the need for expensive precursors, complex synthesis steps and strong tendency of aggregation of formed GQDs are the limitations involved.

1.4. Nitrogen-doped graphene quantum dots (N-GQDs)

Chemical modification of GQDs with heteroatom doping is an effective way by which one can tune the intrinsic structural properties and manipulate the electronic state [43]–[49]. Among elemental doped GQDs, the nitrogen-doped graphene quantum dots (N-GQDs) have received significant attention due to their electronic structure manipulation, which enhances their opto-electronic properties, electrocatalytic and photocatalytic activities [44, 47, 50–54]. Different chemically bonded N atoms (graphitic, pyridinic, pyrrolic) introduce new energy levels in NGQDs, altering their HOMO-LUMO structure and offering new sites for chemical reactivity [55]. The introduction of nitrogen into the defective sites by annealing and hydrothermal treatment of GQDs in the presence of nitrogen-containing compounds can simultaneously overhaul the graphitic structure. Oxidised carbon also can be replaced with nitrogen dopants via electrochemical oxidation and reduction in the presence of nitrogen moieties.

1.5. Titanium dioxide (TiO_2)

Among wide gap semiconductors, TiO_2 is regarded as one of the most pertinent material capable of harvesting solar energy and driving chemical reactions simultaneously because of its high efficiency, non-toxicity, photo- and chemical stability, water insolubility under most conditions [56–60].TiO_2 exists in the anatase, rutile and brookite phases with a band gap of 3.2, 3.02, and 2.96 eV, respectively. TiO_2 is an n-type semiconductor, the valence band (VB) is O_{2p} hybridised with Ti_{3d}, and the conduction band (CB) is Ti_{3d} and Ti_{4s} [61].On irradiation with near- UV light, electrons in the VB are excited to CB leaving behind holes in VB. For a good semiconductor photocatalyst, the probability for e^-/h^+ recombination should be reduced, making the e^- and h^+ available for surface redox reactions. In anatase TiO_2, the surface hole trapping dominates due to spatial charge separation and is regarded as more active photocatalytic component than the rutile form. P25 Degussa is the commercially available TiO_2 which constitute 80% anatase and 20% rutile phase [62–65].

1.6. Titania/graphene quantum dot & titania/N-doped graphene quantum dot nanocomposites

The main drawbacks of TiO_2 photocatalyst are the rapid recombination of photogenerated electrons & holes and its inability to absorb visible light, which is the major portion of sunlight. Hence enormous amount of research work in recent years have been devoted to improve the photocatalytic activity of TiO_2 by modifying it in various ways, for example, with noble metal deposition and sensitizing with organic dyes [66–73]. Photocatalysts doped with carbon nanomaterials have demonstrated a significant enhancement in the photocatalytic activity compared to metal co-doped TiO_2, owing to the tunability of their properties [74]. GQDs are known to exhibit band gap tunability based on their size and are expected to enhance light absorption, including UV and visible radiations [75]. The use of GQDs as sensitizers in photocatalysis is an attractive alternate due to their non-toxic nature and strong photoabsorption in UV–visible regions depending on their size and doping elements [76–78]. Thus, in TiO_2/GQD nanocomposites, the photocatalytic enhancement is usually attributed to electron capture by the carbon material and subsequent reduction in the surface recombination rate. Apart from being a sink for photoexcited electrons, doping of GQD-based materials can modify the band gap, extending the optical absorption of TiO_2 to the visible region. Thus, GQDs can provide enhanced photocatalytic activity making the system better suited for solar energy harvesting [79]. Further, N-doping in GQDs creates less interfacial resistance and favorable band alignment, which significantly improves the potential use of N-doped GQDs as a green sensitizer in TiO_2/NGQD photocatalytic systems [80–82].

1.7. Fluorine-rich graphene quantum dots

Effective chemical functionalization of graphene under mild conditions is still a significant challenge. The search for a two-dimensional graphene-based precursor material with suitable properties and which can be easily cut into graphene quantum dots leads to fluorographite-derived materials. Fluorination is an efficient method to modify the properties of carbon materials, and the high level of fluorination of graphite results in graphite fluoride or fluorographite, $(CF)_n$ [83 –86]. Fluorographite has a graphite-like layered structure with fluorine atoms attached alternately above and below the hexagon layers of carbon atoms [83]. In partially fluorinated systems, interaction between carbon and fluorine can be rather complex and encompasses covalent, semi-ionic, ionic, and van der Waals interactions [84]. However, with less extreme conditions, a lower fluorine content can be introduced that causes significant alterations to the electronic, mechanical, and electrochemical properties without disrupting the planar sp^2-carbon network, and different ratios of carbon-to-fluorine in fluorinated graphite can then be obtained by employing different preparation conditions.

Fluorographene (FG), initially thought as a 2D analogue of Teflon, turned out as a material with high chemical reactivity owing to the strained geometry of F adatoms in the graphene network [85]. It is reported that the highly labile F atoms in FG are susceptible to reductive defluorination [86] and nucleophilic substitution reactions [87]. Thus, fluorographene can be considered a promising precursor material for preparing versatile graphene derivatives such as hydroxy graphene, cyanographene, graphene acid, alkylated, arylated and alkynylated graphene [88–92]. Modification with F has endowed graphene with unique electronic [93], [94], magnetic [95, 96], electrochemical [97, 98], exotic fluorescence [88, 99] and biological properties [100, 101]. There are several recent reports on GQDs doped with N, F, S, and P [44-45, 47–49, 102- 103]. F doping can intensively modulate the chemical, structural, and electronic features of GQDs due to the electronegativity difference between carbon and fluorine. Significant changes in PL properties are observed on cutting fluorographene to fluorinated graphene quantum dots (FGQDs). Red-shifted PL emission is observed in FGQDs when compared to GQDs [104]. FGQDs exhibit strong upconversion PL, excited by visible light, unlike GQDs, which use IR light for optimal excitation. Hence, FGQDs can be used as suitable energy transfer components in photocatalysis [105]. Unlike GQDs, fluorescent graphene fluorooxide quantum dots prepared by Gong et al. can resist pH effects without any surface passivation [106]. The generation of localised spin magnetic moments due to the point defects induced by fluorine atoms in FGQDs increases the paramagnetism five times higher than nonfluorinated ones and finds its potential as a novel contrasting agent for magnetic resonance imaging [107].

1.8. Carbon nano onions

Carbon nano-onion (CNO) or Onion like Carbon (OLC) can be considered as a new member of the carbon nanomaterial family consisting of quasi-spherical and polyhedral-shaped concentric graphitic shells [108]. CNOs basically consist of multiple shells of sp^2 hybridised carbon with shapes varying from spherical to polyhedral, sometimes with hollow core and size between 5-10 nm with varying degrees of carbon ordering within the shell and also the presence of non-sp^2 hybridised carbon. The structure of CNOs is constituted by hexagonal and pentagonal rings of carbon atoms with delocalized π-electrons. The interlayer spacing in CNO is generally 0.335 nm, approximately equal to basal planes of graphite [109]. The graphitic layers with holes, defects and pentagonal carbon rings lead to the appearance of curvature, resulting in amorphous or crystalline quasi-spherical CNOs [110], [111]. Despite its accidental discovery in 1980, this material was overshadowed by the popular and thoroughly investigated carbon nanomaterials such as fullerene (1985), CNT (1991), and graphene (2004). CNOs were first observed in 1980 by Iijima [112]. Nevertheless, this discovery remained unnoticed until 1992, when Daniel Ugarte synthesized carbon nano-onions with a diameter of around 45 nm by irradiating carbon soot with a high-energy electron beam [111]. Since then, a variety of methods have been reported for the synthesis of CNOs, which include thermal annealing of ultra-dispersed nanodiamonds (NDs), [113] arc-discharge, [114] pyrolysis, [115] ion implantation, [116] chemical vapour deposition [117] and electron-beam irradiation, [118] laser irradiation [119] and ball-milling [120]. Soft chemical methods, including solvothermal reduction and hydrothermal treatment with mild conditions, are also reported to synthesise CNOs [121]. Depending on the synthesis condition and precursor, big or small sized, spherical or polyhedral shaped, dense or hollow cored CNOs are obtained [110]. CNOs with small sizes and high surface strain displayed high chemical reactivity [122]. Due to unique physiochemical properties such as high surface-to-volume ratio, wide absorption spectra, high thermal stability and electrical conductivity [122–125], CNOs find applications in the field of supercapacitors, gas and energy storage, catalysis, hyper lubricants, electromagnetic shielding, biological imaging, sensing and water treatment [126]–[142].

1.9. Photocatalytic water splitting

Hydrogen is predicted to be good secondary energy resource and a valuable product of water splitting [143]. Among the various methods utilized for splitting water using solar energy for hydrogen generation, much attention has been focused on photoelectrochemical (PEC) or photocatalytic reactions because they are cost-effective, simple and convenient and have massive potential for further development. In 1972, Honda and Fujishima were the first who reported that H_2 evolution could be observed on a TiO_2 electrode under UV-light irradiation in a PEC cell with Pt as a counter electrode [144]. The principle of PEC hydrogen production was successfully extended using heterogeneous photocatalysis by Allen J. Bard [145]. The first step in heterogeneous photocatalysis is the interaction of semiconductors with light energy equal to or greater than band-gap energy, resulting in the generation of electron-hole pairs in the dispersed semiconductor particles. For photocatalytic hydrogen generation via water splitting, the semiconductor should have a band gap larger than 1.23 eV, and in order to suppress the recombination of photogenerated electrons and holes, sacrificial reagents such as methanol, ethanol and S^{2-}/SO_3^{2-} are generally used [146]. The whole process of photocatalytic water splitting with a semiconductor photocatalyst involves the following steps.

1. Photon absorption by the photocatalyst and generation of electrons and holes with sufficient potential for water splitting.
2. Charge separation and migration of charge carriers to surface reaction sites of the photocatalyst.
3. Hydrogen evolution via the reduction of water by photogenerated electrons and the oxidation of sacrificial agents by the holes at the surface reaction sites of the photocatalyst.

1.10. Fluorescent sensing of metal ions

A clean and hygienic source of water is essential for a healthy life. But increasing industrialisation and improper waste management mainly pollute the water bodies. Water pollution caused by heavy metal ions is a serious concern and has to be handled properly. Metals such as Fe, Na, K, Zn, Cu, Mn, Co, Ni, Mo, and W play crucial roles in biological process like osmotic regulation, catalysis, metabolism, biomineralization and signalling [147]. Even though metal cations have significant role in biological, environmental and chemical systems, if their concentration in water bodies exceeds the threshold level, will pose serious adverse effect on life and hence has to be monitored. Instrumental techniques generally used for metal ion detection include atomic absorption spectrometry [148, 149], UV-Vis spectrophotometry [150-152], voltammetry [153- 156], and inductively coupled plasma - mass spectrometry [157, 158]. Even though these techniques are highly sensitive and selective, they require tedious sample preparation, also expensive and are inconvenient for real-time and onsite detection. On the other hand, optical methods find more advantages in the detection of toxic metal ions, mainly because they are low cost, simple, fast, efficient, and highly sensitive and selective. Commonly used optical methods include fluorescent, electrochemiluminescence (ECL), photoluminescence (PL), colorimetry, and surface plasmon resonance (SPR) sensing [159]. Our studies are focussed on fluorescent sensing which is an easy, economical and effective way for detecting metal ions.

Fluorescent sensing is based on interaction of metal ions with the surface functionalised groups on QDs thereby affecting the surface states and consequently the physiochemical properties of fluorophores such as fluorescence intensity, life time and charge transfer or energy transfer processes, which can be monitored for the quantitative and qualitative determination of the metal ions. The major mechanisms involved in the fluorescence quenching or enhancement are, photoelectron transfer (PET), fluorescence resonance energy transfer (FRET), inner filter effect (IFE), static or dynamic quenching, Dexter energy transfer (DET), crosslink-enhanced emission (CEE), or aggregation-induced emission enhancement (AIEE) [160].

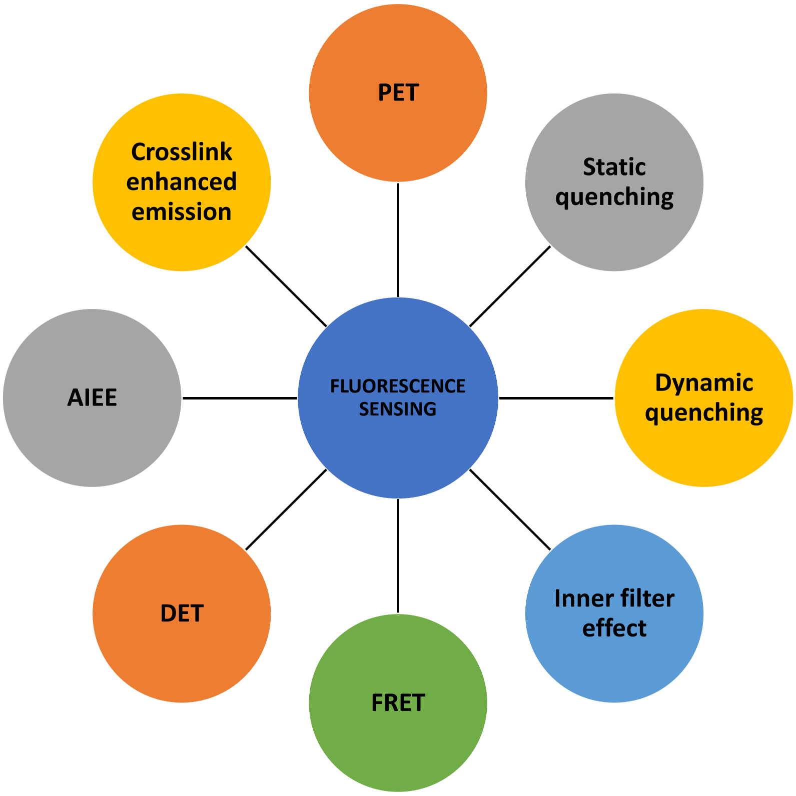

Figure 1.2 Schematic illustration of different mechanisms involved in the quenching and enhancement of fluorescence.

1.11 Anti-cancer and anti-oxidant properties

Zero-dimensional carbon nanomaterials find immense potential applications in biomedical field. These small sized nanomaterials possessing high surface to volume ratio, cell permeability, biocompatibility, optical stability. Strong and excitation dependent photoluminescence enable them to be suitable for biological applications**.** The biomedical utilities of 0-D carbon nanomaterials include drug delivery, bioimaging, cancer therapy, tissue engineering and biosensing [161], [162].

Cancer is perceived as one of the most lethal diseases, and can be the leading cause of death worldwide, according to WHO. Cancer is actually a group of diseases in which the abnormal growth of cells happens as a consequence of mutation caused by several factors. Since cancer cells have the potential to invade or spread to other parts of body, its early detection and diagnosis is essential for the survival of the patient. Nanomaterials can play an important role in early cancer diagnosis.

There are over 100 cancer types affecting human population and among them, most common are lung, breast, colon, prostrate and rectum cancers. Most of the cancers can be almost completely cured if diagnosed and treated at the initial stage itself, especially breast cancer. Even though the survivors from breast cancer have increased over time, even today it remains one of the leading causes of death among women.

MCF-7 (Michigan Cancer Foundation -7) cell line is a human breast cancer cell line which is commonly used in breast cancer research with estrogen, progesterone and glucocorticoid receptors. It is an epithelial cell line isolated from the breast tissue of a patient with metastatic adenocarcinoma [163]. HBL-100 is a normal human breast epithelial cell line extracted from the milk secretion of a nursing mother [164].

Most of the cancer cells lack the anti-oxidant enzymes such as peroxidase, catalase and superoxidase, which results in an increase in concentration of ROS species like H_2O_2 within the cells resulting in oxidative stress. Hydrogen peroxide, in normal case, serve as a secondary messenger to control several cellular events. But the biologically abnormal cancer cells respond differently to the high concentration of H_2O_2 and is used as a weapon to extract the nutrients from the adjacent fibroblast. Therefore, for cancer cells, H_2O_2 is a fuel for their rapid cell proliferation and growth. Thus, a nanomaterial with good radical scavenging ability may also exhibit anti- cancer property [165].

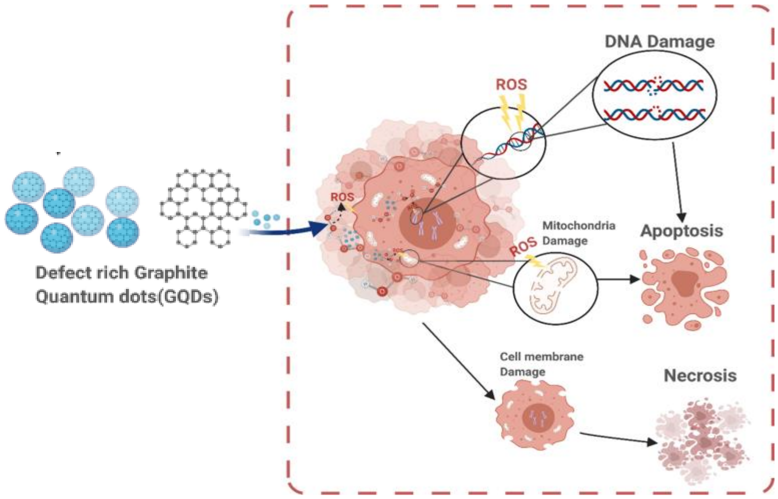

Figure 1.3 Schematic representation of multi-target therapeutic mechanism of graphene quantum dots (GQDs) [166].

1.12. Objectives of the thesis

The aim and objectives of the present research are

1. The synthesis of 0-D carbon nanomaterials – graphene quantum dots, nitrogen doped graphene quantum dots, fluorine rich graphene quantum dots and carbon nano onions by simple and facile hydrothermal methods.
2. To characterise the prepared nanomaterials using various spectroscopic and microscopic techniques such as TEM, SEM, AFM, FTIR, Raman, XPS, and Photoluminescence.
3. To explore the application of the as-synthesised nanomaterials in various fields such as photocatalysis and fluorescent turn-off sensing for the detection of metal ions.
4. To investigate the biological applications such as anti- cancer and anti-oxidant properties, and cell imaging, of the 0-D dimensional nanomaterials prepared.

References

[1] 'Feynman's Talk'. https://www.zyvex.com/nanotech/feynman.html (accessed Nov. 11, 2022).

[2] R. W. Sie, 'NANOSTRUCTURED MATERIALS', p. 21.

[3] P. I. Varghese and T. Pradeep, *A Textbook of Nanoscience and Nanotechnology*. Tata McGraw Hill Education, 2003.

[4] K. S. Novoselov, 'Electric Field Effect in Atomically Thin Carbon Films', *Science*, vol. 306, no. 5696, pp. 666–669, Oct. 2004, doi: 10.1126/science.1102896.

[5] K. S. Novoselov, A. K Geim, S. V Morozov, D. Jiang, M. I Katneslson, S.V Dubonos, A. A. Firsov 'Two-dimensional gas of massless Dirac fermions in graphene', *Nature*, vol. 438, no. 7065, pp. 197–200, Nov. 2005, doi: 10.1038/nature04233.

[6] A. K. Geim and K. S. Novoselov, 'The rise of graphene', *Nature Mater*, vol. 6, no. 3, Art. no. 3, Mar. 2007, doi: 10.1038/nmat1849.

[7] 'Phys. Rev. 71, 622 (1947) - The Band Theory of Graphite'. https://journals.aps.org/pr/abstract/10.1103/PhysRev.71.622 (accessed Nov. 12, 2022).

[8] J. W. McClure, 'Diamagnetism of Graphite', *Phys. Rev.*, vol. 104, no. 3, pp. 666–671, Nov. 1956, doi: 10.1103/PhysRev.104.666.

[9] G. W. Semenoff, 'Condensed-Matter Simulation of a Three-Dimensional Anomaly', *Phys. Rev. Lett.*, vol. 53, no. 26, pp. 2449–2452, Dec. 1984, doi: 10.1103/PhysRevLett.53.2449.

[10] M. Bacon, S. J. Bradley, and T. Nann, 'Graphene Quantum Dots', *Particle & Particle Systems Characterization*, vol. 31, no. 4, pp. 415–428, 2014, doi: 10.1002/ppsc.201300252.

[11] L. Li, G. Wu, G. Yang, J. Peng, J. Zhao, and J.-J. Zhu, 'Focusing on luminescent graphene quantum dots: current status and future perspectives', *Nanoscale*, vol. 5, no. 10, pp. 4015–4039, May 2013, doi: 10.1039/C3NR33849E.

[12] H. Li, X. He, Z. Kang, H. Huang, Y. Liu, J. Liu, S. Lian. 'Water-Soluble Fluorescent Carbon Quantum Dots and Photocatalyst

Design', *Angewandte Chemie International Edition*, vol. 49, no. 26, pp. 4430–4434, 2010, doi: 10.1002/anie.200906154.

[13] D. Pan, J. Zhang, Z. Li, and M. Wu, 'Hydrothermal Route for Cutting Graphene Sheets into Blue-Luminescent Graphene Quantum Dots', *Advanced Materials*, vol. 22, no. 6, pp. 734–738, 2010, doi: 10.1002/adma.200902825.

[14] R. Ye., Z. Peng, A. Metzger, J. Lin, J. A. Mann, K. Huang, C. Xiang, X. Fan, E.L.G Samuel, L.B Alemany, A.A Marti, J.M Tour, 'Bandgap Engineering of Coal-Derived Graphene Quantum Dots', *ACS Appl. Mater. Interfaces*, vol. 7, no. 12, pp. 7041–7048, Apr. 2015, doi: 10.1021/acsami.5b01419.

[15] L. Tang, R. Ji, X. Cao, J. Lin, H Jiang, X. Li, K.S Teng, C.M. Luk, S. Zeng, J. Hao, S.P. Lau, 'Deep Ultraviolet Photoluminescence of Water-Soluble Self-Passivated Graphene Quantum Dots', May 10, 2012. https://pubs.acs.org/doi/abs/10.1021/nn300760g (accessed Aug. 01, 2020).

[16] S. Zhu, Y. Song, X. Zhao, J. Shao, J. Zhang, and B. Yang, 'The photoluminescence mechanism in carbon dots (graphene quantum dots, carbon nanodots, and polymer dots): current state and future perspective', *Nano Res.*, vol. 8, no. 2, pp. 355–381, Feb. 2015, doi: 10.1007/s12274-014-0644-3.

[17] Q.-R. Dong, 'Electrical linear control of the electronic structure of graphene quantum dots', *Journal of Applied Physics*, vol. 113, no. 23, p. 234304, Jun. 2013, doi: 10.1063/1.4811519.

[18] S. Chen, N. Ullah, T. Wang, and R. Zhang, 'Tuning the optical properties of graphene quantum dots by selective oxidation: a theoretical perspective', *J. Mater. Chem. C*, vol. 6, no. 25, pp. 6875–6883, Jun. 2018, doi: 10.1039/C8TC02083C.

[19] M. Zhang, L. Bai, W. Shang, W. Xie, H. Ma, Y. Fu, D. Fang, H. Sun, L. Fan, M. Han, C. Liu, S. Fang, 'Facile synthesis of water-soluble, highly fluorescent graphene quantum dots as a robust biological label for stem cells', *J. Mater. Chem.*, vol. 22, no. 15, pp. 7461–7467, Mar. 2012, doi: 10.1039/C2JM16835A.

[20] X. T. Zheng, A. Ananthanarayanan, K. Q. Luo, and P. Chen, 'Glowing graphene quantum dots and carbon dots: properties,

syntheses, and biological applications’, *Small*, vol. 11, no. 14, pp. 1620–1636, Apr. 2015, doi: 10.1002/smll.201402648.

[21] S. Zhu, J. Zhang, C. Qiao, S. Tang, Y. Li, W. Yuan, B. Li, L. Tian, F. Liu, R. Hu, H. Gao, H. Wei, H. Zhang, H. Sun, B.Yang. ‘Strongly green-photoluminescent graphene quantum dots for bioimaging applications’, *Chem. Commun. (Camb.)*, vol. 47, no. 24, pp. 6858–6860, Jun. 2011, doi: 10.1039/c1cc11122a.

[22] Z. Xue, Q. Sun, L. Zhang, Z. Kang, L. Liang, Q. Wang, ‘Graphene quantum dot assisted translocation of drugs into a cell membrane’, *Nanoscale*, vol. 11, no. 10, pp. 4503–4514, Mar. 2019, doi: 10.1039/C8NR10091H.

[23] H. Wang, X. Wu, W. Dong, S.-L. Lee, Q. Yuan, and W. Gan, ‘One-step preparation of single-layered graphene quantum dots for the detection of Fe^{3+}’, *Spectrochimica Acta Part A: Molecular and Biomolecular Spectroscopy*, vol. 226, p. 117626, Feb. 2020, doi: 10.1016/j.saa.2019.117626.

[24] F. Wang, Z. Gu, W. Lei, W. Wang, X. Xia, and Q. Hao, ‘Graphene quantum dots as a fluorescent sensing platform for highly efficient detection of copper(II) ions’, *Sensors and Actuators B: Chemical*, vol. 190, pp. 516–522, Jan. 2014, doi: 10.1016/j.snb.2013.09.009.

[25] M. K. Chini, V. Kumar, A. Javed, and S. Satapathi, ‘Graphene quantum dots and carbon nano dots for the FRET based detection of heavy metal ions’, *Nano-Structures & Nano-Objects*, vol. 19, p. 100347, Jul. 2019, doi: 10.1016/j.nanoso.2019.100347.

[26] H. Chakraborti, S. Sinha, S. Ghosh, and S. K. Pal, ‘Interfacing water soluble nanomaterials with fluorescence chemosensing: Graphene quantum dot to detect Hg^{2+} in 100% aqueous solution’, *Materials Letters*, vol. 97, pp. 78–80, Apr. 2013, doi: 10.1016/j.matlet.2013.01.094.

[27] B. Wang, S. Zhuo, L. Chen, and Y. Zhang, ‘Fluorescent graphene quantum dot nanoprobes for the sensitive and selective detection of mercury ions’, *Spectrochimica Acta Part A: Molecular and Biomolecular Spectroscopy*, vol. 131, pp. 384–387, Oct. 2014, doi: 10.1016/j.saa.2014.04.129.

[28] Z. Li, Y. Wang, Y. Ni, and S. Kokot, ‘A rapid and label-free dual detection of Hg (II) and cysteine with the use of fluorescence

switching of graphene quantum dots', *Sensors and Actuators B: Chemical*, vol. 207, pp. 490–497, Feb. 2015, doi: 10.1016/j.snb.2014.10.071.

[29] X. Liu, W. Gao, X. Zhou, and Y. Ma, 'Pristine graphene quantum dots for detection of copper ions', *J. Mater. Res.*, vol. 29, no. 13, pp. 1401–1407, Jul. 2014, doi: 10.1557/jmr.2014.145.

[30] P. Kaewanan, P. Sricharoen, N. Limchoowong, T. Sripakdee, P. Nuengmatcha, and S. Chanthai, 'A fluorescence switching sensor based on graphene quantum dots decorated with Hg $^{2+}$ and hydrolyzed thioacetamide for highly Ag $^{+}$ -sensitive and selective detection', *RSC Adv.*, vol. 7, no. 76, pp. 48058–48067, 2017, doi: 10.1039/C7RA09126E.

[31] X.-E. Zhao, C. Lei, Y. Gao, H. Gao, S. Zhu, X. Yang, J. You, H. Wang, 'A ratiometric fluorescent nanosensor for the detection of silver ions using graphene quantum dots', *Sensors and Actuators B: Chemical*, vol. 253, pp. 239–246, Dec. 2017, doi: 10.1016/j.snb.2017.06.086.

[32] H. Huang, L. Liao, X. Xu, M. Zou, F. Liu, and N. Li, 'The electron-transfer based interaction between transition metal ions and photoluminescent graphene quantum dots (GQDs): A platform for metal ion sensing', *Talanta*, vol. 117, pp. 152–157, Dec. 2013, doi: 10.1016/j.talanta.2013.08.055.

[33] S. Jayanthi, R. Kaur, and F. Erogbogbo, 'Graphene Quantum Dot - Titania Nanoparticle Composite for Photocatalytic Water Splitting', *MRS Advances*, vol. 1, pp. 1–7, Jun. 2016, doi: 10.1557/adv.2016.470.

[34] Q. Zhang, J. Jie, S. Diao, Z. Shao, Q. Zhang, L. Wang, W. Deng, W. Hu, H. Xia, X. Yuan and S. Lee, 'Solution-processed graphene quantum dot deep-UV photodetectors', *ACS Nano*, vol. 9, no. 2, pp. 1561–1570, Feb. 2015, doi: 10.1021/acsnano.5b00437.

[35] M. Dutta, S. Sarkar, T. Ghosh, and D. Basak, 'ZnO/Graphene Quantum Dot Solid-State Solar Cell', *The Journal of Physical Chemistry C*, vol. 116, pp. 20127–20131, Sep. 2012, doi: 10.1021/jp302992k.

[36] T. Fan, W. Zeng, W. Tang, C. Yuan, S. Tong, K. Cai, Y. Liu, W. Huang, Y. Min and A. J Epstein 'Controllable size-selective method

to prepare graphene quantum dots from graphene oxide', *Nanoscale Res Lett*, vol. 10, p. 55, Feb. 2015, doi: 10.1186/s11671-015-0783-9.

[37] F. Liu, M.-H. Jang, H. D. Ha, J.-H. Kim, Y.-H. Cho, and T. S. Seo, 'Facile Synthetic Method for Pristine Graphene Quantum Dots and Graphene Oxide Quantum Dots: Origin of Blue and Green Luminescence', *Advanced Materials*, vol. 25, no. 27, pp. 3657–3662, 2013, doi: 10.1002/adma.201300233.

[38] S. H. Jin, D. H. Kim, G. H. Jun, S. H. Hong, and S. Jeon, 'Tuning the Photoluminescence of Graphene Quantum Dots through the Charge Transfer Effect of Functional Groups', *ACS Nano*, vol. 7, no. 2, pp. 1239–1245, Feb. 2013, doi: 10.1021/nn304675g.

[39] L. A. Ponomarenko, F. Schedin, M. I Katsnelson, R. Yang, E.W Hill, K.S Novoselov, A.K Geim, 'Chaotic Dirac Billiard in Graphene Quantum Dots', *Science*, vol. 320, no. 5874, pp. 356–358, Apr. 2008, doi: 10.1126/science.1154663.

[40] S. Zhu, J. Zhang, X. Liu, B. Li, X. Wang, S. Tang, Q. Meng, Y. Liu, C. Shi, R. Hu, and B. Yang, 'Graphene quantum dots with controllable surface oxidation, tunable fluorescence and up-conversion emission', *RSC Adv.*, vol. 2, no. 7, pp. 2717–2720, Mar. 2012, doi: 10.1039/C2RA20182H.

[41] R. Liu, D. Wu, X. Feng, and K. Müllen, 'Bottom-up fabrication of photoluminescent graphene quantum dots with uniform morphology', *J. Am. Chem. Soc.*, vol. 133, no. 39, pp. 15221–15223, Oct. 2011, doi: 10.1021/ja204953k.

[42] J. Lu, P. S. E. Yeo, C. K. Gan, P. Wu, and K. P. Loh, 'Transforming C_{60} molecules into graphene quantum dots', *Nat Nanotechnol*, vol. 6, no. 4, pp. 247–252, Apr. 2011, doi: 10.1038/nnano.2011.30.

[43] S. Kim, D. H. Shin, C.O. Kim, S.S. Kang, K.W. Lee, J. Kim, S. H. Choi and S.W. Hwang 'Effect of nitrogen doping on the structural and the optical variations of graphene quantum dots by using hydrazine treatment', *Journal of the Korean Physical Society*, vol. 67, no. 4, pp. 746–751, Aug. 2015, doi: 10.3938/jkps.67.746.

[44] Y. Li, Y. Zhao, H. Cheng, Y. Hu, G. Shi, L. Dai and L. Qu, 'Nitrogen-Doped Graphene Quantum Dots with Oxygen-Rich Functional Groups', *J. Am. Chem. Soc.*, vol. 134, no. 1, pp. 15–18, Jan. 2012, doi: 10.1021/ja206030c.

[45] C. Hu, Y. Liu, Y. Yang, J. Cui, Z. Huang, Y. Wang, L. Yang, H. Wang, Y.Xiao and J. Rong ‘One-step preparation of nitrogen-doped graphene quantum dots from oxidized debris of graphene oxide’, *J. Mater. Chem. B*, vol. 1, no. 1, pp. 39–42, Nov. 2012, doi: 10.1039/C2TB00189F.

[46] M. Hassan, E. Haque, K. R. Reddy, A. I. Minett, J. Chen, and V. G. Gomes, ‘Edge-enriched graphene quantum dots for enhanced photo-luminescence and supercapacitance’, *Nanoscale*, vol. 6, no. 20, pp. 11988–11994, Sep. 2014, doi: 10.1039/C4NR02365J.

[47] L. Tang, R. Ji, X. Li, G. Bai, C.P. Liu, J. Hao, J. Lin, H. Jiang, K.S. Teng, Z. Yang and S.P. Lau, ‘Deep ultraviolet to near-infrared emission and photoresponse in layered N-doped graphene quantum dots’, *ACS Nano*, vol. 8, no. 6, pp. 6312–6320, Jun. 2014, doi: 10.1021/nn501796r.

[48] A. Ananthanarayanan, Y. Wang, P. Routh, M. Sk Alam,A. Than, M. Lin, J. Zhang, J. Chen, H. Sun, and P. Chen, ‘Nitrogen and phosphorus co-doped graphene quantum dots: synthesis from adenosine triphosphate, optical properties, and cellular imaging’, *Nanoscale*, vol. 7, no. 17, pp. 8159–8165, 2015, doi: 10.1039/C5NR01519G.

[49] S. Kundu, R. M. Yadav, T. N Narayanan, M.V Shelke, R. Vajtai, P.M Ajayan and V.K. Pillai ‘Synthesis of N, F and S co-doped graphene quantum dots’, *Nanoscale*, vol. 7, no. 27, pp. 11515–11519, Jul. 2015, doi: 10.1039/C5NR02427G.

[50] J. Ju and W. Chen, ‘Synthesis of highly fluorescent nitrogen-doped graphene quantum dots for sensitive, label-free detection of Fe (III) in aqueous media’, *Biosensors and Bioelectronics*, vol. 58, pp. 219–225, Aug. 2014, doi: 10.1016/j.bios.2014.02.061.

[51] Q. Li, S. Zhang, L. Dai, and L. Li, ‘Nitrogen-Doped Colloidal Graphene Quantum Dots and Their Size-Dependent Electrocatalytic Activity for the Oxygen Reduction Reaction’, *J. Am. Chem. Soc.*, vol. 134, no. 46, pp. 18932–18935, Nov. 2012, doi: 10.1021/ja309270h.

[52] D. Jiang, Y. Zhang, H. Chu, J. Liu, J. Wan, and M. Chen, ‘N-doped graphene quantum dots as an effective photocatalyst for the photochemical synthesis of silver deposited porous graphitic C_3N_4 nanocomposites for nonenzymatic electrochemical H_2O_2 sensing’,

RSC Adv., vol. 4, no. 31, pp. 16163–16171, Mar. 2014, doi: 10.1039/C4RA00601A.

[53] T.-F. Yeh, C.-Y. Teng, S.-J. Chen, and H. Teng, 'Nitrogen-Doped Graphene Oxide Quantum Dots as Photocatalysts for Overall Water-Splitting under Visible Light Illumination', *Advanced Materials*, vol. 26, no. 20, pp. 3297–3303, 2014, doi: 10.1002/adma.201305299.

[54] Q. Liu, B. Guo, Z. Rao, B. Zhang, and J. R. Gong, 'Strong two-photon-induced fluorescence from photostable, biocompatible nitrogen-doped graphene quantum dots for cellular and deep-tissue imaging', *Nano Lett*, vol. 13, no. 6, pp. 2436–2441, Jun. 2013, doi: 10.1021/nl400368v.

[55] R. Yadav and C. Dixit, 'Review on: Synthesis, Characterization and Potential application of Nitrogen-doped Graphene', *Journal of Science: Advanced Materials and Devices*, vol. 2, May 2017, doi: 10.1016/j.jsamd.2017.05.007.

[56] X. Chen, S. Shen, L. Guo, and S. S. Mao, 'Semiconductor-based Photocatalytic Hydrogen Generation', *Chem. Rev.*, vol. 110, no. 11, pp. 6503–6570, Nov. 2010, doi: 10.1021/cr1001645.

[57] C.-H. Liao, C.-W. Huang, and J. C. S. Wu, 'Hydrogen Production from Semiconductor-based Photocatalysis via Water Splitting', *Catalysts*, vol. 2, no. 4, Art. no. 4, Dec. 2012, doi: 10.3390/catal2040490.

[58] 'Direct splitting of water under visible light irradiation with an oxide semiconductor photocatalyst | Nature'. https://www.nature.com/articles/414625a (accessed Nov. 16, 2022).

[59] V. Etacheri, C. Di Valentin, J. Schneider, D. Bahnemann, and S. C. Pillai, 'Visible-light activation of TiO_2 photocatalysts: Advances in theory and experiments', *Journal of Photochemistry and Photobiology C: Photochemistry Reviews*, vol. 25, pp. 1–29, Dec. 2015, doi: 10.1016/j.jphotochemrev.2015.08.003.

[60] Z. Luo, A.S Poyraz, C.H Kuo, R. Miao, Y. Meng, S. Y Chen, T. Jiang, C. Wenos and S.L Suib 'Crystalline Mixed Phase (Anatase/Rutile) Mesoporous Titanium Dioxides for Visible Light Photocatalytic Activity', *Chem. Mater.*, vol. 27, no. 1, pp. 6–17, Jan. 2015, doi: 10.1021/cm5035112.

[61] ‘TiO2 Band Gap, Doping, and Modifying’, *Ebrary*. https://ebrary.net/182944/engineering/TiO$_2$_band_doping_modifying (accessed Nov. 14, 2022).

[62] O. Carp, ‘Photoinduced reactivity of titanium dioxide’, *Progress in Solid State Chemistry*, vol. 32, no. 1–2, pp. 33–177, 2004, doi: 10.1016/j.progsolidstchem.2004.08.001.

[63] A. L. Linsebigler, G. Lu, and J. T. Jr. Yates, ‘Photocatalysis on TiO_2 Surfaces: Principles, Mechanisms, and Selected Results’, *Chem. Rev.*, vol. 95, no. 3, pp. 735–758, May 1995, doi: 10.1021/cr00035a013.

[64] R. Li, Y. Weng,X. Zhou, X. Wang, Y. Mi, R. Chong, H. Han and C. Li ‘Achieving overall water splitting using titanium dioxide-based photocatalysts of different phases’, *Energy Environ. Sci.*, vol. 8, no. 8, pp. 2377–2382, Jul. 2015, doi: 10.1039/C5EE01398D.

[65] C. Dette, M.A Perez-Osorio, C.S Kley, P. Punke, C.E Patrick, P. Jacobson, F. Giustino and S.J Jung ‘TiO_2 Anatase with a Bandgap in the Visible Region’, *Nano Lett.*, vol. 14, no. 11, pp. 6533–6538, Nov. 2014, doi: 10.1021/nl503131s.

[66] T. Sreethawong and S. Yoshikawa, ‘Comparative investigation on photocatalytic hydrogen evolution over Cu-, Pd-, and Au-loaded mesoporous TiO_2 photocatalysts’, *Catalysis Communications*, vol. 6, no. 10, pp. 661–668, Oct. 2005, doi: 10.1016/j.catcom.2005.06.004.

[67] X. Wang, R. Long, D. Liu, D. Yang, C. Wang, and Y. Xiong, ‘Enhanced full-spectrum water splitting by confining plasmonic Au nanoparticles in N-doped TiO_2 bowl nanoarrays’, *Nano Energy*, vol. 24, pp. 87–93, Jun. 2016, doi: 10.1016/j.nanoen.2016.04.013.

[68] W. Zhou, W. Li, J.Q Wang, Y. Qu, Y. Yang, Y. Xie, K. Zhang, L. Wang, H. Fu and D. Zhao ‘Ordered Mesoporous Black TiO_2 as Highly Efficient Hydrogen Evolution Photocatalyst’, *J. Am. Chem. Soc.*, vol. 136, no. 26, pp. 9280–9283, Jul. 2014, doi: 10.1021/ja504802q.

[69] E. Pulido Melián, O. Diaz Gonzalez, A. Mendez Ortega, C.R Lopez, D. Hevia and J. Pena Perez, ‘Efficient and affordable hydrogen production by water photo-splitting using TiO_2-based photocatalysts’, *International Journal of Hydrogen Energy*, vol. 38,

no. 5, pp. 2144–2155, Feb. 2013, doi: 10.1016/j.ijhydene.2012.12.005.

[70] V. J. Babu, S. Vempati, T. Uyar, and S. Ramakrishna, ‘Review of one-dimensional and two-dimensional nanostructured materials for hydrogen generation’, *Phys. Chem. Chem. Phys.*, vol. 17, no. 5, pp. 2960–2986, Jan. 2015, doi: 10.1039/C4CP04245J.

[71] B. Wu, D. Liu, S. Mubeen, T. T. Chuong, M. Moskovits, and G. D. Stucky, ‘Anisotropic Growth of TiO_2 onto Gold Nanorods for Plasmon-Enhanced Hydrogen Production from Water Reduction’, *J. Am. Chem. Soc.*, vol. 138, no. 4, pp. 1114–1117, Feb. 2016, doi: 10.1021/jacs.5b11341.

[72] S. Tanigawa and H. Irie, ‘Visible-light-sensitive two-step overall water-splitting based on band structure control of titanium dioxide’, *Applied Catalysis B: Environmental*, vol. 180, pp. 1–5, Jan. 2016, doi: 10.1016/j.apcatb.2015.06.008.

[73] W. J. Youngblood, S.H Lee, Y. Kobayashi, P.G Hoertz, T. A Moore, A. L Moore, D. Gust and T. E Mallouk, ‘Photoassisted overall water splitting in a visible light-absorbing dye-sensitized photoelectrochemical cell’, *J Am Chem Soc*, vol. 131, no. 3, pp. 926–927, Jan. 2009, doi: 10.1021/ja809108y.

[74] ‘Novel Carbon-Doped TiO_2 Nanotube Arrays with High Aspect Ratios for Efficient Solar Water Splitting | Nano Letters’. https://pubs.acs.org/doi/10.1021/nl051807y (accessed Nov. 17, 2022).

[75] D. Pan, J. Jiao, Z. Li, Y. Guo, C. Feng, Y. Liu, L. Wang and M. Wu, ‘Efficient Separation of Electron–Hole Pairs in Graphene Quantum Dots by TiO_2 Heterojunctions for Dye Degradation’, *ACS Sustainable Chem. Eng.*, vol. 3, no. 10, pp. 2405–2413, Oct. 2015, doi: 10.1021/acssuschemeng.5b00771.

[76] Y. Sun, S. Wang, C. Li, P. Luo, L. Tao, Y. Wei and G. Shi ‘Large scale preparation of graphene quantum dots from graphite with tunable fluorescence properties’, *Phys. Chem. Chem. Phys.*, vol. 15, no. 24, pp. 9907–9913, May 2013, doi: 10.1039/C3CP50691F.

[77] P. Roy, A.P. Periasamy, C. Chuang, Y.R Liou, Y.F Chen, J. Joly, C.T Liang, H T Chang, ‘Plant leaf-derived graphene quantum dots

and applications for white LEDs', *New J. Chem.*, vol. 38, no. 10, pp. 4946–4951, Sep. 2014, doi: 10.1039/C4NJ01185F.

[78] Q. Xue, H. Huang, L. Wang, Z. Chen, M. Wu, Z. Li, D. Pan, 'Nearly monodisperse graphene quantum dots fabricated by amine-assisted cutting and ultrafiltration', *Nanoscale*, vol. 5, no. 24, pp. 12098–12103, Nov. 2013, doi: 10.1039/C3NR03623E.

[79] Y. Zheng, 'TiO_2/graphene quantum dots heterostructure composite with enhanced photocatalytic activity under visible light irradiation', in *Advanced Materials and Energy Sustainability*, WORLD SCIENTIFIC, 2017, pp. 97–104. doi: 10.1142/9789813220393_0012.

[80] R. Shi, Z. Li, H. Yu, L. Shang, C. Zhou, G.I.N. WATERHOUSE, I.Z Wu, T. Zhang, 'Effect of Nitrogen Doping Level on the Performance of N-Doped Carbon Quantum Dot/TiO_2 Composites for Photocatalytic Hydrogen Evolution', *ChemSusChem*, vol. 10, no. 22, pp. 4650–4656, 2017, doi: 10.1002/cssc.201700943.

[81] Solar Light Harvesting N-Graphene Quantum Dots Decorated TiO_2 for Enhanced Photocatalytic Activity'. https://www.researchgate.net/publication/329185160_Solar_Light_Harvesting_NGraphene_Quantum_Dots_Decorated_TiO_2_for_Enhanced_Photocatalytic_Activity.

[82] X. Sun, H.J. Li, N. Ou, B. Lyu, B. Gui, S. Tian, D. Qian, X. Wang, J. Yang, 'Visible-Light Driven TiO_2 Photocatalyst Coated with Graphene Quantum Dots of Tunable Nitrogen Doping', *Molecules*, vol. 24, no. 2, p. 344, Jan. 2019, doi: 10.3390/molecules24020344.

[83] X. Wang, Y. Dai, J. Gao, J. Huang, B. Li, C. Fan, J. Yang, X. Liu, 'High-Yield Production of Highly Fluorinated Graphene by Direct Heating Fluorination of Graphene-oxide', *ACS Appl. Mater. Interfaces*, vol. 5, no. 17, pp. 8294–8299, Sep. 2013, doi: 10.1021/am402958p.

[84] H. Touhara and F. Okino, 'Property control of carbon materials by fluorination', *Carbon*, vol. 38, no. 2, pp. 241–267, Jan. 2000, doi: 10.1016/S0008-6223(99)00140-2.

[85] D. D. Chronopoulos, A. Bakandritsos, M. Pykal, R. Zbořil, and M. Otyepka, 'Chemistry, properties, and applications of

fluorographene', *Applied Materials Today*, vol. 9, pp. 60–70, Dec. 2017, doi: 10.1016/j.apmt.2017.05.004.

[86] R. Zbořil, F. Karlicky, A.B. Bourlinos, T.A Steriotis, A.K Georgakilas, V.K Safarova, D. Jancik, C. Trapalis, M. Oteypka, 'Graphene Fluoride: A Stable Stoichiometric Graphene Derivative and its Chemical Conversion to Graphene', *Small*, vol. 6, no. 24, pp. 2885–2891, 2010, doi: 10.1002/smll.201001401.

[87] M. Dubecký, E. Otyepkova, P.Lazar, F. Karlicky, M. Petr, K. Cepe, P. Banas, R. Zboril, M. Otyepka, 'Reactivity of Fluorographene: A Facile Way toward Graphene Derivatives', *J. Phys. Chem. Lett.*, vol. 6, no. 8, pp. 1430–1434, Apr. 2015, doi: 10.1021/acs.jpclett.5b00565.

[88] P. Gong, J. Wang, W. Sun, D. Wu, Z. Wang, Z. Fan, H. Wang, X. Han, S. Yang, 'Tunable photoluminescence and spectrum split from fluorinated to hydroxylated graphene', *Nanoscale*, vol. 6, no. 6, pp. 3316–3324, Feb. 2014, doi: 10.1039/C3NR05725A.

[89] A. Bakandritsos, M. Pykal, P. Btonski, P. Jakubec, D.D. Chronopoulos, K. Polakova, V. Georgakilas, K. Cepe, O. Tomanec, V. Ranc, A.B. Bourlinos, R. Zboril, M. Oteypka, 'Cyanographene and Graphene Acid: Emerging Derivatives Enabling High-Yield and Selective Functionalization of Graphene', *ACS Nano*, vol. 11, no. 3, pp. 2982–2991, Mar. 2017, doi: 10.1021/acsnano.6b08449.

[90] D. D. Chronopoulos, A. Bakandritsos, P. Lazar, M. Pykal, K. Cepe, R. Zboril, M.Oteypka, 'High-Yield Alkylation and Arylation of Graphene via Grignard Reaction with Fluorographene', *Chem. Mater.*, vol. 29, no. 3, pp. 926–930, Feb. 2017, doi: 10.1021/acs.chemmater.6b05040.

[91] W. La , J. Liu, L. Luo, X. Wang, T. He, K. Fan, X. Liu 'The Friedel–Crafts reaction of fluorinated graphene for high-yield arylation of graphene', *Chem. Commun.*, vol. 54, no. 72, pp. 10168–10171, Sep. 2018, doi: 10.1039/C8CC05762A.

[92] D. D. Chronopoulos , M. Medved, P Błoński, Z. Nováček, P. Jakubec, O. Tomanec, A. Bakandritsos, V. Novotná, R. Zbořil, M. Otyepka, 'Alkynylation of graphene via the Sonogashira C–C cross-coupling reaction on fluorographene', *Chemical Communications*, vol. 55, no. 8, pp. 1088–1091, 2019, doi: 10.1039/C8CC08492K.

[93] J. T. Robinson, J. S. Burgess, C. E. Junkermeier, S. C Badescu, T. L Reinecke, F. K. Perkins, M. K. Zalalutdniov, J. W. Baldwin, J.C. Culbertson, P. E. Sheehan, E. S. Snow, 'Properties of fluorinated graphene films', *Nano Lett.*, vol. 10, no. 8, pp. 3001–3005, Aug. 2010, doi: 10.1021/nl101437p.

[94] W. Feng, P. Long, Y. Feng, and Y. Li, 'Two-Dimensional Fluorinated Graphene: Synthesis, Structures, Properties and Applications', *Advanced Science*, vol. 3, no. 7, p. 1500413, 2016, doi: 10.1002/advs.201500413.

[95] Q. Feng, N. Tang, F. Liu, Q. Cao, W. Zheng, W. Ren, X. Wan, Y. Du, Obtaining High Localized Spin Magnetic Moments by Fluorination of Reduced Graphene Oxide', *ACS Nano*, vol. 7, no. 8, pp. 6729–6734, Aug. 2013, doi: 10.1021/nn4027905.

[96] X. Hong, S. H. Cheng, C. Herding, and J. Zhu, 'Colossal negative magnetoresistance in dilute fluorinated graphene', *Giant-magnetoresistance anomaly associated with a magnetization process in UFe4Al8*, vol. 83, no. 8, p. 085410, Feb. 2011, doi: 10.1103/PhysRevB.83.085410.

[97] P. Meduri, H. Chen, J. Xiao, J. J. Martinez, C. T. Carlson, J. G. Zhang, Z. D. Deng, 'Tunable electrochemical properties of fluorinated graphene', *J. Mater. Chem. A*, vol. 1, no. 27, pp. 7866–7869, Jun. 2013, doi: 10.1039/C3TA11710C.

[98] Y. Yang, G. Lu, Y. Li, Z. Liu, and X. Huang, 'One-Step Preparation of Fluorographene: A Highly Efficient, Low-Cost, and Large-Scale Approach of Exfoliating Fluorographite', *ACS Appl. Mater. Interfaces*, vol. 5, no. 24, pp. 13478–13483, Dec. 2013, doi: 10.1021/am405046u.

[99] K.-J. Jeon, Z. Lee, E. Pollak, L. Moreschini, A. Bostwick, C.M. Park, R. Mendelsberg, V. Radmilovic, R. Kostecki, T.J. Richardson, E. Rotenberg, 'Fluorographene: A Wide Bandgap Semiconductor with Ultraviolet Luminescence', *ACS Nano*, vol. 5, no. 2, pp. 1042–1046, Feb. 2011, doi: 10.1021/nn1025274.

[100] R. Romero-Aburto, T. N. Narayanan, Y. Nagaoka, T. Hasumura, T. M. Mitcham, T. Fukuda, P. J. Cox, R. R. Bouchard, T. Maekawa, D. S. Kumar, S. V. Torti, S. A. Mani, P. M. Ajayan, 'Fluorinated Graphene Oxide; a New Multimodal Material for Biological

Applications', *Advanced Materials*, vol. 25, no. 39, pp. 5632–5637, 2013, doi: 10.1002/adma201301804.

[101] Y. Wang, W. C. Lee, K. K. Manga, P. K. Ang, J. Lu, Y. P. Liu, C. T. Lim, K. P. Loh, 'Fluorinated Graphene for Promoting Neuro-Induction of Stem Cells', *Advanced Materials*, vol. 24, no. 31, pp. 4285–4290, 2012, doi: 10.1002/adma.201200846.

[102] F. Qian, X. Li, L. Tang, S. K. Lai, C. Lu, and S. P. Lau, 'Potassium doping: Tuning the optical properties of graphene quantum dots', *AIP Advances*, vol. 6, no. 7, p. 075116, Jul. 2016, doi: 10.1063/1.4959906.

[103] W. Wang, S. Xu, N. Li, Z. Huang, B. Su, and X. Chen, 'Sulfur and phosphorus co-doped graphene quantum dots for fluorescent monitoring of nitrite in pickles', *Spectrochimica Acta Part A: Molecular and Biomolecular Spectroscopy*, vol. 221, p. 117211, May 2019, doi: 10.1016/j.saa.2019.117211.

[104] Q. Feng, Q. Cao, M. Li, F. Liu, N. Tang, and Y. Du, 'Synthesis and photoluminescence of fluorinated graphene quantum dots', *Appl. Phys. Lett.*, vol. 102, no. 1, p. 013111, Jan. 2013, doi: 10.1063/1.4774264.

[105] J. Shen, Y. Zhu, C. Chen, X. Yang, and C. Li, 'Facile preparation and upconversion luminescence of graphene quantum dots', *Chem. Commun.*, vol. 47, no. 9, pp. 2580–2582, Feb. 2011, doi: 10.1039/C0CC04812G.

[106] P. Gong, Z. Yang, W. Hong, Z. Wang, K. Hou, J. Wang, S. Yang, 'To lose is to gain: Effective synthesis of water-soluble graphene fluoroxide quantum dots by sacrificing certain fluorine atoms from exfoliated fluorinated graphene', *Carbon*, vol. 83, pp. 152–161, Mar. 2015, doi: 10.1016/j.carbon.2014.11.027.

[107] P. Gong, J. Wang, K. Hou, Z. Yang, Z. Wang, Z. Liu, X. Han, S. Yang, 'Small but strong: The influence of fluorine atoms on formation and performance of graphene quantum dots using a gradient F-sacrifice strategy', *Carbon*, vol. 112, pp. 63–71, Feb. 2017, doi: 10.1016/j.carbon.2016.10.091.

[108] O. Mykhailiv, H. Zubyk, and M. E. Plonska-Brzezinska, 'Carbon nano-onions: Unique carbon nanostructures with fascinating

properties and their potential applications’, *Inorganica Chimica Acta*, vol. 468, pp. 49–66, Nov. 2017, doi: 10.1016/j.ica.2017.07.021.

[109] R. Bacon, ‘Growth, Structure, and Properties of Graphite Whiskers’, *Journal of Applied Physics*, vol. 31, no. 2, p. 283, Jun. 2004, doi: 10.1063/1.1735559.

[110] O. Mykhailiv, H. Zubyk, and M. E. Plonska-Brzezinska, ‘Carbon nano-onions: Unique carbon nanostructures with fascinating properties and their potential applications’, *Inorganica Chimica Acta*, vol. 468, pp. 49–66, Nov. 2017, doi: 10.1016/j.ica.2017.07.021.

[111] D. Ugarte, ‘Curling and closure of graphitic networks under electron-beam irradiation’, *Nature*, vol. 359, no. 6397, Art. no. 6397, Oct. 1992, doi: 10.1038/359707a0.

[112] S. Iijima, ‘Direct observation of the tetrahedral bonding in graphitized carbon black by high resolution electron microscopy’, *Journal of Crystal Growth*, vol. 50, no. 3, pp. 675–683, Nov. 1980, doi: 10.1016/0022-0248(80)90013-5.

[113] V. Kuznetsov, A. Chuvilin, Y. V. Butenko, I. Mal’kov, and V. Titov, ‘Onion-like carbon from ultra-disperse diamond’, 1994, doi: 10.1016/0009-2614(94)87072-1.

[114] N. Sano, H. Wang, M. Chhowalla, I. Alexandrou, and G. A. Amaratunga, ‘Synthesis of carbon “onions” in water’, *Nature*, vol. 414, no. 6863, pp. 506–507, Nov. 2001, doi: 10.1038/35107141.

[115] M. Choucair and J. A. Stride, ‘The gram-scale synthesis of carbon onions’, *Carbon*, vol. 50, no. 3, pp. 1109–1115, Mar. 2012, doi: 10.1016/j.carbon.2011.10.023.

[116] T. Cabioc’h, M. Jaouen, E. Thune, P. Guérin, C. Fayoux, and M. F. Denanot, ‘Carbon onions formation by high-dose carbon ion implantation into copper and silver’, *Surface & Coatings Technology*, no. 128–129, pp. 43–50, 2000.

[117] X. Chen, F. Deng, J. Wang, H. Yang, G. Wu, X. Zhang, J. Peng, W. Li, ‘New method of carbon onion growth by radio-frequency plasma-enhanced chemical vapor deposition’, *Chemical Physics Letters - CHEM PHYS LETT*, vol. 336, pp. 201–204, Mar. 2001, doi: 10.1016/S0009-2614(01)00085-9.

[118] M. Choi, I. S. Altman, Y. J. Kim, P.V. Pikhitsa, S. Lee, G.S. Park, G T. Jeong, J.B. Yoo, ‘Formation of Shell-Shaped Carbon Nanoparticles Above a Critical Laser Power in Irradiated Acetylene’, *Advanced Materials,* vol. 16, no. 19, pp. 1721–1725, 2004, doi: 10.1002/adma.200400179.

[119] T. Gorelik, S. Urban, F. Falk, U. Kaiser, and U. Glatzel, ‘Carbon onions produced by laser irradiation of amorphous silicon carbide’, *Chemical Physics Letters*, vol. 373, pp. 642–645, May 2003, doi: 10.1016/S0009-2614(03)00677-8.

[120] X. H. Chen, H. S. Yang, G. T. Wu, M. Wang, F. M. Deng, X. B. Zhang, J. C. Peng, W. Z. Li, ‘Generation of curved or closed-shell carbon nanostructures by ball-milling of graphite’, *Journal of Crystal Growth*, vol. 218, no. 1, pp. 57–61, Sep. 2000, doi: 10.1016/S0022-0248(00)00486-3.

[121] A. Guo, K. Bao, S. Sang, X. Zhang, B. Shao, C. Zhang, Y. Wang, F. Cui, X. Yang, ‘Soft-chemistry synthesis, solubility and interlayer spacing of carbon nano-onions’, *RSC Adv.*, vol. 11, no. 12, pp. 6850–6858, Feb. 2021, doi: 10.1039/D0RA09410B.

[122] A. Palkar, F. Melin, C. M. Cardona, B. Elliott, A. K. Naskar, D.D. Edie, A. Kumbhar, L. Echegoyen, ‘Reactivity Differences between Carbon Nano Onions (CNOs) Prepared by Different Methods’, *Chem. Asian J.*, vol. 2, no. 5, pp. 625–633, May 2007, doi: 10.1002/asia.200600426.

[123] M. Zeiger, N. Jäckel, M. Aslan, D. Weingarth, and V. Presser, ‘Understanding structure and porosity of nanodiamond-derived carbon onions’, *Carbon*, vol. 84, pp. 584–598, Apr. 2015, doi: 10.1016/j.carbon.2014.12.050.

[124] C. Portet, G. Yushin, and Y. Gogotsi, ‘Electrochemical performance of carbon onions, nanodiamonds, carbon black and multiwalled nanotubes in electrical double layer capacitors’, *Carbon*, vol. 45, no. 13, pp. 2511–2518, Nov. 2007, doi: 10.1016/j.carbon.2007.08.024.

[125] V. Kuznetsov, S. Moseenkov, A. Ischenko, A. Romanenko, T. Buryakov, O. Anikeeva, S. Maksimenko, P. Kuzhir, D. Bychanok, A. Gusinski, O. Ruhavets, O. Shenderova, P. Lambin, Controllable electromagnetic response of onion-like carbon based materials’, *physica status solidi (b)*, vol. 245, no. 10, pp. 2051–2054, 2008, doi: 10.1002/pssb.200879603.

[126] D. Pech, M. Brunet, H. Durou, P. Huang, V. Mochalin, Y. Gogotsi, P. L. Taberna, P. Simon, ‘Ultrahigh-power micrometre-sized supercapacitors based on onion-like carbon’, *Nature Nanotech*, vol. 5, no. 9, Art. no. 9, Sep. 2010, doi: 10.1038/nnano.2010.162.

[127] G. Moussa, C. Matei Ghimbeu, P.-L. Taberna, P. Simon, and C. Vix-Guterl, ‘Relationship between the carbon nano-onions (CNOs) surface chemistry/defects and their capacitance in aqueous and organic electrolytes’, *Carbon*, vol. 105, pp. 628–637, Aug. 2016, doi: 10.1016/j.carbon.2016.05.010.

[128] K. L. Van Aken, K. Maleski, T. S. Mathis, J. P. Breslin, and Y. Gogotsi, ‘Processing of Onion-like Carbon for Electrochemical Capacitors’, *ECS J. Solid State Sci. Technol.*, vol. 6, no. 6, pp. M3103–M3108, 2017, doi: 10.1149/2.0181706jss.

[129] R. Borgohain, J. Li, J. P. Selegue, and Y.-T. Cheng, ‘Electrochemical Study of Functionalized Carbon Nano-Onions for High-Performance Supercapacitor Electrodes’, *J. Phys. Chem. C*, vol. 116, no. 28, pp. 15068–15075, Jul. 2012, doi: 10.1021/jp301642s.

[130] M. Zeiger, N. Jäckel, V. N. Mochalin, and V. Presser, ‘Review: carbon onions for electrochemical energy storage’, *J. Mater. Chem. A*, vol. 4, no. 9, pp. 3172–3196, 2016, doi: 10.1039/C5TA08295A.

[131] A. V. Raghu, K. K. Karuppanan, and B. Pullithadathil, ‘Highly Surface Active Phosphorus-Doped Onion-Like Carbon Nanostructures: Ultrasensitive, Fully Reversible, and Portable NH $_3$ Gas Sensors’, *ACS Appl. Electron. Mater.*, vol. 1, no. 11, pp. 2208–2219, Nov. 2019, doi: 10.1021/acsaelm.9b00412.

[132] K. M. Tripathi, T. S. Tran, Y. J. Kim, and T. Kim, ‘Green Fluorescent Onion-like Carbon Nanoparticles From Flaxseed Oil for Visible Light-Induced Photocatalytic Applications and Label-Free Detection of Al(III) Ions’, p. 28.

[133] M. B. Seymour, C. Su, Y. Gao, Y. Lu, and Y. Li, ‘Characterization of carbon nano-onions for heavy metal ion remediation’, *J Nanopart Res*, vol. 14, no. 9, p. 1087, Sep. 2012, doi: 10.1007/s11051-012-1087-y.

[134] S. Lettieri, M. d’Amora, A. Camisasca, A. Diaspro, and S. Giordani, ‘Carbon nano-onions as fluorescent on/off modulated nanoprobes for

diagnostics', *Beilstein J. Nanotechnol.*, vol. 8, pp. 1878–1888, Sep. 2017, doi: 10.3762/bjnano.8.188.

[135] L. Joly-Pottuz, B. Vacher, N. Ohmae, J. M. Martin, and T. Epicier, 'Anti-wear and Friction Reducing Mechanisms of Carbon Nano-onions as Lubricant Additives', *Tribol Lett*, vol. 30, no. 1, pp. 69–80, Apr. 2008, doi: 10.1007/s11249-008-9316-3.

[136] J. Xu, X. Chen, P. Grützmacher, A. Rosenkranz, J. Li, J. Jin, C. Zhang, J. Luo, 'Tribochemical Behaviors of Onion-Like Carbon Films as High-Performance Solid Lubricants with Variable Interfacial Nanostructures', p. 5.

[137] A. F. Hassan, 'Synthesis of carbon nano-onion embedded metal–organic frameworks as an efficient adsorbent for cadmium ions: kinetic and thermodynamic studies', *Environ Sci Pollut Res*, vol. 26, no. 23, pp. 24099–24111, Aug. 2019, doi: 10.1007/s11356-019-05581-5.

[138] P. P. Kuzhir, D.S. Bychanok, S. A. Maksimenko, A. V. Gusinski, O. V. Ruhavets, V. L. Kuznetsov, S. I. Moseenkov, C. Jones, O. Shenderova, Ph. Lambin, 'Onion-like carbon based polymer composite films in microwaves', *Solid State Sciences*, vol. 11, no. 10, pp. 1762–1767, Oct. 2009, doi: 10.1016/j.solidstatesciences.2008.12.003.

[139] S. K. Sonkar, M. Roy, D. G. Babar, and S. Sarkar, 'Water soluble carbon nano-onions from wood wool as growth promoters for gram plants', *Nanoscale*, vol. 4, no. 24, p. 7670, 2012, doi: 10.1039/c2nr32408c.

[140] N. Keller, N. I. Maksimova, V. V. Roddatis, M. Schur, G. Mestl, Y. V. Butenko, V. L. Kuznetsov, R. Schlögl, 'The catalytic use of onion-like carbon materials for styrene synthesis by oxidative dehydrogenation of ethylbenzene', *Angew Chem Int Ed Engl*, vol. 41, no. 11, pp. 1885–1888, Jun. 2002, doi: 10.1002/1521-3773(20020603)41:11<1885::aid-anie1885>3.0.co;2-5.

[141] D. Su, N. Maksimova, G. Mestl, V. Kuznetsov, V. Keller, R. Schlögl, N. Keller, 'Oxidative dehydrogenation of ethylbenzene to styrene over ultra-dispersed diamond and onion-like carbon', *Carbon*, vol. 45, pp. 2145–2151, Oct. 2007, doi: 10.1016/j.carbon.2007.07.005.

[142] S. Giordani, J, Bartelmess, M. Frasconi, I. Biondi, S. Cheung, M. Grossi, D. Wu, L. Echegoyen, D.F O'Shea, 'NIR fluorescence labelled carbon nano-onions: synthesis, analysis and cellular imaging', *J. Mater. Chem. B*, vol. 2, no. 42, pp. 7459–7463, 2014, doi: 10.1039/C4TB01087F.

[143] J. A. Turner, 'A Realizable Renewable Energy Future', *Science*, vol. 285, no. 5428, pp. 687–689, Jul. 1999, doi: 10.1126/science.285.5428.687.

[144] A. Fujishima and K. Honda, 'Electrochemical Photolysis of Water at a Semiconductor Electrode', *Nature*, vol. 238, no. 5358, Art. no. 5358, Jul. 1972, doi: 10.1038/238037a0.

[145] A. J. Bard, 'Design of semiconductor photoelectrochemical systems for solar energy conversion', *J. Phys. Chem.*, vol. 86, no. 2, pp. 172–177, Jan. 1982, doi: 10.1021/j100391a008.

[146] A. Kudo and Y. Miseki, 'Heterogeneous photocatalyst materials for water splitting', *Chem. Soc. Rev.*, vol. 38, no. 1, pp. 253–278, Dec. 2008, doi: 10.1039/B800489G.

[147] K. P. Carter, A. M. Young, and A. E. Palmer, 'Fluorescent Sensors for Measuring Metal Ions in Living Systems', *Chem. Rev.*, vol. 114, no. 8, pp. 4564–4601, Apr. 2014, doi: 10.1021/cr400546e.

[148] Andersen, J. E. T. A Novel Method for the Filterless Preconcentration of Iron. *The Analyst* **2005**, *130* (3), 385. https://doi.org/10.1039/b412061b

[149] Grotti, M.; Abelmoschi, M. L.; Soggia, F.; Frache, R. Determination of Ultratrace Elements in Natural Waters by Solid-Phase Extraction and Atomic Spectrometry Methods. *Anal. Bioanal. Chem.* **2003**, *375* (2), 242–247. https://doi.org/10.1007/s00216-002-1676-1.

[150] Narayanaswamy, N.; Govindaraju, T. Aldazine-Based Colorimetric Sensors for Cu^{2+} and Fe^{3+}. *Sens. Actuators B Chem.* **2012**, *161* (1), 304–310. https://doi.org/10.1016/j.snb.2011.10.036.

[151] Liang, Z.-Q.; Wang, C.-X.; Yang, J.-X.; Gao, H.-W.; Tian, Y.-P.; Tao, X.-T.; Jiang, M.-H. A Highly Selective Colorimetric Chemosensor for Detecting the Respective Amounts of Iron(Ii) and Iron(Iii) Ions in Water. *New J. Chem.* **2007**, *31* (6), 906. https://doi.org/10.1039/b701201m.

[152] Lunvongsa, S.; Oshima, M.; Motomizu, S. Determination of Total and Dissolved Amount of Iron in Water Samples Using Catalytic Spectrophotometric Flow Injection Analysis. *Talanta* **2006**, *68* (3), 969–973. https://doi.org/10.1016/j.talanta.2005.06.067.

[153] Van den Berg, C. M. G. Chemical Speciation of Iron in Seawater by Cathodic Stripping Voltammetry with Dihydroxynaphthalene. *Anal. Chem.* **2006**, *78* (1), 156–163. https://doi.org/10.1021/ac051441+.

[154] Cheize, M.; Sarthou, G.; Croot, P. L.; Bucciarelli, E.; Baudoux, A.-C.; Baker, A. R. Iron Organic Speciation Determination in Rainwater Using Cathodic Stripping Voltammetry. *Anal. Chim. Acta* **2012**, *736*, 45–54. https://doi.org/10.1016/j.aca.2012.05.011.

[155] Gun, J.; Salaün, P.; van den Berg, C. M. G. Advantages of Using a Mercury Coated, Micro-Wire, Electrode in Adsorptive Cathodic Stripping Voltammetry. *Anal. Chim. Acta* **2006**, *571* (1), 86–92. https://doi.org/10.1016/j.aca.2006.04.043.

[156] Zhu, Y.; Hu, X.; Pan, D.; Han, H.; Lin, M.; Lu, Y.; Wang, C.; Zhu, R. Speciation Determination of Iron and Its Spatial and Seasonal Distribution in Coastal River. *Sci. Rep.* **2018**, *8* (1), 2576. https://doi.org/10.1038/s41598-018-20991-0.

[157] Matusch, A.; Depboylu, C.; Palm, C.; Wu, B.; Höglinger, G. U.; Schäfer, M. K.-H.; Becker, J. S. Cerebral Bioimaging of Cu, Fe, Zn, and Mn in the MPTP Mouse Model of Parkinson's Disease Using Laser Ablation Inductively Coupled Plasma Mass Spectrometry (LA-ICP-MS). *J. Am. Soc. Mass Spectrom.* **2010**, *21* (1), 161.

[158] Wu, J.; Boyle, E. A. Determination of Iron in Seawater by High-Resolution Isotope Dilution Inductively Coupled Plasma Mass Spectrometry after $Mg(OH)_2$ Coprecipitation. *Anal. Chim. Acta* **1998**, *367* (1–3), 183–191. https://doi.org/10.1016/S0003-2670(98)00145-7.

[159] N. A. A. Anas, Y. W. Fen, N. A. S. Omar, W. M. E. M. M. Daniyal, N. S. M. Ramdzan, and S. Saleviter, "Development of Graphene Quantum Dots-Based Optical Sensor for Toxic Metal Ion Detection," *Sensors*, vol. 19, no. 18, p. 3850, Sep. 2019, doi: 10.3390/s19183850.

[160] The Huy, B.; Thangadurai, D. T.; Sharipov, M.; Ngoc Nghia, N.; Van Cuong, N.; Lee, Y.-I. Recent Advances in Turn Off-on Fluorescence Sensing Strategies for Sensitive Biochemical Analysis -

A Mechanistic Approach. *Microchem.J.*2022,*179*,107511. https://doi.org/10.1016/j.microc.2022.107511.

[161] "Graphene Quantum Dots and Their Applications in Bioimaging, Biosensing, and Therapy - Chung - 2021 - Advanced Materials - Wiley OnlineLibrary."https://onlinelibrary.wiley.com/doi/10.1002/adma.201904362 (accessed Dec. 26, 2022).

[162] H. Sun, L. Wu, W. Wei, and X. Qu, "Recent advances in graphene quantum dots for sensing," *Mater. Today*, vol. 16, no. 11, pp. 433–442, Nov. 2013, doi: 10.1016/j.mattod.2013.10.020.

[163] "mcf7-cell-line-profile.pdf." Accessed: Dec. 26, 2022. [Online]. Available: https://www.culturecollections.org.uk/media/130237/mcf7-cell-line-profile.pd.

[164] C. Caron de Fromentel, P. C. Nardeux, T. Soussi, C. Lavialle, S. Estrade, G. Carloni, K. Chandrasekaran, R. Cassingena, "Epithelial HBL-100 cell line derived from milk of an apparently healthy woman harbours SV40 genetic information," *Exp. Cell Res.*, vol. 160, no. 1, pp. 83–94, Sep. 1985, doi: 10.1016/0014-4827(85)90238

[165] M. P. Lisanti, U. E. Martinez-Outschoorn, Z. Lin, S. Pavlides, D. Whitaker-Menezes, R. G.Pestell, A. Howell, F. Sotgia, "Hydrogen peroxide fuels aging, inflammation, cancer metabolism and metastasis: The seed and soil also needs 'fertilizer,'" *Cell Cycle*, vol. 10, no. 15, p. 2440, Aug. 2011, doi: 10.4161/cc.10.15.16870.

[166] Wang, X.; Hu, C.; Gu, Z.; Dai, L. Understanding of Catalytic ROS Generation from Defect-Rich Graphene Quantum-Dots for Therapeutic Effects in Tumor Microenvironment. *J. Nanobiotechnology* 2021, *19* (1), 340.https://doi.org/10.1186/s12951-021-01053-6.

CHAPTER 2

MATERIALS AND METHODS

2.1 Experimental Procedures

This chapter describes the experimental methods used for the preparation of graphene quantum dots, nitrogen-doped graphene quantum dots, titania and composites of titania with graphene quantum dots, carbon nano onions and fluorine-rich graphene quantum dots. The various techniques used for the characterisations of synthesised nanomaterial are discussed here. The experimental procedure used for the investigation of photocatalytic water splitting, fluorescent sensing of metal ions, anti-cancer and radical scavenging properties, and fluorescent cell imaging using the prepared zero-dimensional nanomaterials are also described in this chapter. The various chemicals used for the preparation and application studies are given in Table 2.1

Table 2.1 List of Chemicals used in the works

SI No.	Chemicals utilised	Manufacturer
1	Graphite	Sigma Aldrich
2	Fluorographite	Sigma
3	Sulphuric acid	Loba Chemie
4	Potassium permanganate	Merck
5	Sodium nitrate	Loba Chemie
6	Hydrogen peroxide	Merck
7	Ethanol	Changshu Hongsheng Fine Chemicals
8	Acetone	Loba Chemie
9	Hydrochloric acid	Nice Chemicals
10	Titanium dioxide	Degussa P25
11	Nitric acid	Nice Chemicals

SI No.	Chemicals utilised	Manufacturer
12	Titanium isopropoxide	Merck
13	Methanol	Merck
14	Ferric chloride	Sigma Aldrich
15	Ferrous sulphate	Merck
16	Aluminium nitrate, cadmium sulphate, zinc acetate, potassium chloride	Nice Chemicals
18	Manganese chloride, cobalt nitrate, calcium chloride, and nickel nitrate	Loba Chemie
19	Lead nitrate	Sd Fine Chemicals
20	Mercuric chloride	Fischer Scientific
21	Magnesium sulphate, sodium chloride	Merck
32	Silver nitrate	SRL Pvt Ltd
33	MCF-7 & HBL-100 cell lines	National Center for Cell Sciences (NCCS), Pune
34	3-(4,5-dimethylthiazol-2yl)-2,5-diphenyltetrazolium bromide (MTT)	Sigma Aldrich
35	Dulbecco’s modified eagles’ medium (DMEM)	Sigma Aldrich
36	Foetal bovine serum	Sigma Aldrich

2.2. Experimental section

2.2.1 Preparation of Graphene oxide

Graphene oxide was used as the precursor in the preparation of GQDs and CNOs. Modified Hummer’s method was used to prepare graphite oxide from graphite [1]. In this method, 2 g of graphite flakes and 1 g of sodium nitrate were thoroughly mixed and slowly added into 96 ml of conc. sulphuric acid taken in a 500 ml beaker, which was kept in an ice bath with continuous stirring. 6 g of $KMnO_4$ was added to this mixture, keeping the temperature of the ice bath below 20 °C. Removing the ice bath, the mixture was stirred for another 18 h at room temperature, followed by a very slow addition of 150 ml of distilled water, maintaining the temperature below 50 °C. The mixture was further diluted with 240 ml water, followed by adding 5 ml of 30% H_2O_2 and stirring was continued for another 2 h, followed by filtration and washing with 10% HCl, distilled water and acetone and then dried at 60 °C to obtain graphite oxide. The ultrasonication (6.5 L bath sonicator 200 W) of graphite oxide in water for 30 min produced a stable graphene oxide dispersion.

2.2.2. Preparation of Graphene quantum dots

2.2.2.1. Preparation of GQDs of sizes (10-20 nm) used in photocatalytic water splitting studies

Graphene oxide was used as the precursor for the synthesis of graphene quantum dots via hydrothermal method. Graphite oxide was prepared from graphite by Modified Hummer’s method as per the procedure detailed in 2.2.1.

0.2 g of as prepared graphite oxide was dissolved in 200 ml of distilled water and sonicated for 30 min (6.5 L bath sonicator 200 W) to obtain graphene oxide dispersion. Graphene quantum dots were prepared hydrothermally by treating 200 ml of graphene oxide with 20 ml of 30% hydrogen peroxide in a Teflon lined stainless steel autoclave kept in an oven at 180 °C for 1 h. The obtained stable aqueous dispersion of graphene quantum dots were stored at 4 °C for further use.

2.2.2.2. Preparation of GQDs of sizes (1-3 nm) used in biological studies

The synthesis of small sized (1- 3 nm) graphene quantum dots were achieved by increasing the reaction time of hydrothermal treatment.

Briefly, Graphite oxide was prepared from graphite powder using Modified Hummer's method as described in 2.2.1. The ultrasonication (6.5 L bath sonicator 200 W) of 0.2 g of as-synthesised graphite oxide in 200 ml of distilled water for 30 min resulted in graphene oxide dispersion. The hydrothermal treatment of obtained 200 ml of graphene oxide dispersion with 20 ml of 30% H_2O_2 was performed in a Teflon-lined stainless-steel autoclave, kept in an oven at 180 °C for 1.5 h. The obtained small sized GQDs were centrifuged at 10000 rpm for 20 min and stored at 4 °C for further use.

2.2.3. Preparation of nitrogen-doped graphene quantum dots (NGQDs)

Facile hydrothermal method was used for the preparation of nitrogen doped graphene quantum dots (NGQDs). Modified Hummer's method, detailed in 2.2.1, was used for the preparation of graphite oxide. From the prepared graphite oxide 0.6 g was dispersed in 600 ml of distilled water by ultrasonication for 30 min to obtain graphene oxide. N-GQD was prepared by the hydrothermal treatment of 600 ml graphene oxide dispersion with 60 ml of 30% hydrogen peroxide and 120 ml of ammonia, in a Teflon lined stainless steel autoclave kept in an oven at 180 °C for 12 h. The solution and solid part were separated. The solution containing N-GQDs was used for further studies.

In another method, mono-dispersed N-GQDs were synthesised from the oxidised debris attached to graphene oxide. In this method, N-GQDs were prepared via hydrothermal method of treating 600 ml of graphene oxide dispersion with 120 ml of ammonia, taken in a Teflon lined stainless steel autoclave and kept in an oven at 180 °C for 12 h. In the absence of hydrogen peroxide, during the hydrothermal treatment of graphene oxide in alkaline medium, the oxidised debris attached to graphene oxide was converted to crystalline small-sized N-GQDs. [2]

2.2.4. Preparation of titania

The sol-gel method was employed for the preparation of TiO_2. To a solution of 234.8 ml water and 2.2 ml nitric acid, 19.4 ml of titanium isopropoxide was added. The resulting mixture was stirred at around 1490 rpm for 24 h with a mechanical stirrer to obtain the sol and dried at 80 °C to obtain the gel. The obtained gel of titania was then calcined at 250 °C.

2.2.4.1 Preparation of TiO_2/GQD and TiO_2/N-GQD nanocomposites

To prepare these nanocomposites, a similar procedure was adapted. In a typical procedure, 19.4 ml of titanium isopropoxide was added to 234.8 ml water and 2.2 ml nitric acid solution, stirred at 1490 rpm for 24 h. To the obtained sol, a 10 ml of GQD/N-GQD solution was added, which was dried at 80 °C, and the obtained gel of TiO_2/GQD or TiO_2/N-GQD nanocomposite was calcined at 250 °C.

2.2.4.2 Preparation of P25 TiO_2/NGQD nanocomposites

The nanocomposites of P25 TiO_2/NGQD were synthesised by adding 10 ml of NGQDs, prepared from the oxidised debris attached to graphene oxide to 0.1 g commercial Degussa P25 TiO_2. Then, the reaction mixture was ultrasonicated for 2 h (6.5 L bath sonicator 200 W), dried and calcined at 250 °C.

2.2.5. Preparation of CNOs

Graphite oxide was prepared from graphite flake using the modified Hummer's method as detailed in 2.2.1.

0.6 g of obtained graphite oxide was dispersed in 600 ml distilled water, ultrasonicated for 2 h to obtain graphene oxide dispersion (GO). The as-prepared graphene oxide was hydrothermally treated with 30% hydrogen peroxide in two different reaction conditions.

In one method, the hydrothermal treatment of 500 ml of prepared graphene oxide dispersion with 30 ml of 30% hydrogen peroxide was carried out in a stainless-steel autoclave, kept in an oven at a temperature of 180 °C for 1 h. This resulted in a clear dispersion of spherical dense core CNOs and was stored at 4 °C.

In another procedure, 100 ml of prepared graphene oxide dispersion was hydrothermally treated with 10 ml of 30% hydrogen peroxide in a Teflon- lined stainless-steel autoclave, kept in an oven at 180 °C for just 30 min. The resulting clear solution of faceted hollow core CNOs was centrifuged at 10000 rpm for 20 min and stored at 4 °C for further studies.

2.2.6. Preparation of FGQDs

To 100 mg of fluorographite, 10 ml of sodium hydroxide solution (10 g NaOH dissolved in 90:10 ethanol-water mixture) was added, and the reaction mixture was refluxed at 100 °C for 24 h. The resulting black-coloured dispersion was centrifuged and washed with distilled water and ethanol. The material was finally dried in an oven at 60 °C. From the obtained product,10 mg was re-dispersed in 100 ml distilled water by ultrasonication for 3 h (1.5 L bath sonicator 100 W), resulted in hydroxy fluorographene (HFG) dispersion.

For the synthesis of fluorine rich graphene quantum dots (FGQDs), 80 ml of HFG dispersion was hydrothermally treated with 8 ml of 30% hydrogen peroxide in a 100 ml Teflon-lined stainless-steel autoclave and kept in an oven at 180 °C for 1 h. The obtained FGQDs were then centrifuged at 10000 rpm for 15 min and stored at 4 °C for further use.

2.3. Hydrogen production by photocatalytic water splitting

The photocatalytic water splitting experiments were carried out in a fabricated 316 stainless steel photoreactor with a sapphire window and a septum. The hydrogen production was evaluated using a gas chromatograph (GC-2010 Plus Shimadzu) equipped with a 5A molecular sieve column, using argon as career gas and a TCD detector. In a typical photocatalytic hydrogen production experiment, 20 mg of the photocatalyst was suspended in 50 ml of water containing 10 ml methanol as the sacrificial agent, taken in the photoreactor and kept under continuous magnetic stirring. The visible light from a 450 W high-pressure mercury lamp (placed 5 cm away from the photoreactor) was used to illuminate the chamber through the sapphire window. Degassing was made before irradiation by passing nitrogen gas into the reaction mixture before sealing. The experiment was performed for a total of 5 h period. At every 1 h interval, 1 ml of gaseous product formed within the photoreactor was taken out through the septum and injected into a gas chromatograph, thus, monitoring the amount of produced hydrogen.

2.4. Fluorescent sensing of metal ions

2.4.1. Detection of Fe^{2+} ions

Standard solutions of different metal ions (ferric chloride hexahydrate, ferrous sulphate, sodium hydroxide, manganese chloride, cobalt nitrate, calcium chloride, nickel nitrate, aluminium nitrate, cadmium sulphate, zinc acetate, potassium chloride, lead nitrate, mercuric chloride, magnesium sulphate, sodium chloride, silver nitrate.) were prepared, and the fluorescent sensing of metal ions by CNOs was performed at room temperature. To evaluate the selectivity, 200 µL of CNO solution was added to 2 mL of double distilled water taken in the cuvette. To this, 20 µL of prepared metal ion solution was added and incubated for 1 min, and each time, the corresponding PL spectrum was recorded at 330 nm excitation wavelength using FL 6500 Perkin Elmer fluorescence spectrofluorometer. To evaluate the sensitivity of CNO towards Fe^{2+}, different concentrations of Fe^{2+} were added to the aqueous solution of CNO, incubated and recorded the PL spectrum.

2.4.2. Detection of Fe^{3+} ions

In a typical assay, 200 µL of FGQDs dispersion was added to 2 mL of double distilled water in a cuvette. The fluorescence spectrum was recorded at room temperature at an excitation wavelength of 335 nm. The selectivity of FGQDs was confirmed by adding 20 µL of 0.01 M standard solutions of different metal ions (ferric chloride hexahydrate, ferrous sulphate, sodium hydroxide, manganese chloride, cobalt nitrate, calcium chloride, nickel nitrate, aluminium nitrate, cadmium sulphate, zinc acetate, potassium chloride, lead nitrate, mercuric chloride, magnesium sulphate, sodium chloride, silver nitrate) into the sensor system. After every 2 min of incubation, the PL spectrum was recorded in each case. For the sensitivity studies, ferric ions of varying concentrations ranging from 0 to 90 µM were added to the system. The fluorescence intensity changes were consequently measured at 335 nm excitation wavelength.

2.5. Biological applications

2.5.1. Cell culture

The cancer cells were maintained in Dulbecco’s modified eagles’ medium (DMEM) supplemented with 2 mM l-glutamine and balanced salt solution (BSS). The BSS was altered to contain 1.5 g/L Na_2CO_3, 0.1 mM nonessential amino acids, 1 mM sodium pyruvate, 2 mM l-glutamine, 1.5 g/L glucose, 10 mM (4-(2-hydroxyethyl)-1-piperazineethane sulfonic acid) (HEPES), and 10% foetal bovine serum in order to maintain the cancer cells. Streptomycin and penicillin (100 IU/100 g) were changed to 1 mL/L. The cells were kept in a humidified CO_2 incubator at 37 ℃ with 5% CO_2.

2.5.2. Evaluation of cytotoxicity (MTT Assay)

Through the use of MTT [3-(4,5-dimethylthiazol-2-yl)-2,5-diphenyltetrazolium bromide] assay, the inhibitory concentration (IC_{50}) value was calculated. In a 96-well plate with 100 µL of Dulbecco's modified eagles’ medium, cancer cells were cultured for 48 h to reach 75% confluence ($1x10^4$ cells/well). The medium was changed, and the cells were given 48 h of incubation in fresh medium of serially diluted as-synthesized GQDs/CNOs. Following the removal of the culture media, 100 µL of the MTT solution (3-(4,5-dimethylthiozol-2-yl)-3,5-diphenyltetrazolium bromide) was added to each well before being incubated for 4 hours at 37 °C. After the removal of supernatant 50 µL of DMSO was added to each well, which was then incubated for 10 min to solubilize the formazan crystals before the absorbance measurements were taken. The percentage of viability of cells were calculated from the optical density (OD) values using the following formula.

$$\%\ \text{of viability} = \frac{\text{OD value of experimental sample}}{\text{OD value of experimental control}} \times 100$$

2.5.3. Morphological analysis

MCF-7 cells grown in DMEM media were exposed to GQDs/CNOs at their IC_{25}, IC_{50}, and IC_{75} concentrations for 48 h before being fixed in a 3:1 combination of methanol and acetic acid. Inverted phase contrast microscopy was used to examine the cell morphology after the precipitated cells had been washed three times with PBS. To examine the nuclear morphology, cells washed with PBS were then stained with 1 mg/mL DAPI (4, 6-diamidino-2-phenylindole, dihydrochloride) for 20 min in the dark. Images of the stained objects were captured using a fluorescence microscope.

2.5.4 In vitro antioxidant assays

Using the DPPH radical (1,1-diphenyl-2-picryl hydrazyl radicals), hydroxyl radicals, and hydrogen peroxide, the *in vitro* antioxidant experiments can be conducted to assess the free radical scavenging capacity [3]–[5].

2.5.4.1. Hydrogen peroxide scavenging assay

By using the technique described by Shimada et al. [6], using a hydrogen peroxide solution, the hydrogen peroxide scavenging activity of GQDs at concentrations of 10–50 g/mL was calculated. In phosphate buffer, a solution of hydrogen peroxide (2 mmol/L) was created (pH 7.4). The hydrogen peroxide solution received the GQDs (10, 20, 3, 40, and 50 µg/mL) as an addition (0.6 mL). The blank was made up of phosphate buffer (3.3 mL) and GQDs. After 10 min, the hydrogen peroxide absorbance at 230 nm was measured in comparison to a blank solution made of phosphate buffer without hydrogen peroxide.

2.5.5. Cell incubation and Bio-imaging

DMEM supplemented with FBS (10%), antibiotic-antimycotic (1%), L-glutamine (2 mM), and non-essential amino acids (1%), in 5% CO_2 at 37 ºC, was used to sustain the cells. Cells were planted in 96-well plates at an initial cell density of 1×10^4 cells per mL prior to measurements. The mixture of a polybrene solution (8 mg mL^{-1}, 0.1 mL) and a concentrated aqueous GQDs solution (10x, 3.6 mg/mL-1, 0.9 mL) was then equilibrated at 37 ºC for 30 min. Each well received an aliquot (100 µL) of the GQDs and polybrene combination, which was then incubated for 24 h. The Trypan Blue exclusion method and the Alamar Blue method were then used to calculate the number of cells and viability of the cells in each well, respectively. Before being employed for bright field and PL imaging measurements with a fluorescent microscope (Nikon Eclipse, Inc., Japan) at 40X magnification, the precipitated cells were washed three times with PBS. The excitation wavelengths were set in the ranges of 510-590 nm, 460-480 nm, and 360-380 nm due to the limitations of the microscopic system.

2.6. Characterisation techniques

The prepared zero-dimensional nanomaterials are characterised using various techniques such as Transmission electron microscopy (TEM), Scanning electron microscopy (SEM), Fourier Transform Infrared (FTIR) spectroscopy, Raman spectroscopy, X-ray diffraction (XRD), X-ray photoelectron spectroscopy (XPS), Photoluminescence spectroscopy (PL), UV-Vis diffused reflectance spectroscopy (DRS), Zeta potential and Fluorescence decay (Lifetime measurement) analysis. A brief description on these analytical techniques is summarised in this section.

2.6.1. Transmission Electron microscopy (TEM)

TEM is an electron microscopic technique for determining the morphology, particle size and shape of the nanomaterials. In a TEM instrument, an accelerated high-energy electron beam passes through the ultra-thin sample and due to interaction with the atoms in the specimen, the electron beam may get transmitted or scattered. The transmitted beam of electrons is focussed and hits on the fluorescent screen to produce the image. The scattered beam of electrons from the same direction gives the selected area diffraction pattern, which provide information on crystalline/amorphous nature of the sample [7], [8]. The TEM images of the prepared zero-dimensional nanomaterials (GQDs, N-GQDs, CNOs, FGQDs) were obtained from JEOL/JEM 2100 TEM by drop casting an aqueous solution of the sample on the carbon-coated copper grid and mounting it on the sample probe.

2.6.2. Scanning electron microscopy (SEM)

SEM provides topographical and elemental information about the material with a large depth of field by scanning the specimen surface with a focussed beam of electrons in a raster pattern. The electron beam interaction across the sample surface generates secondary electrons, backscattered electrons and characteristic X-rays, which are collected by the detectors to form the images. The secondary signal originating from the sample surface provides the topographical information, while the imaging of backscattered electrons originating from the bulk provides spatial distribution of elements [9], [10]. SEM images of the samples prepared were obtained on a ZEISS Gemini SEM 300 with EDAX model Octane Plus instrument.

2.6.3. FTIR (Fourier Transform Infra-Red) Spectroscopy

FTIR spectroscopy is a powerful analytical tool concerned with the vibration of the molecule and is used for the chemical identification of the material. When IR radiation passes through the sample, certain specific frequency radiation is absorbed, and rest is transmitted. The interaction of IR radiation causes a change in the dipole moment of the molecule corresponding to the vibrational energy [11].

In this investigation, the surface oxygen group functionalisation in GQDs and CNOs, the presence of covalent and semi-ionic C-F bonds in FGQDs, N-doping in N-GQDs and also the formation of TiO_2/N-GQDs are confirmed by FTIR analysis. FTIR measurements were carried out using a Perkin Elmer Spectrum two L1600300 Fourier Transformation Infra-Red (FTIR) spectrophotometer in the range 4000 cm^{-1} to 400 cm^{-1}.

2.6.4. Raman spectroscopy

Raman spectroscopy is a non-destructive, vibrational spectroscopic technique that relies on light's inelastic scattering. When the sample is irradiated with a laser beam, scattering occurs, and most of the scattered light has the same frequency (Rayleigh scattering), while some photons are scattered with a frequency higher (Stokes line) or lower (anti-Stokes) than incident photons because of the absorption by the vibrating molecules. The energy absorbed will be equivalent to the vibrational energies of the molecules present in the sample and the technique is called Raman spectroscopy [12]. Information regarding the material's molecular structure and surface characteristics are obtained from Raman spectroscopy. In this work, the surface defects in the prepared zero-dimensional nanomaterials are confirmed by Raman spectroscopy which was recorded using WITec alpha control 300RA with a 532 nm Argon laser.

2.6.5. X-ray diffraction (XRD)

XRD is a powerful technique for the qualitative and quantitative determination of crystalline material. XRD analyses reveal crystal size, crystal purity, crystal structure and phase identification information. In this work, Rigaku MiniFlex 600 diffractometer with 2θ from 0 to 90° and CuKα of $\lambda = 0.154$ nm as a radiation source was used for the XRD analyses of TiO_2/NGQD and P25TiO_2/NGQD nanocomposite.

X-ray diffraction is based on the constructive interference of monochromatic X-rays and the atomic planes of the crystal, which is obtained from Bragg's equation, $n\lambda=2d\sin\theta$ where λ is the wavelength of X-ray used, n is the order, d is the atomic plane spacing, and θ is the diffraction angle [13].

2.6.6. X-ray photoelectron spectroscopy (XPS)

XPS, or electron spectroscopy for chemical analysis, is a surface-sensitive technique used to measure the elemental composition and its chemical state by measuring the binding energy. X-ray photoelectron spectra are recorded using (Kratos Analytical) monochromated Al-Kα (1486.6 eV) radiations (15 kV; 250 W, λ=1.5418).

XPS is based on the photoelectric effect. When a sample is irradiated with a beam of x-rays, electrons are ejected, and the kinetic energies of these ejected electrons are measured, from which the binding energy of the core electron can be calculated using $E_{B.E}= E_{photon} - (E_{k.E} + \varphi)$. From the binding energy and peak intensity, identification and quantification of surface elements are possible [14] .

2.6.7. Ultraviolet-Visible absorption spectroscopy.

UV -Visible spectroscopy is an absorption analytical technique used to determine the optical properties of materials. In UV-Visible spectroscopy, when a sample is irradiated with UV-Visible light (200-800 nm), absorption occurs if the incident light energy is equal to the energy difference between the ground and excited electronic energy states of the molecule. The absorption of UV-Visible light by molecules containing π and non-bonding electrons results in the excitation of electrons to higher anti-bonding orbitals, while in semiconductor materials, the electronic transition occurs from the valence band to the conduction band. The UV-Vis DRS spectra provide both an indication of absorption of UV-Vis light by semiconductor and a method for evaluating the band gap energy using the Kubelka-Munk plot [15]. The UV-Visible DRS measurement of prepared titania-based photocatalysts was carried out using a Varian, Cary 5000 instrument with a spectral range of 175 – 3300 nm.

2.6.8. Fluorescence spectroscopy

Fluorescence or photoluminescence spectroscopy is a light emission spectroscopic technique which analyses the fluorescence properties exhibited by a fluorescent material. In this work, the quantum dots and CNOs investigated exhibited strong fluorescence. Their fluorescent properties are thoroughly analysed using FL 6500 Perkin Elmer fluorescence spectrofluorometer.

The basic principle of fluorescence spectroscopy is the processes called photo-excitation and subsequent emission. When a monochromatic light source is directed through a sample, the photons cause the excitation of the molecule to a singlet excited state. When the excited molecule returns to its ground state, it emits photons of lower energy, (in the form of visible light) than the absorbed photon, resulting in fluorescence [16].

2.6.9. Lifetime (Fluorescence decay) measurement

Lifetime measurement is a decisive method to distinguish between static and dynamic fluorescence quenching. The fluorescence lifetime of FGQDs was monitored using a Horiba Fluorolog fluorescence spectrometer with TCSPC at an excitation wavelength of 330 nm.

Fluorescence lifetime is the average time a fluorophore stays in an excited state before returning to the ground state via photon emission. Fluorescence lifetime is an intrinsic property of a fluorophore and typically ranges from 10^{-9} to 10^{-7} s. Both radiative and non-radiative transitions are included in the decaying process. Hence lifetime τ is the time taken for the number of excited molecules to decay to 1/e of the original population via fluorescence or non-radiative processes. Time-correlated single photon counting (TCSPC) enables quantitative photon counting since, after an exciting pulse, the probability of a single photon detection will be proportional to the fluorescence intensity at that time [17].

2.6.10. Quantum yield measurements

The fluorescence quantum yield of the prepared FGQDs was determined with quinine sulfate as the standard. The calculation was carried out according to the following equation.

$$\mathbf{Q = Q_{ref}\ (\eta^2/\eta^2_{ref})(\ I/\ I_{ref}\ )(A_{ref}/\ A)}$$

Where, η = Refractive Index of the solvent used, η = 1.33 for water, η_{ref} = 1.33 for 0.1 M H_2SO_4 solution, Q_{ref} = 0.54 (Quantum yield of quinine sulfate), I = Integrated fluorescence intensity of the sample, I_{ref} = Integrate fluorescence intensity of the reference, A = Absorbance at the excitation wavelength of the sample, A_{ref} = Absorbance at the excitation wavelength of the reference [16]

2.6.11. Zeta potential analyser

Zeta potential is the characterisation technique used to determine the surface charge of nanoparticles to have an idea about the stability of the dispersion. A high positive or negative value (-30 mV to 30 mV) of the Zeta potential of nanocrystals indicates good stability of nanosuspensions, and in this work, Zeta potential measurements are made using Horiba SZ-100 instrument. The solution of charged particles is surrounded by a thin layer of oppositely charged ions called the Stern layer and a diffused layer of loosely attached ions. Due to the movement of these layers, a boundary is formed, and the electrostatic potential at the interfacial double layer is referred as zeta potential [18].

References

[1] W. S. Jr. Hummers and R. E. Offeman, "Preparation of Graphitic Oxide," *J. Am. Chem. Soc.*, vol. 80, no. 6, pp. 1339–1339, Mar. 1958, doi: 10.1021/ja01539a017.

[2] C. Hu, Y. Liu, Y. Yang, J. Cui, Z. Huang, Y. Wang, L. Yang, H. Wang, Y. Xiao, J. Rong, "One-step preparation of nitrogen-doped graphenequantum dots from oxidized debris of graphene oxide," *J Mater Chem B,* vol. 1, no. 1, pp. 39–42, 2013, doi: 10.1039/C2TB00189F.

[3] "Antioxidant Determinations by the Use of a Stable Free Radical | Nature." https://www.nature.com/articles/1811199a0 (accessed Dec. 14, 2022).

[4] "Hydroxyl Radical-scavenging Effects of Spices and Scavengers from Brown Mustard (Brassica nigra): Bioscience, Biotechnology, and Biochemistry: Vol 61, No 1." https://www.tandfonline.com/doi/abs/10.1271/bbb.61.118 (accessed Dec. 14, 2022).

[5] N. Benkeblia, "Free-radical scavenging capacity and antioxidant properties of some selected onions (Allium cepa L.) and garlic (Allium sativum L.) extracts," *Braz. Arch. Biol. Technol.*, vol. 48, no. 5, pp. 753–759, Sep. 2005, doi: 10.1590/S1516-89132005000600011.

[6] Kazuko. Shimada, Kuniko. Fujikawa, Keiko. Yahara, and Takashi. Nakamura, "Antioxidative properties of xanthan on the autoxidation of soybean oil in cyclodextrin emulsion," *J. Agric. Food Chem.*, vol. 40, no. 6, pp. 945–948, Jun. 1992, doi: 10.1021/jf00018a005.

[7] D. B. Williams and C. B. Carter, *Transmission Electron Microscopy: A Textbook for Materials Science*, 2nd edition. New York: Springer, 2009.

[8] "Transmission Electron Microscopy - an overview | ScienceDirect Topics." https://www.sciencedirect.com/topics/physics-and-astronomy/transmission-electron-microscopy (accessed Dec. 14, 2022).

[9] “Scanning Electron Microscopy (SEM),” *Techniques*. https://serc.carleton.edu/research_education/geochemsheets/techniques/SEM.html (accessed Dec. 14, 2022).

[10] “A Beginners’ Guide to Scanning Electron Microscopy | SpringerLink.” https://link.springer.com/book/10.1007/978-3-319-98482-7 (accessed Dec. 14, 2022).

[11] “FTIR Spectroscopy (Overview),” *JASCO Inc*. https://jascoinc.com/learning-center/theory/spectroscopy/fundamentals-ftir-spectroscopy/ (accessed Dec. 14, 2022).

[12] “Principles of Raman spectroscopy (1) What is Raman spectroscopy? | JASCO Global.” https://www.jasco-global.com/principle/1-what-is-raman-spectroscopy/ (accessed Dec. 14, 2022).

[13] “Fundamentals of analytical chemistry (Skoog, Douglas A.; West, Donald M.) | Journal of Chemical Education.” https://pubs.acs.org/doi/10.1021/ed040p614.2 (accessed Dec. 14, 2022).

[14] “X-Ray Photoelectron Spectroscopy - IN.” https://www.thermofisher.com/in/en/home/materials-science/xps-technology.html (accessed Dec. 14, 2022).

[15] H.-H. Perkampus, *UV-VIS Spectroscopy and Its Applications*. Berlin, Heidelberg: Springer, 1992. doi: 10.1007/978-3-642-77477-5.

[16] J. R. Lakowicz, *Principles of Fluorescence Spectroscopy*, 3rd ed. 2006. Corr. 5th printing 2010 edition. New York: Springer, 2010.

[17] “Chapter 5 Optical transducers: Optical molecular sensing and spectroscopy - Dimensions.” https://app.dimensions.ai/details/publication/pub.1111370931 (accessed Dec. 14, 2022).

[18] E. Joseph and G. Singhvi, “Chapter 4 - Multifunctional nanocrystals for cancer therapy: a potential nanocarrier,” in *Nanomaterials for Drug Delivery and Therapy*, A. M. Grumezescu, Ed. William Andrew Publishing, 2019, pp. 91–116. doi: 10.1016/B978-0-12-816505-8.00007-2.

CHAPTER 3

PHOTOCATALYTIC WATER SPLITTING USING TiO_2-NGQD NANOCOMPOSITES

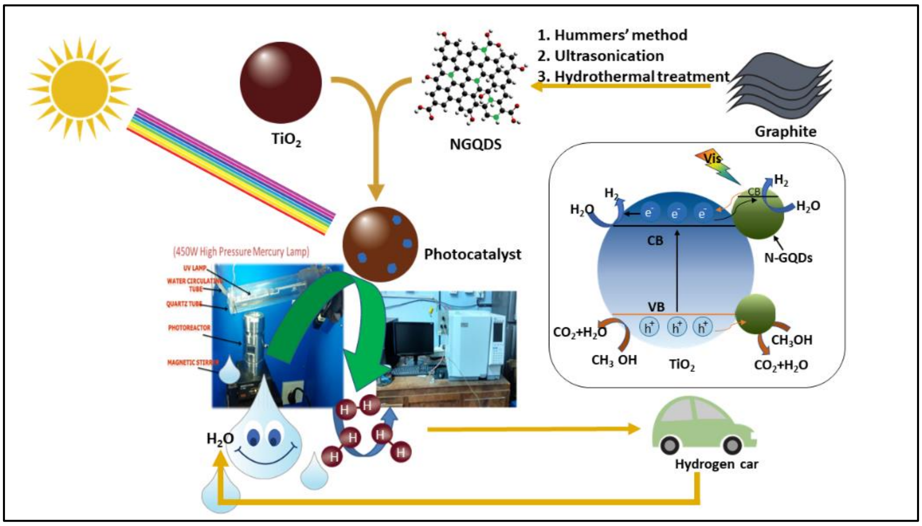

3.1 Introduction

As a part of the universal urge for renewable and clean energy, the conversion of solar energy into “solar fuels” is an area where there has been a considerable research focus in recent years. Hydrogen is considered a highly efficient clean solar fuel [1]. Among the various methods currently in use for splitting of water using solar energy for hydrogen generation, much attention has been focused on photocatalytic reactions because they are cost-effective, simple, sustainable and convenient. TiO_2 is the most investigated photocatalyst mainly because of its high efficiency, low cost, non-toxicity, and photostability [2]–[4]. The fast recombination of photogenerated electrons and holes and the large bandgap (3.2 eV) of TiO_2 are the major challenges in TiO_2 photocatalysis [5], [6]. Various strategies have been adopted to overcome its limitations, such as doping with noble metals [7], [8] and sensitizing with organic dyes [9], [10]. The combination of TiO_2 with metal-free carbon materials has attracted special attention since it could efficiently enhance photocatalytic activity due to their superior charge transport properties and thereby reduce the recombination rate of photogenerated charge carriers [11]–[14].

Graphene quantum dots (GQDs), nanometer-sized graphene fragments, have attracted considerable interest recently, mainly because of their high water-solubility, better chemical stability, low toxicity, excellent biocompatibility and unique photoelectrical properties. GQDs are also known to exhibit band gap tunability based on their size and can be an efficient photosensitizer [7]. The elemental doping of GQDs can further enhance the performance of TiO_2

photocatalysts by improving their visible light harvesting capability [8]. Nitrogen-doped graphene quantum dots (NGQDs) have received considerable attention due to their ready manipulation of the electronic structure compared to pristine GQDs, which may be exploited for diverse applications. N-doping in GQDs creates less interfacial resistance and improves band alignment, significantly improving its sensitizer properties.

There are several reports for using doped and undoped GQDs/ TiO_2 nanocomposites for photocatalytic water splitting. The TiO_2/GQDs hybrid system with intimate interface developed by Jia et al. displayed excellent photocatalytic water splitting under infrared light due to efficient transfer of photo-generated electrons from GQDs to TiO_2 [15]. According to Xao et al., GQDs can act as an electron reservoir as well as a photosensitizer for the efficient photocatalytic hydrogen evolution in GQDs/ TiO_2 hybrid prepared via in-situ photo-assisted strategy [16]. Sui et al. reported that CQDs/ TiO_2 nanosheets with majority of (001) facets showed photocatalytic activity due to synergetic effect of TiO_2-001 and CQDs [17]. The carbon nitrogen quantum dots developed by Chen et al. act as a co-catalyst and enhance the photocatalytic hydrogen productivity of TiO_2 nanofibres [18]. Xie et al. reported that S, N co-doped GQDs/TiO_2 nanocomposite, prepared via hydrothermal method exhibited excellent photocatalytic hydrogen generation with extended light absorption range [19]. According to Shi et al., controlled nitrogen doping enhanced the photocatalytic hydrogen evolution of NCDs/ P25 TiO_2 hybrid system under both UV and visible illumination [20].

In the present chapter, we prepared sol-gel TiO_2, GQDs by an oxidative etching process of nanosheets of graphene oxide (GO) employing hydrogen peroxide and their nanocomposite with the prepared sol-gel titania (TiO_2-GQDs), nitrogen doped GQDs (NGQDs) as well as their nanocomposites with sol-gel titania (TiO_2-NGQDs), NGQDs from oxidised debris attached to GO without the use of hydrogen peroxide in the hydrothermal treatment and their nanocomposites (P25TiO_2-NGQDs) with commercial Degussa P25 titania (P25TiO_2). The effect of GQDs/NGQDs on the photocatalytic performance of TiO_2 was studied by comparing its performance with that of the bare titania prepared. The performance of the prepared photocatalytic systems was evaluated using the hydrogen generation via photocatalytic water-splitting reaction.

3.2 Experimental methods

The chemicals used and the procedure adopted for the synthesis of GQDs, NGQDs, sol gel TiO_2 and the composites of TiO_2 are detailed in chapter 2.

The synthesis of graphene oxide using Modified Hummer's method are detailed in 2.2.1. Graphene quantum dots was prepared by the hydrothermal oxidative cleavage of graphene oxide in presence of hydrogen peroxide which is detailed in 2.2.2.1. NGQDs are prepared by the hydrothermal treatment of graphene oxide dispersion with ammonia and hydrogen peroxide, discussed in 2.2.3. The sol-gel method of titania synthesis is discussed in 2.2.4. The in-situ sol-gel synthesis of TiO_2/GQDs and TiO_2/NGQDs are explained in 2.2.4.1. Mono-dispersed NGQDs prepared from oxidised debris are discussed in 2.2.3. and the preparation of its composite (P25 TiO_2/NGQDs) with P25 TiO_2 using ultrasonication method is discussed in 2.2.4.2.

3.3 Results and Discussion

3.3.1 TEM analysis

The morphology of the prepared graphene oxide was examined using high-resolution transmission electron microscopy. The HR TEM images obtained are presented in figure 3.3.1.(i). Figure 3.3.1(i) (a) shows thin exfoliated graphene oxide nanosheets which indicate good exfoliation of crystalline graphite oxide by means of ultrasonication. Figure 3.3.1(i) (b) is its corresponding selected area electron diffraction (SAED) pattern pointing towards slight turbostratic nature of the graphene layers present. The TEM images of GQDs reveal that the formed GQDs are of 10 to 20 nm size range and found to be quite crystalline, as evident from the SAED pattern. The SAED pattern of crystalline graphene quantum dots can be indexed to lattice spacings of 0.32 nm and 0.21 nm, corresponding to (002) and (100) planes of graphene respectively, consistent with the reported values [21], [22]. The morphological properties of the TiO_2-GQDs nanocomposites prepared were also investigated by analysing the lattice fringes present in the HR-TEM image, which also reveals their crystalline nature with lattice spacing of 0.35 nm, 0.28 nm and 0.32 nm, indicating the (101) and (004) planes of anatase TiO_2 and (002) of graphitic plane respectively. The SAED pattern obtained also was in consistent with this observation.[14]

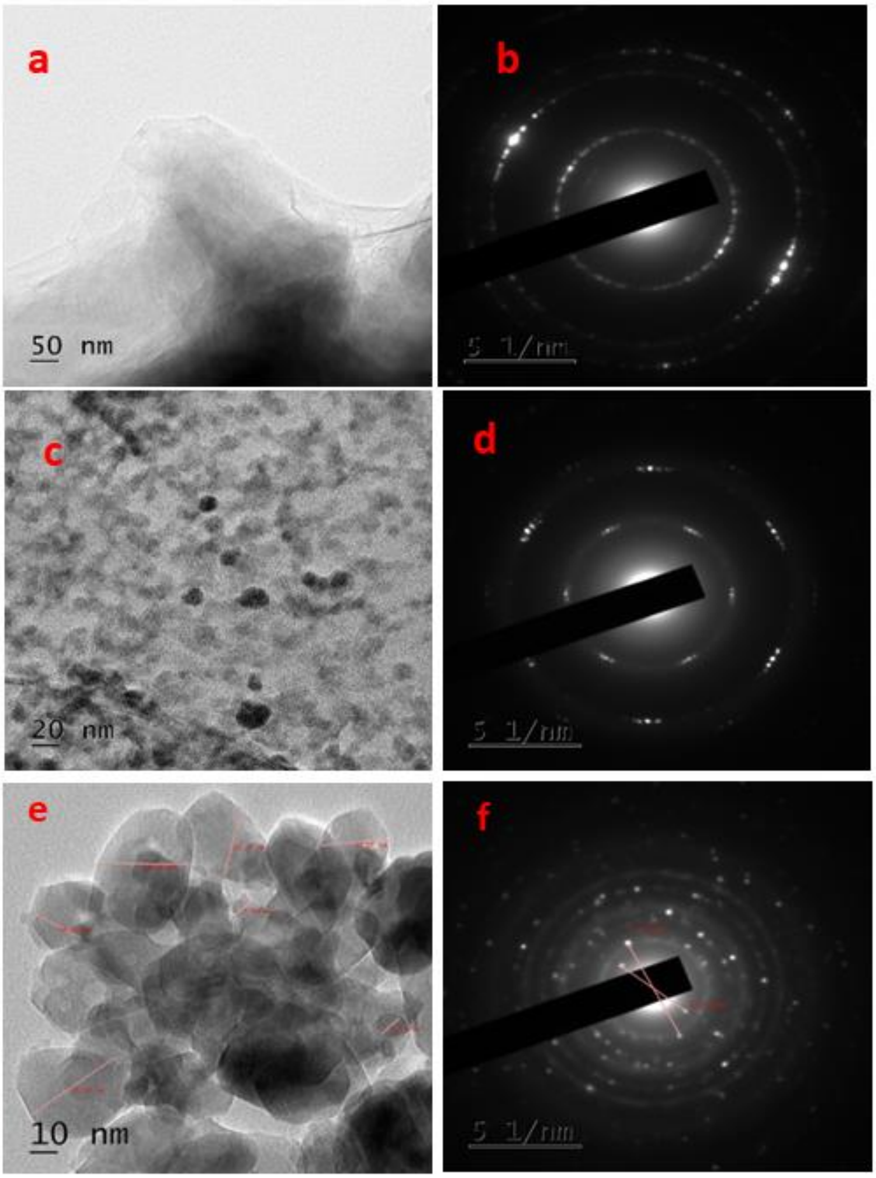

Figure 3.3.1(ⅰ): **(a, c & e)** TEM images of GO, GQDs, TiO_2-GQDs nanocomposite and **(b, d & f)** their corresponding SAED patterns.

Figure 3.3.1(ii) (a) & (b) show the high-resolution TEM images and the size distributions of NGQDs. It is found that NGQDs are in the size range of 10-20 nm in size and of irregular shapes. As a result of H_2O_2 etching, a cleavage of the GO sheet into small fragments have occurred, as evident by the TEM analysis. In Figure 3.3.1(ii) (b), the lattice fringes are clearly visible with a lattice spacing of 0.24 nm, consistent with the in-plane lattice constant of graphite. The SAED pattern shows the crystalline nature of the NGQDs (Figure 3.3.1(ii) (c) and the diffraction patterns corresponding to (100) and (002) planes of graphene are observed.

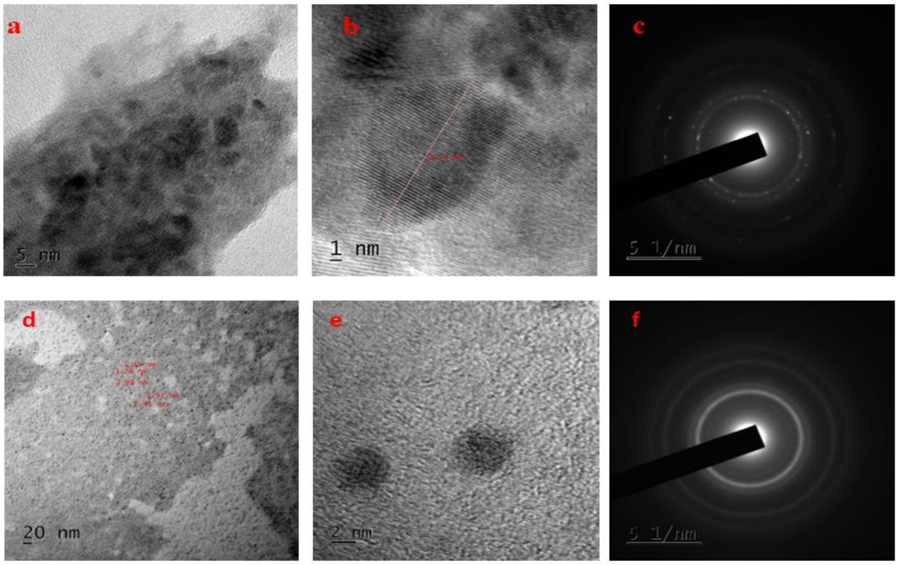

Figure 3.3.1. (ii): TEM images of (a, b) NGQDs prepared using NH_3 and H_2O_2, **(c)** corresponding SAED pattern, **(d, e)** NGQDs obtained from oxidised debris and **(f)** the corresponding SAED pattern.

For the NGQDs prepared without using H_2O_2, the quantum dots obtained are much smaller, in the size range 1-5 nm, as observed from the high-resolution TEM micrographs presented in Figure 3.3.2. (ii) (d) & (e). In a similar study by Hu et. al., the authors suggested that NGQDs might have originated by the detachment of amorphous oxidation debris adsorbed to GO sheets in the presence of NH_3, which eventually get converted to crystalline NGQDs in hydrothermal conditions. In our study as well, the origin of the NGQDs must be from the attached oxidation debris because no oxidative cleaving agent like H_2O_2 was used here [23].

3.3.2 PL spectral analysis

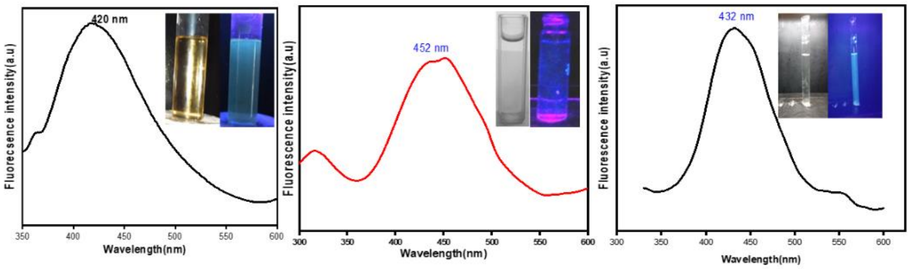

Figure 3.3.2: **(a)** Emission spectrum of GQDs showing a λ_{max} at 420 nm when excited at 325 nm (inset shows the photograph of GQDs illuminated with visible light and with UV light) **(b)** Emission spectrum of NGQDs showing a λ_{max} at 452 nm when excited 365 nm (inset shows the photograph of NGQDs with visible light and UV light illumination) **(c)** Emission spectrum of NGQDs obtained from oxidized debris showing a λ_{max} at 432 nm when excited with 365 nm radiation (inset shows the photograph of NGQDs with visible light and UV light illumination).

One of the most fascinating features of GQDs is their photoluminescence, and depending on size, and functionalisation, GQDs exhibit different PL colors. It is assumed that the factors such as quantum confinement effect, emissive traps, free zigzag sites and edge defects intensively contribute to the origin of fluorescence, Even now, the exact mechanism for the PL of GQDs are not yet fully understood [24]–[26]. The PL might have originated from intrinsic state emission (induced by either quantum size effect, recombination of localized electron–hole pairs or edge effects) as well as defect state emission (arises from energy traps). In several studies, authors have pointed out that doping with heteroatoms enhance the fluorescence emission of GQDs due to modulation of its electronic structure [27]-[29]. In nitrogen doped GQDs, the fluorescence is thought to be dominated by the n to π^* transition between N atom and the core graphitic structure. Figure 3.3.2 depicts the emission peaks of GQDs and NGQDs obtained from oxidative cutting and from oxidized debris. GQDs exhibited a strong bluish green fluorescence with an emission maximum at 420 nm when excited with 325 nm. NGQDs prepared via oxidative cutting showed an emission spectrum with a λ_{max} at 452 nm when excited at 365 nm and NGQDs obtained from oxidised debris exhibited strong fluoresecence with a emission maximum at 432 nm on excitation with 365 nm.

3.3.3 XRD analysis

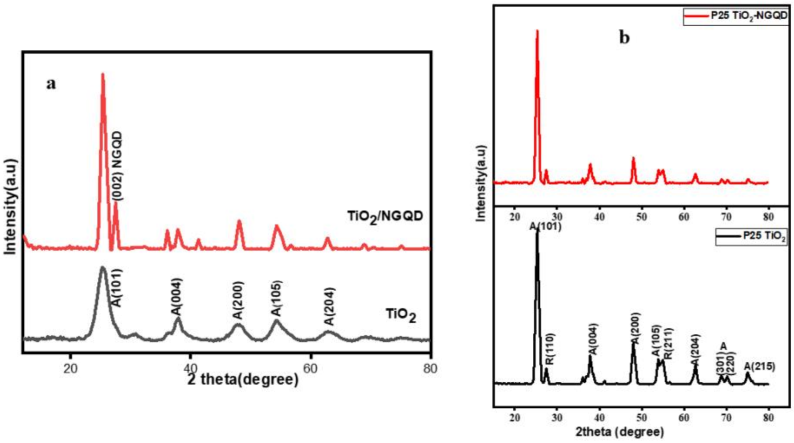

Figure 3.3.3: XRD patterns of **(a)** TiO_2 &TiO_2-NGQDs **(b)** P25 TiO_2 & P25TiO_2-NGQDs

Figure 3.3.3 shows the XRD pattern of the photocatalysts investigated (TiO_2 &TiO_2-NGQDs and P25 TiO_2 & P25TiO_2-NGQDs). In both TiO_2 &TiO_2-NGQDs, anatase phase of TiO_2 is found to be the major component. Titania prepared by sol-gel method shows the diffraction peaks at 25.2°, 36.1°, 37.8°, 48.1°, 54.2°, 62.7°, 68.9°, 75.3° corresponding to (101), (101), (004), (200), (105), (204), (301), (215) planes respectively [30] as shown in figure 3.3.3 (a). In the XRD pattern of TiO_2-NGQDs nanocomposite, the peaks are much sharper indicating the attainment of much more crystallinity and a small graphene peak corresponding to the (002) plane is visible in between the characteristic peaks of anatase. The diffraction peak of P25 titania is centered at 25.2° (101), 27.4° (110), 37.7° (004), 48.1° (200), 53.9° (105), 56° (211), 62.6° (204), 68.8° (301), 70.2° (220), 75.6° (215) and no peak corresponding to the graphitic plane is visible in this nanocomposite (figure 3.3.3 (b)). Thus, the XRD analysis of the as-synthesised nanocomposites have revealed that the modification of TiO_2 using NGQDs has, by and large, not altered the crystal structure and phase morphology of TiO_2.

3.3.4 FTIR spectral analysis

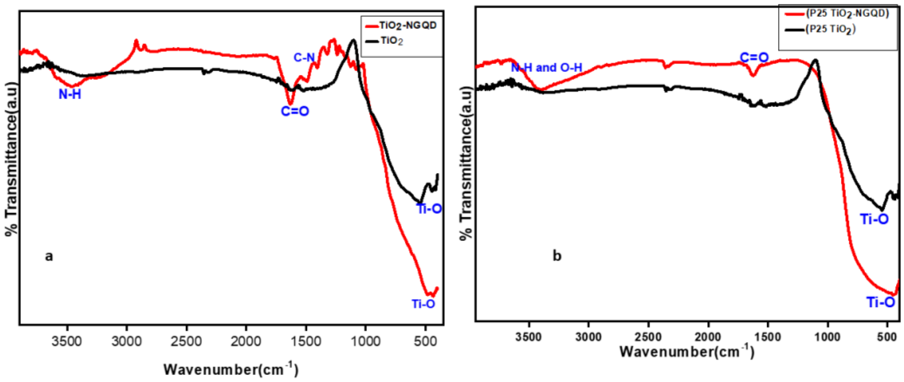

Figure 3.3.4: FTIR spectra of **(a)** TiO_2 &TiO_2-NGQDs **(b)**P25 TiO_2 & P25TiO_2-NGQDs

FTIR spectra of the sol-gel TiO_2 & its nanocomposite TiO_2-NGQDs and the commercial P25TiO_2 & its nanocomposite P25TiO_2-NGQDs are presented in Figure 3.3.4. The broad IR absorption band present in all the spectra in the region of 450-800 cm^{-1} can be attributed to Ti-O stretching vibrations [30]. In bare titania, this band is centred around 500-800 which after the nanocomposite formation, is red shifted to 450-800 cm^{-1}. This points to the fact that the composite formation involved the adsorption of NGQDs on the surface of TiO_2 or P25 TiO_2 and no evidence of Ti-C chemical bond is found in the spectra of the nanocomposites. It is reported that an improved visible light absorption of TiO_2-GQDs composite is enabled by the formation of Ti-O-C bond [31]. As shown in figure 3.3.4 (a), N-H and O-H stretching (broad band at 3100-3500 cm^{-1}), C=O stretching (1635 cm^{-1}), C-N bending (1330 cm^{-1}), C-O bending (1236 cm^{-1}), vibrational frequencies are visible in the FTIR analysis which confirm the incorporation of N-GQDs with sol -gel TiO_2 [20], [32]. The formation of P25TiO_2-NGQDs nanocomposite revealed by the presence of Ti-O (broad band from 450-800 cm^{-1}), C=O stretching (1621cm^{-1}), O-H and N-H stretching (broad band at 3200-3500 cm^{-1}), as presented in figure 3.3.4 (b) [23], [33].

3.3.5 UV-Visible diffuse reflectance spectroscopy

From UV-visible diffuse reflectance spectral measurements, it can be observed that the band gaps of titania had been modified for the prepared nanocomposite samples. In figure 3.3.5 (a), the absorption edge of TiO_2-NGQD is red shifted to the visible region compared to bare titania, making it more suitable for visible light harvesting [32], [34].

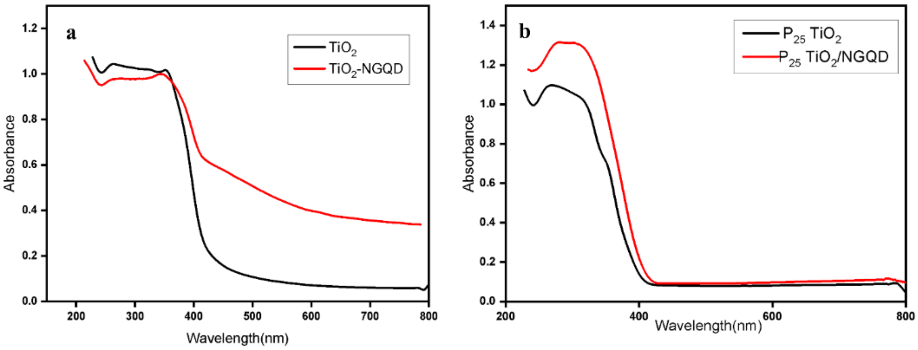

Figure 3.3.5: UV-DRS spectra of (a) TiO_2 &TiO_2-NGQDs (b) P25 TiO_2 & P25TiO_2-NGQDs

3.3.6 Kubelka- Munk plot

The optical band gaps were calculated using Kubelka-Munk plots. In figure 3.3.6 (a) & (b), the plots of Kubelka-Munk function with light energy are presented. The band gap obtained for sol-gel TiO_2 and TiO_2-NGQDs composite were 2.52 eV, and 2.8 eV respectively. Thus, the better photocatalytic performance of the TiO_2-NGQDs nanocomposite catalyst in visible light assisted photocatalytic water splitting can be attributed to the decrease in the band gap as a result of nitrogen doping as well as the improved photosensitization by NGQDs.

The UV-Visible spectra of P25TiO_2 and P25TiO_2-NGQD are presented in figure 3.3.5 (b). As shown, the band gap of P25TiO_2 calculated from Kubelka-Munk plot was 3.2 eV and the composite P25TiO_2-NGQD shows a decrease in the band gap to a value of 3.04 eV in the Kubelka–Munk plot. This substantial improvement in band gap reduction enhances the photocatalytic performance of the composite.

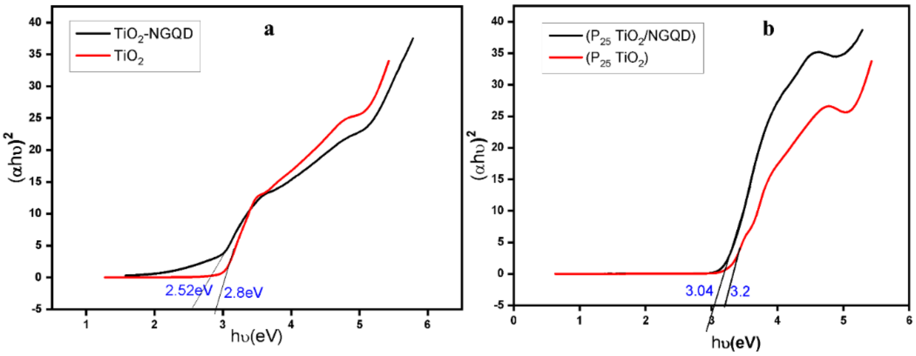

Figure 3.3.6: Kubelka –Munk plots for (a) TiO_2 & TiO_2 -NGQDs (b) P25 TiO_2 & P25TiO_2 -NGQDs

3.3.7 PL spectral analysis

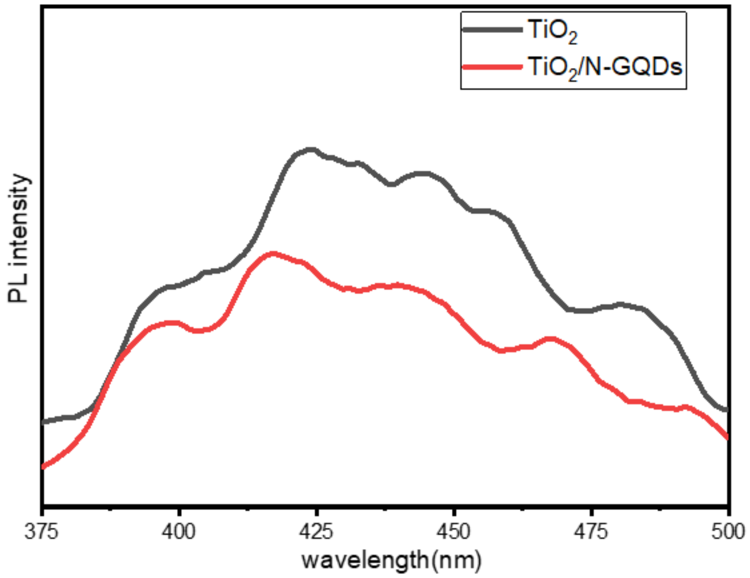

Figure 3.3.7: Photoluminescence spectra of TiO_2 and TiO_2-NGQDs

The PL spectra of TiO_2 and TiO_2-NGQDs are presented in figure 3.3.7. The electron hole recombination is the main factor that contributes to PL intensity which is found to be reduced in TiO_2-NGQDs composite compared to bare titania. Thus, in addition to the role as a photosensitizer, NGQDs can also act as an electron transfer reagent by the injection of electron from NGQDs to TiO_2 and the drainage of hole from the TiO_2 to NGQDs. Thus an efficient electron-hole separation is achieved due to the formation of Ti-O-C bond [16], [31].

3.3.8 Photocatalytic water splitting studies

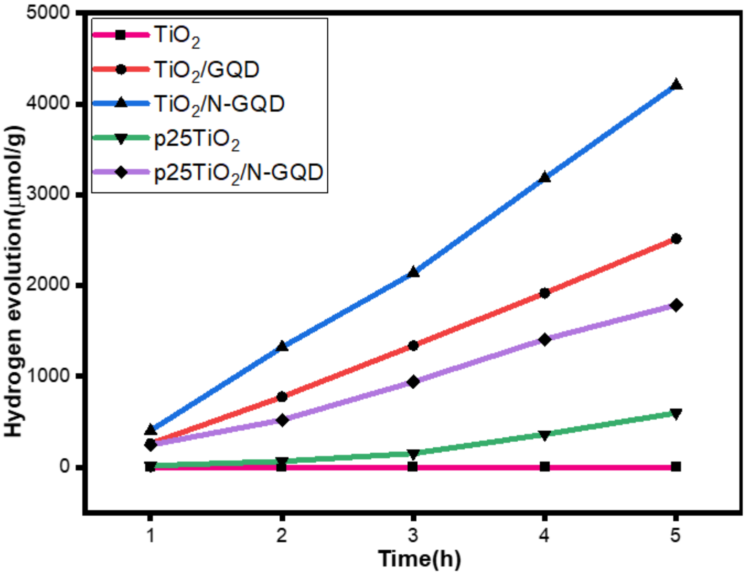

Figure 3.3.8.1: Comparison of Hydrogen evolution

The hydrogen production via water splitting was carried out with the prepared photocatalyst in a fabricated photoreactor using 450 W high pressure mercury lamp as the radiation source and methanol as a sacrificial agent. The plots of the photocatalytic hydrogen production against time are provided in Figure 3.3.8.1. In all samples studied except in the case of sol-gel TiO_2, it was observed that hydrogen production kept on increasing with increase in irradiation time. The initial hydrogen production rate was found to be slow in all the cases. When the nanocomposites were used as photocatalysts, an increase in the rate could be observed. Among the prepared samples, the composites of sol-gel TiO_2 was found to exhibit better performance than P25TiO_2 based nanocomposite. When compared to TiO_2-GQDs, hydrogen production was found to be higher for TiO_2-NGQDs.

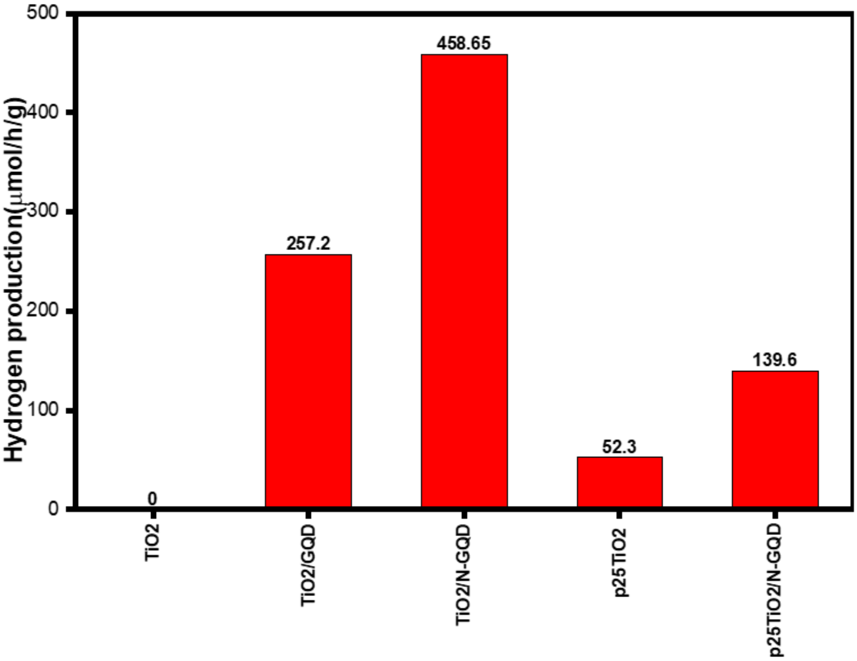

Figure 3.3.8.2: Comparison of maximum rate of hydrogen evolution using prepared photocatalyst

Figure 3.3.8.2. presents the maximum rate of hydrogen production observed with the prepared photocatalysts. A comparison of investigations on TiO_2-GQDs nanocomposites employed for photocatalytic water-splitting from the existing literature are presented in Table 1 and it can be observed that the developed nanocomposites exhibit excellent performance as visible light photocatalysts in the hydrogen generation by photocatalytic water splitting.

The increase in maximum rate of hydrogen generation by TiO_2-GQDs and TiO_2-NGQDs can be explained on the basis of band gap narrowing mechanism. According to Wang et al. [31], besides the formation of Ti-O-C bond, the band gap narrowing can also significantly improve the visible light harvesting of TiO_2-GQD composite. In GQDs sensitized TiO_2 photocatalyst, the formation of Ti-O-C bond introduces additional energy states between the conduction band and valence band of TiO_2 and GQDs and the position of these energy states are highly quantum confined. Hence larger the size of GQDs, narrow will be the band gap of the composite and hence absorption edge could be extended more to the visible region [16], [31], [35]. In our work, NGQDs and GQDs prepared via oxidative cutting were larger in size compared to NGQDs prepared from oxidized debris. Hence the enhanced hydrogen production in TiO_2-NGQDs nanocomposite may be attributed to nitrogen doping and narrow band gap mechanism.

Table 1: Rate of hydrogen production by different titania and graphene quantum dot based photocatalysts.

Photocatalyst	**H_2 generation rate**	**Reference**
TiO_2/ GQD	60.4 µmol/h/g	[15]
GQDs/{001}TiO_2	79.3 µmol/h/g	[36]
CNQDs/TiO_2 NF	112.4 µmol/h/g	[18]
S,N-GQD/P25	5.7 µmol/h	[19]
TiO_2/NGQD	458.6 µmol/h/g	This work

3.4 Conclusions

In summary, GQDs and two different types of Nitrogen-doped GQDs were prepared following hydrothermal strategies and were successfully loaded onto TiO_2 photocatalysts in two different methods. The performance of the TiO_2-GQDs, TiO_2-NGQDs and P25TiO_2-NGQDs hybrid catalysts were evaluated using hydrogen generation via photocatalytic water-splitting and compared with that of pristine titania photocatalysts. The NGQD-sensitized TiO_2 photocatalysts were found to be superior to the bare sol-gel titania catalysts in their photocatalytic performances. GQDs and NGQDs are anticipated to have an exciting future as green sensitizers in various semiconductor-based catalytic systems for their performance enhancement in visible light harvesting. The unique optical and physical properties of NGQDs can be attributed to be the high performance of NGQDs-sensitized photocatalysts, enabling them a promising material for commercial photocatalytic applications in the near future.

REFERENCES

[1] R. Chamousis, "HYDROGEN: FUEL OF THE FUTURE".

[2] Q. Guo, C. Zhou, Z. Ma, Z. Ren, H. Fan, and X. Yang, "Elementary photocatalytic chemistry on TiO_2 surfaces," *Chem. Soc. Rev.*, vol. 45, no. 13, pp. 3701–3730, Jun. 2016, doi: 10.1039/C5CS00448A.

[3] V. Etacheri, C. Di Valentin, J. Schneider, D. Bahnemann, and S. C. Pillai, "Visible-light activation of TiO_2 photocatalysts: Advances in theory and experiments," *J. Photochem. Photobiol. C Photochem. Rev.*, vol. 25, pp. 1–29, Dec. 2015, doi: 10.1016/j.jphotochemrev.2015.08.003.

[4] Z. Luo, A. S. Poyraz, C. H. Kuo, R. Miao, Y. Meng, S.Y. Chen, T. Jiang, C. Wenos, S. L Suib, "Crystalline Mixed Phase (Anatase/Rutile) Mesoporous Titanium Dioxides for Visible Light Photocatalytic Activity," *Chem. Mater.*, vol. 27, no. 1, pp. 6–17, Jan. 2015, doi: 10.1021/cm5035112.

[5] H. H. Do, D. L. T. Nguyen, X. C. Nguyen, T. H Le, T. P. Nguyen, Q. T. Trinh, S. H. Ahn, D. V. N. Vo, S. Y. Kim, Q. V. Le, "Recent progress in TiO_2-based photocatalysts for hydrogen evolution reaction: A review," *Arab. J. Chem.*, vol. 13, no. 2, pp. 3653–3671, Feb. 2020, doi: 10.1016/j.arabjc.2019.12.012.

[6] M. T. Noman, M. A. Ashraf, and A. Ali, "Synthesis and applications of nano-TiO_2: a review," *Environ. Sci. Pollut. Res.*, vol. 26, no. 4, pp. 3262–3291, Feb. 2019, doi: 10.1007/s11356-018-3884-z.

[7] T. Sreethawong and S. Yoshikawa, "Comparative investigation on photocatalytic hydrogen evolution over Cu-, Pd-, and Au-loaded mesoporous TiO_2 photocatalysts," *Catal. Commun.*, vol. 6, no. 10, pp. 661–668, Oct. 2005, doi: 10.1016/j.catcom.2005.06.004.

[8] X. Wang, R. Long, D. Liu, D. Y. Yang, and Y. Xiong, "Enhanced full-spectrum water splitting by confining plasmonic Au nanoparticles in N-doped TiO_2 bowl nanoarrays," *Nano Energy*, vol. 24, pp. 87–93, Jun. 2016, doi: 10.1016/j.nanoen.2016.04.013.

[9] G. R. Kandregula, J. Sivanadanam, and K. Ramanujam, "Drastic improvement in dye-sensitized solar cell efficiency by electrosorption based dye staining of titania semiconductor photoanode," *Electrochimica Acta*, vol. 349, p. 136344, Jul. 2020, doi: 10.1016/j.electacta.2020.136344.

[10] E. Savinkina, L. Obolenskaya, and G. Kuz’micheva, “Efficiency of sensitizing nano-titania with organic dyes and peroxo complexes,” *Appl. Nanosci.*, vol. 5, Feb. 2014, doi: 10.1007/s13204-014-0299-0.

[11] T. Jiang, L. Zhang, M. Ji, Q. Wang, Q. Zhao, X. Fu, H. Yin, “Carbon nanotubes/TiO_2 nanotubes composite photocatalysts for efficient degradation of methyl orange dye,” *Particuology*, vol. 11, no. 6, pp. 737–742, Dec. 2013, doi: 10.1016/j.partic.2012.07.008.

[12] J. Suave, S. M. Amorim, J. Ângelo, L. Andrade, A. Mendes, and R. F. P. M. Moreira, “TiO_2/reduced graphene oxide composites for photocatalytic degradation in aqueous and gaseous medium,” *J. Photochem. Photobiol. Chem.*, vol. 348, pp. 326–336, Nov. 2017, doi: 10.1016/j.jphotochem.2017.08.064.

[13] J. Rawal, U. Kamran, M. Park, B. Pant, and S.-J. Park, “Nitrogen and Sulfur Co-Doped Graphene Quantum Dots Anchored TiO_2 Nanocomposites for Enhanced Photocatalytic Activity,” *Catalysts*, vol. 12, no. 5, Art. no. 5, May 2022, doi: 10.3390/catal12050548.

[14] H. Tian, K. Shen, X. Hu, L. Qiao, and W. Zheng, “N, S co-doped graphene quantum dots-graphene-TiO_2 nanotubes composite with enhanced photocatalytic activity,” *J. Alloys Compd.*, vol. 691, pp. 369–377, Jan. 2017, doi: 10.1016/j.jallcom.2016.08.261.

[15] D. Jia, X. Li, Q. Chi, J. Low, P. Deng, W. Wu, Y.Wang, K. Zhu, W. Li, M. Xu, X. Xu, G. Jia, W. Ye, P. Gao, Y. Xiong, “Direct Electron Transfer from Upconversion Graphene Quantum Dots to TiO_2 Enabling Infrared Light-Driven Overall Water Splitting,” *Research*, vol. 2022, pp. 1–9, Apr. 2022, doi: 10.34133/2022/9781453.

[16] X. Hao, Z. Jin, J. Xu, S. Min, and G. Lu, “Functionalization of TiO_2 with graphene quantum dots for efficient photocatalytic hydrogen evolution,” *Superlattices Microstruct.*, vol. 94, pp. 237–244, Jun. 2016, doi: 10.1016/j.spmi.2016.04.024.

[18] Z. Chen, Y. Wu, Q. Wang, Z. Wang, L. He, Y. Lei, Z. Wang, “Oxygen-rich carbon-nitrogen quantum dots as cocatalysts for enhanced photocatalytic H_2 production activity of TiO_2 nanofibers,” *Prog. Nat. Sci. Mater. Int.*, vol. 27, no. 3, pp. 333–337, Jun. 2017, doi: 10.1016/j.pnsc.2017.04.011.

[19] H. Xie, C. Hou, H. Wang, Q. Zhang, and Y. Li, “S, N Co-Doped Graphene Quantum Dot/TiO_2 Composites for Efficient Photocatalytic Hydrogen Generation,” *Nanoscale Res. Lett.*, vol. 12, no. 1, p. 400, Dec. 2017, doi: 10.1186/s11671-017-2101-1.

[20] R. Shi, Z. Li, H. Yu, L. Shang, C. Zhou, G. I. N Waterhouse, L. Z. Wu, T. Zhang, "Effect of Nitrogen Doping Level on the Performance of N-Doped Carbon Quantum Dot/TiO_2 Composites for Photocatalytic Hydrogen Evolution," *ChemSusChem*, vol. 10, no. 22, pp. 4650–4656, 2017, doi: 10.1002/cssc.201700943.

[21] H. Ding, L.-W. Cheng, Y.-Y. Ma, J.-L. Kong, and H.-M. Xiong, "Luminescent carbon quantum dots and their application in cell imaging," *New J. Chem.*, vol. 37, no. 8, pp. 2515–2520, Jul. 2013, doi: 10.1039/C3NJ00366C.

[22] D. Pan, J. Jiao, Z. Li, Y. Guo, C. Feng, Y. Liu, L. Wang, M. Wu, "Efficient Separation of Electron–Hole Pairs in Graphene Quantum Dots by TiO_2 Heterojunctions for Dye Degradation," *ACS Sustain. Chem. Eng.*, vol. 3, no. 10, pp. 2405–2413, Oct. 2015, doi: 10.1021/acssuschemeng.5b00771.

[23] C. Hu, Y. Liu, Y. Yang, J. Cui, Z. Huang, Y. Wang, L. Yang, H. Wang, Y. Xiao, J. Rong, "One-step preparation of nitrogen-doped graphene quantum dots from oxidized debris of graphene oxide," *J Mater Chem B*, vol. 1, no. 1, pp. 39–42, 2013, doi: 10.1039/C2TB00189F.

[24] L. Li, G. Wu, G. Yang, J. Peng, J. Zhao, and J.-J. Zhu, "Focusing on luminescent graphene quantum dots: Current status and future perspectives," *Nanoscale*, vol. 5, Apr. 2013, doi: 10.1039/c3nr33849e.

[25] L. Lin, M. Rong, F. Luo, D. Chen, Y. Wang, and X. Chen, "Luminescent graphene quantum dots as new fluorescent materials for environmental and biological applications," *TrAC Trends Anal. Chem.*, vol. 54, pp. 83–102, Feb. 2014, doi: 10.1016/j.trac.2013.11.001.

[26] "Photoluminescence in graphene quantum dots," *Materials Today*. https://www.materialstoday.com/optical-materials/comment/photoluminescence-in-graphene-quantum-dots/ (accessed Dec. 20, 2022).

[27] "Nitrogen-Doped Graphene Quantum Dots with Oxygen-Rich Functional Groups | Journal of the American Chemical Society." https://pubs.acs.org/doi/10.1021/ja206030c (accessed Dec. 23, 2022).

[28] Q. Liu, B. Guo, Z. Rao, B. Zhang, and J. R. Gong, "Strong two-photon-induced fluorescence from photostable, biocompatible nitrogen-doped graphene quantum dots for cellular and deep-tissue

imaging," *Nano Lett.*, vol. 13, no. 6, pp. 2436–2441, Jun. 2013, doi: 10.1021/nl400368v.

[29] Q. Li, S. Zhang, L. Dai, and L.-S. Li, "Nitrogen-Doped Colloidal Graphene Quantum Dots and Their Size-Dependent Electrocatalytic Activity for the Oxygen Reduction Reaction," *J. Am. Chem. Soc.*, vol. 134, Nov. 2012, doi: 10.1021/ja309270h.

[30] A. Raghavan, S. Sarkar, L. R. Nagappagari, S. Bojja, S. MuthukondaVenkatakrishnan, and S. Ghosh, "Decoration of Graphene Quantum Dots on TiO_2 Nanostructures: Photosensitizer and Cocatalyst Role for Enhanced Hydrogen Generation," *Ind. Eng. Chem. Res.*, vol. 59, no. 29, pp. 13060–13068, Jul. 2020, doi: 10.1021/acs.iecr.0c01663.

[31] S. Wang, I. S. Cole, and Q. Li, "Quantum-confined bandgap narrowing of TiO_2 nanoparticles by graphene quantum dots for visible-light-driven applications," *Chem. Commun.*, vol. 52, no. 59, pp. 9208–9211, 2016, doi: 10.1039/C6CC03302D.

[32] P. Ramachandran, C. Y. Lee, R.-A. Doong, C. E. Oon, N. T. Kim Thanh, and H. L. Lee, "A titanium dioxide/nitrogen-doped graphene quantum dot nanocomposite to mitigate cytotoxicity: synthesis, characterisation, and cell viability evaluation," *RSC Adv.*, vol. 10, no. 37, pp. 21795–21805, 2020, doi: 10.1039/D0RA02907F.

[33] Y. Fu, G. Gao, and J. Zhi, "Electrochemical synthesis of multicolor fluorescent N-doped graphene quantum dots as a ferric ion sensor and their application in bioimaging," *J. Mater. Chem. B*, vol. 7, Feb. 2019, doi: 10.1039/C8TB03103G.

[34] A. Bokare, S. Chinnusamy, and F. Erogbogbo, "TiO_2-Graphene Quantum Dots Nanocomposites for Photocatalysis in Energy and Biomedical Applications," *Catalysts*, vol. 11, p. 319, Feb. 2021, doi: 10.3390/catal11030319.

[35] Y. Yan, J. Chen, N. Li, J. Tian, K. Li, J. Jiang, J. Liu, Q. Tian, P. Chen, "Systematic Bandgap Engineering of Graphene Quantum Dots and Applications for Photocatalytic Water Splitting and CO_2 Reduction," *ACS Nano*, vol. 12, no. 4, pp. 3523–3532, Apr. 2018, doi: 10.1021/acsnano.8b00498.

[36] S. Yu, Y.-Q. Zhong, B.-Q. Yu, S.-Y. Cai, L.-Z. Wu, and Y. Zhou, "Graphene quantum dots to enhance the photocatalytic hydrogen evolution efficiency of anatase TiO_2 with exposed {001} facet," *Phys. Chem. Chem. Phys.*, vol. 18, no. 30, pp. 20338–20344, 2016, doi: 10.1039/C6CP02561G.

CHAPTER 4

PREPARATION, CHARACTERISATIONS AND BIOLOGICAL APPLICATIONS OF SMALL-SIZED FLUORESCENT GRAPHENE QUANTUM DOTS

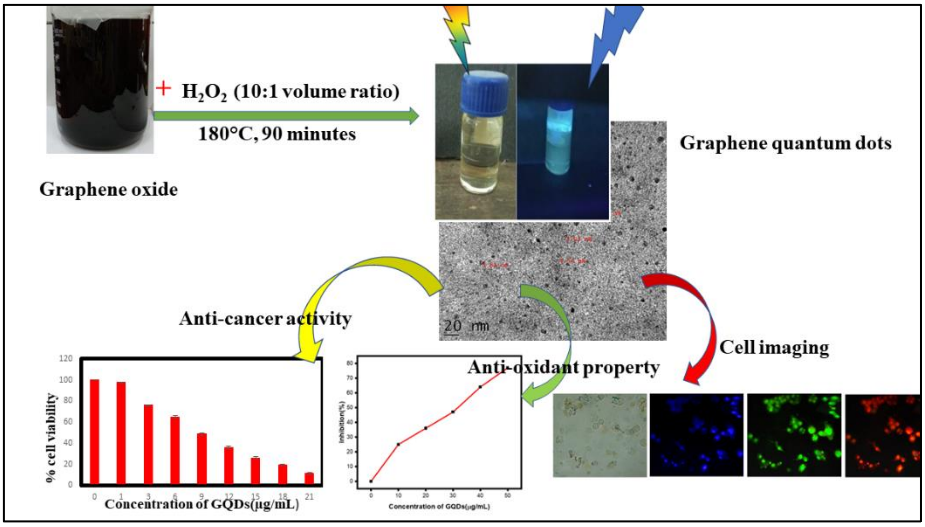

4.1 Introduction

After the first successful synthesis of GQDs [1] with fascinating fluorescent properties, innumerable experimental studies have been come out in this field of research. Being a zero-dimensional carbon nanomaterial with small size, non-toxicity, biocompatibility, strong fluorescence, ease of functionalisation, high water solubility and photo-stability, GQDs find potential applications in the field of bio-imaging, bio-sensing, drug-delivery and cancer theragnostics [2], [3].

So far, several methods have been reported for synthesising graphene quantum dots, and the hydro/solvothermal processes are particularly noteworthy. This simplified approach to the preparation of blue luminescent GQDs by the hydrothermal exfoliation of graphene oxide was first reported by Pan et al. in 2010. Zhao et al. reported a highly efficient hydrothermal approach for fabricating GQDs using potassium superoxide [4]. In another method, Chen et al. reported a green and eco-friendly preparation of GQDs by one-pot hydrothermal exfoliation of starch [5]. Gu et al. prepared GQDs via the hydrothermal method using glucose [6]. A greener method for the hydrothermal synthesis of GQDs by the exfoliation of graphene oxide in the presence of hydrogen peroxide was reported by Halder et al. [7]. The hydrothermal cutting of graphene oxide sheets with the aid of H_2O_2 in the presence of MnO_2 was carried out by Tian et al. [8]. H_2O_2 can effectively drive the scissoring of GO sheets and does not require dialysis for further purification of GQDs [2], [7].

The GQDs overcome the major limitation of inorganic quantum dots via., their intrinsic non-toxicity. Several biomedical applications using differently functionalised GQDs have been reported to date [2]. Apart from providing high solubility to GQDs, these chemical modifications such as edge-functionalised carboxyl, carbonyl, hydroxyl and epoxy groups are also capable of interacting with proteins, enzymes and antibodies [9]. A comparitive study on the cytotoxicity and autophagy induction of COOH-GQDs, OH-GQDs and NH_2-GQDs was performed by Xi et al. [10]. The high surface area to volume ratio of GQDs and π-conjugation enables efficient drug loading [11]–[13]. The inherent photoluminescence properties of GQDs help in the in-vivo tracking of drug delivery. The therapeutic applications of GQDs are mainly focused on cancer research [11], [13], [14]. Besides imaging probes, GQDs also find application as a potential photosensitiser in photodynamic therapy. The ROS production-induced cytotoxicity is dealt by the irradiation of GQDs.This novel strategy spreads a new light in the field of cancer therapy [15]–[17].

According to the “seed and soil” hypothesis by Dr Stephen Paget, cancer can grow, spread and metastasize in the proper microenvironment [18]. Studies have shown that excessive hydrogen peroxide production offers the necessary fertilizer for cancer metabolism in most cancer cells and associated fibroblasts. The cancer cells and fibroblasts mimic the behavior of immune cells through the secretion of hydrogen peroxide. Thus, to prevent tumour-stroma co-evolution and metastasis, synthesising catalase or antioxidants to neutralise cancer-associated hydrogen peroxide production is significant [19]. Several studies have shown that GQDs exhibit anti-oxidant properties and protect cells against oxidative stress by effectively scavenging free radicals. The presence of surface defects and π-conjugated structure indicates the potential of GQDs for quenching reactive ROS [20]–[24].

Studies have shown that biocompatible GQDs with small sizes, robust and stable photoluminescence can be successfully used for live cell nucleus imaging [25]. Cellular or sub-cellular labelling, especially nucleus labelling, is very crucial in cancer therapeutics for the selective targeting of drug delivery [25]–[27]. Conventionally used organic and peptide-based nuclear staining dyes suffer from photobleaching. But GQDs- based nuclear staining is a better alternative, merited with non-photobleaching, multi-photon emission, and good cellular distribution [16], [28]

This chapter discusses small-sized, highly fluorescent and water-soluble graphene quantum dots prepared by a simple hydrothermal cutting of graphene oxide with mild oxidising agent H_2O_2. We could successfully synthesise mono-dispersed graphene quantum dots within less time than earlier reports and also the prepared graphene quantum dots did not require further purification. TEM, FTIR, Raman and PL analysis were used to characterise graphene quantum dots. The anti-cancer activity of GQDs was evaluated. The prepared GQDs exhibited concentration-dependent cytotoxicity towards MCF-7 cells. On the other hand, negligible toxicity was shown towards normal cells. The unique excitation-dependent emission property of GQDs was utilised in cellular labelling.

4.2 Experimental methods

The chemicals used and the synthesis procedure of small sized graphene dots are discussed in chapter 2. Graphene oxide prepared via Modified Hummer’s method was used as the precursor for the synthesis of small sized GQDs, detailed in 2.2.1. Small sized GQDs was prepared by the hydrothermal treatment of graphene oxide dispersion in the presence of oxidative cleaving agent H_2O_2 for a time of one and half hour at 180 ℃, as discussed in 2.2.2.2.

4.3 Results and discussion

4.3.1 TEM analysis

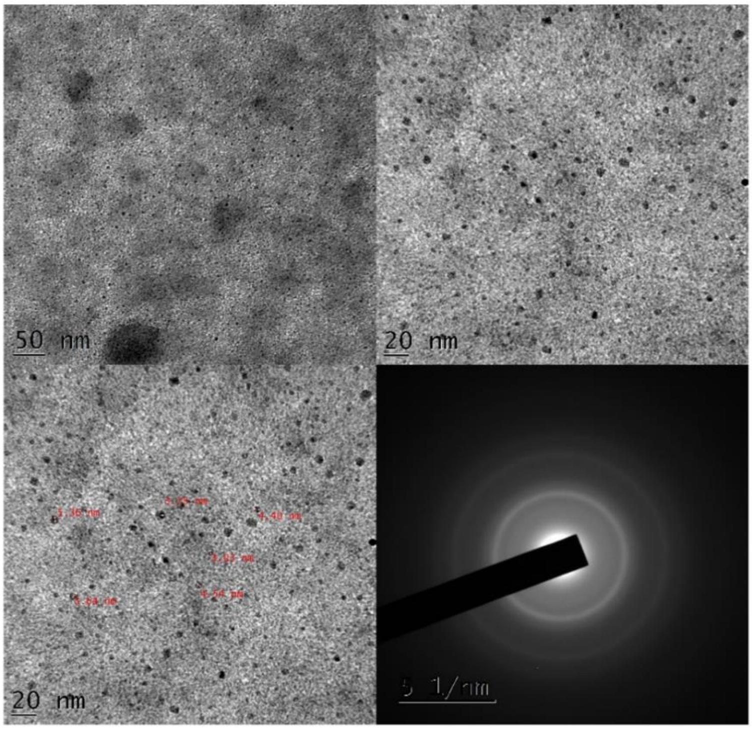

Figure 4.3.1(a-c) TEM images of GQDs (d)SAED pattern.

In Figure 4.3.1, the transmission microscopy images of the prepared GQDs having a relatively narrow size distribution between 1 and 3 nm are shown. Different hydrothermal temperatures and time can significantly affect the particle size distribution of GQDs. Since we have increased the hydrothermal treatment time to one and half hour, GQDs of even small sizes were formed compared to the GQDs discussed in the previous chapter. In figure 4.3.1(d), the corresponding SAED pattern is given, which can be atributed to the polycrystalline nature of the material. According to the mechanism proposed by Tian et al., at a higher temperature, H_2O_2 dissociate into ·OH radicals which drive the fragmentation of graphene sheets.

4.3.2 FTIR analysis

FTIR spectrum confirm the oxygen-rich functionalisation in GQDs, which imparts its solubility and strong fluorescence. The analysed peak position corresponds to 3262 cm^{-1} (O-H stretching vibration), 1716 cm^{-1} (C=O stretching vibration), 1638 cm^{-1} (C=C stretching vibration),1403 cm^{-1}(O-H bending vibrations), 1091 cm^{-1} (C-O stretching vibrations) as shown in figure 4.3.2.

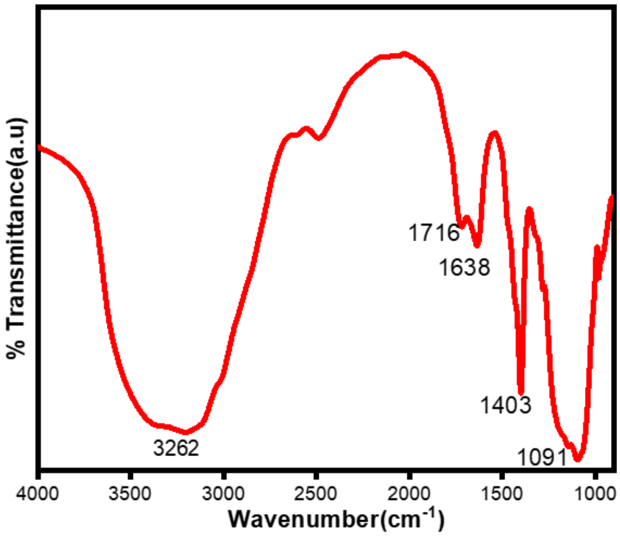

Figure 4.3.2 FTIR spectrum of GQDs

4.3.3 Raman spectroscopic analysis

Raman spectroscopic analysis of GQDs reveals the presence of the D band (1351 cm^{-1}) and G band (1601 cm^{-1}) in figure 4.3.3. The relative intensity ratio, I_D/I_G is found to be 1.2, which is an indication of the surface defects in GQDs due to the incorporation of oxygen functional groups, as hinted by FTIR data.

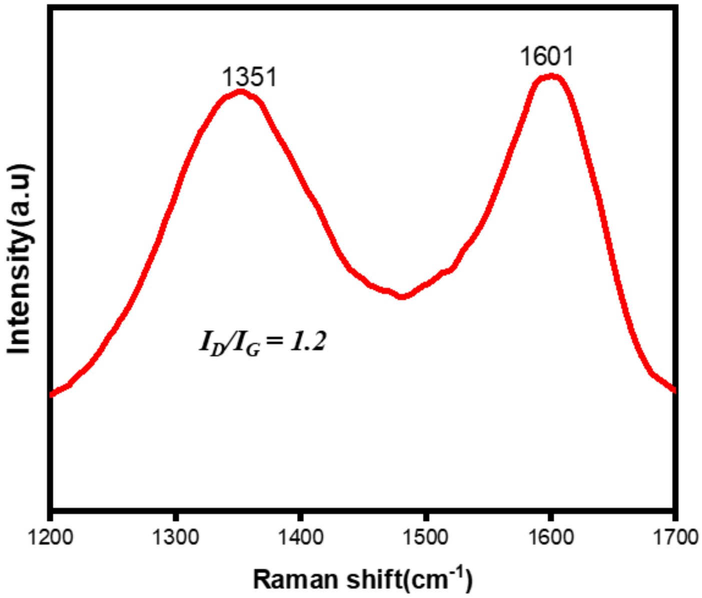

Figure 4.3.3. Raman spectrum of GQDs

4.3.4 Fluorescence spectral analysis

The optical properties of GQDs were investigated, and as depicted in figure 4.3.4. GQDs exhibited intense blue-coloured fluorescence with an emission peak at 485 nm when illuminated with 365 nm wavelength. The fluorescence band overlap of different oxygen functional groups results in the broadness of the peak [7]. The UV-Visible spectrum showed strong absorption in the UV region which decreased gradually and extended into the visible region. Consistent with earlier reports, prepared GQDs also displayed an excitation-dependent emission violating Kasha’s rule [29] (shown in figure 4.3.4(b)). The presence of the edge-functional groups and the emissive surface traps contribute towards the multi-colour emission property of GQDs [30], [25]

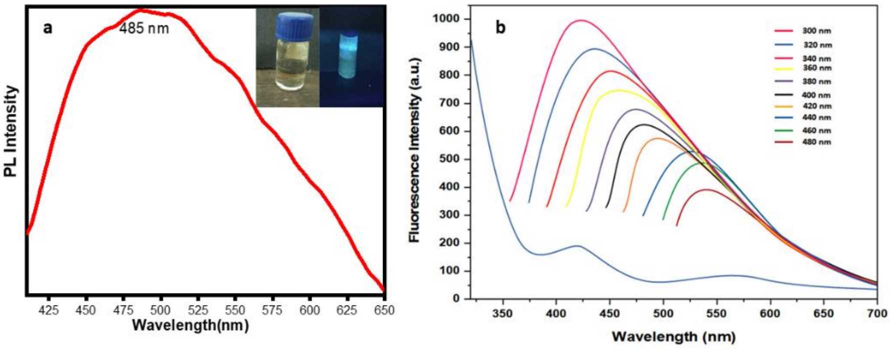

Figure 4.3.4(a): Fluorescence spectrum of GQDs at 365 nm excitation (inset is the photographs of GQDs when illuminated under visible light and 365 nm UV light) and (b) Excitation-dependent emission spectra of GQDs.

4.3.5 Anti-cancer activity of GQDs

4.3.5.1 Cell viability analysis

MTT assay was performed to evaluate the cytotoxicity of GQDs towards MCF-7 cell and HBL-100 and the results are presented in figure 4.2.5.1. The results demonstrated the in-vitro cytotoxic effect of GQDs on breast cancer MCF-7 cells. On increasing the concentration of GQDs from 0 to 21 µg/mL, the cancerous cell activity was found to be decreased, and cell death was 80% with an IC_{50} value of 9 µg/mL. While a concentration-dependent inhibition of cell proliferation was observed in MCF-7 cells, GQDs were found to be biocompatible to HBL-100 cells up to a concentration of 100µg/mL, ensuring its therapeutic applicability as an anti-cancer agent.

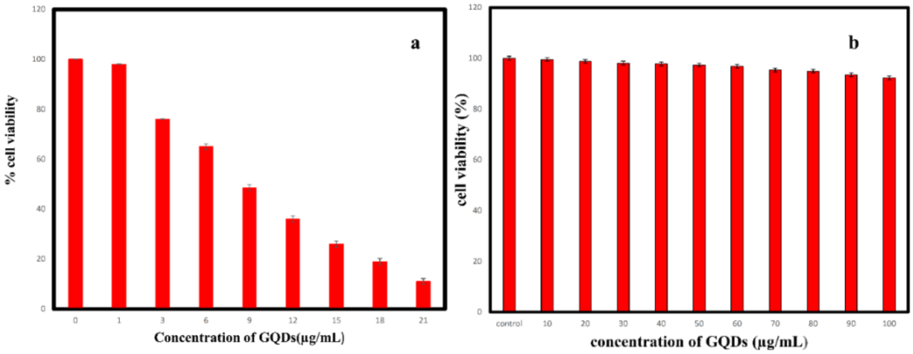

Figure 4.3.5.1:Cell viability analysis using different concentrations of GQDs towards (a) MCF-7 cells and (b) HBL-100 cells.

4.3.5.2 Possible mechanism for anti-cancer activity of GQDs

The specific toxicity of GQDs towards MCF-7 can be attributed to the overproduction of H_2O_2 in these cells compared to normal cells. Hydrogen peroxide is a second messenger, regulating fundamental biological processes [31]–[34] and is involved in wound healing, anti-bacterial defence, and stem-cell proliferation [33], [35]–[37]. But the over-expression of H_2O_2 within cells leads to severe issues like cancer, ageing, diabetes and neurodegenerative diseases [38]–[43]. Several studies have shown that the progressive mitochondrial defects in mutated cells lead to increased hydrogen peroxide production and result in a tumour microenvironment. The cancer cells use excess production of H_2O_2 to extract the nutrients from the nearby fibroblast. Outschoorn et al. studied the H_2O_2 metabolism in the tumour microenvironment using co-culturing MCF-7 breast cancer cells with immortalized fibroblasts [44]. They observed that cancer cells initially secrete hydrogen peroxide, which triggers oxidative stress in neighbouring fibroblasts, driving stromal inflammation, aerobic glycolysis, and autophagy. These autophagy, mitophagy and aerobic glycolysis in cancer-associated fibroblasts provide high-energy nutrients to “feed” cancer cells and further promote mitochondrial biogenesis and oxidative mitochondrial metabolism in cancer cells driving tumour growth. Since the anti-oxidant property of GQDs (rich in carboxyl and hydroxyl functional groups) are already established. The prepared GQDs might be capable of acting as excellent anti-oxidant and radical scavengers which might have resulted in growth inhibition and apoptosis in MCF-7 cells.

4.3.6 Anti-Oxidant property of GQDs

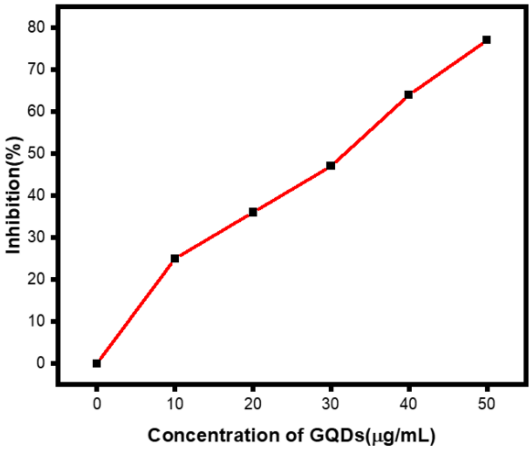

Figure 4.3.6. Percentage inhibition of H_2O_2 radicals with increasing concentration of GQDs

The hydrogen peroxide scavenging assay further confirmed the anti-oxidant property of GQDs prepared. Therefore, the anti-cancer activity of GQDs can be attributed to their radical scavenging ability. As shown in figure 4.3.6, an efficient H_2O_2 radical scavenging activity was displayed by GQDs on increasing concentration from 0 to 50 µg/mL. The IC_{50} is calculated for GQDs based on % inhibition and is found to be 30.9 µg/mL.

4.3.7 Morphology study of GQDs treated MCF-7 cells

The morphology of the MCF-7 in the presence and absence of GQDs was analysed with an inverted phase contrast microscopy. As shown in figure 4.3.7, the spindle-shaped MCF-7 cells, after treatment with GQDs, show an irregular cell membrane with more signs of blebbing, which confirms that GQDs could induce cell apoptosis in breast cancer MCF-7 cells.

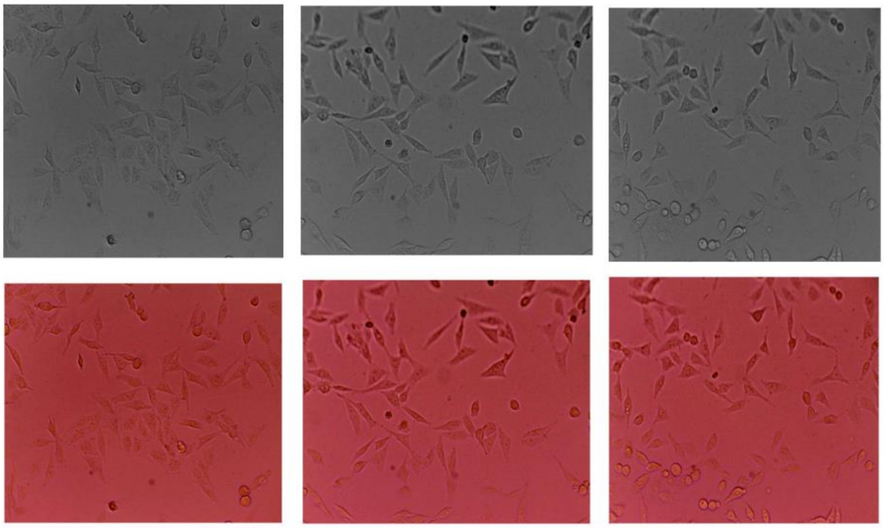

Figure 4.3.7. Morphologies of MCF-7 cell lines under control, treated with GQDs at IC_{25} concentration and IC_{50} concentration respectively.

4.3.8 Cell imaging of HBL-100 cells

Figure 4.3.8. shows the fluorescence microscopic images of HBL-100 cells treated with GQDs under different excitation

wavelengths. The multi-colour emission (blue, green and red) observed is because of the excitation-dependent emission property of GQDs [45]. Earlier reports confirm that due to lower toxicity and small size, GQDs provide better cell uptake ability compared to traditional nanoplatforms [46]. Thus, as-synthesised GQDs with excellent hydrophilic nature and small size were demonstrated to be capable of readily undergo cellular internalization via the endocytosis mechanism [47], [48] without hampering the cell activity.

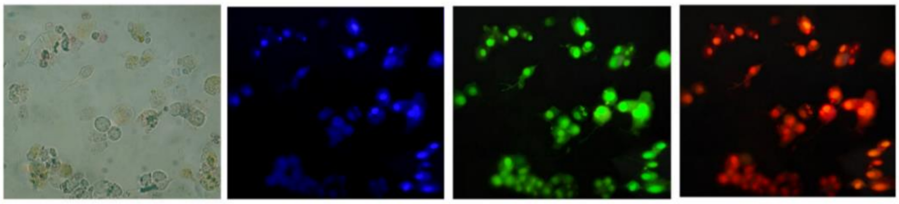

Figure 4.3.8. Fluorescence microscopic images of HBL-100 cells under control and treated with GQDs under different excitation wavelengths. (a) control (b) under excitation of 360-380 nm, (c) 460-480 nm, and (d) 510-590 nm wavelength.

4.4 Conclusions

In summary, graphene quantum dots with small size, high water solubility and strong fluorescence were prepared through a simple and rapid hydrothermal method employing graphene oxide and H_2O_2 at a temperature of 180 °C for 1.5 h reaction time. The synthesised GQDs exhibited anti-cancer properties and were also used for cellular imaging. MTT assays reveal the concentration-dependent cell growth inhibition of human breast cancer cells treated with GQDs in in-vitro conditions. Only negligible cytotoxicity was observed towards normal breast cells. The IC_{50} value of GQDs calculated is 9 µg/mL. The anti-oxidant property of GQDs was confirmed from the H_2O_2 scavenging assay. GQDs also exhibited cell penetration into the nucleus and multi-color fluorescence emission in HBL-100 cells.

References

[1] D. Pan, J. Zhang, Z. Li, and M. Wu, “Hydrothermal Route for Cutting Graphene Sheets into Blue-Luminescent Graphene Quantum Dots,” *Adv. Mater.*, vol. 22, no. 6, pp. 734–738, Feb. 2010, doi: 10.1002/adma.200902825.

[2] M. R. Younis, G. He, J. Lin, and P. Huang, “Recent Advances on Graphene Quantum Dots for Bioimaging Applications,” *Front. Chem.*, vol. 8, p. 424, Jun. 2020, doi: 10.3389/fchem.2020.00424.

[3] J. Lin, X. Chen, and P. Huang, “Graphene-based nanomaterials for bioimaging,” *Adv. Drug Deliv. Rev.*, vol. 105, no. Pt B, pp. 242–254, Oct. 2016, doi: 10.1016/j.addr.2016.05.013.

[4] “A facile and high-efficient approach to yellow emissive graphene quantum dots from graphene oxide | Request PDF.” https://www.researchgate.net/publication/319486342_A_facile_and_high-efficient_approach_to_yellow_emissive_graphene_quantum_dots_from_graphene_oxide.

[5] “Synthesis of graphene quantum dots from natural polymer starch for cell imaging - Green Chemistry (RSC Publishing).” https://pubs.rsc.org/en/content/articlelanding/2018/gc/c8gc02106f.

[6] J. GU, M. Hu, C. Guo, Z. Ding, X. Sun, and J. Yang, “High-yield Synthesis of Graphene Quantum Dots with Strong Green Photoluminescence,” *RSC Adv*, vol. 4, Oct. 2014, doi: 10.1039/C4RA10011E.

[7] A. Halder, M. Godoy-Gallardo, J. Ashley, X. Feng, T. Zhou, L. Hosta-Rigau, Y. Sun, “One-Pot Green Synthesis of Biocompatible Graphene Quantum Dots and Their Cell Uptake Studies,” *ACS Appl. Bio Mater.*, vol. 1, no. 2, pp. 452–461, Aug. 2018, doi: 10.1021/acsabm.8b00170.

[8] R. Tian, S. Zhong, J. Wu, W. Jiang, and T. Wang, “Facile hydrothermal method to prepare graphene quantum dots from graphene oxide with different photoluminescences,” *RSC Adv.*, vol. 6, no. 46, pp. 40422–40426, 2016, doi: 10.1039/C6RA00780E.

[9] K. E. Sapsford, W.R. Algar, L. Berti, K.B. Gemmill, B.J. Casey, E. Oh, M. H. Stewart, I. L Medintz, "Functionalizing Nanoparticles with Biological Molecules: Developing Chemistries that Facilitate Nanotechnology," *Chem. Rev.*, vol. 113, no. 3, pp. 1904–2074, Mar. 2013, doi: 10.1021/cr300143v.

[10] Y. Xie, B. Wan, Y. Yang, X. Cui, Y. Xin, and L.-H. Guo, "Cytotoxicity and autophagy induction by graphene quantum dots with different functional groups," *J. Environ. Sci.*, vol. 77, pp. 198–209, Mar. 2019, doi: 10.1016/j.jes.2018.07.014.

[11] D. Iannazzo, A. Pistone, M. Salamò, S. Galvagno, R. Romeo, S. V. Giofré, C. Branca, G. Visalli, A. Di Pietro, "Graphene quantum dots for cancer targeted drug delivery," *Int. J. Pharm.*, vol. 518, no. 1, pp. 185–192, Feb. 2017, doi: 10.1016/j.ijpharm.2016.12.060.

[12] F. Khodadadei, S. Safarian, and N. Ghanbari, "Methotrexate-loaded nitrogen-doped graphene quantum dots nanocarriers as an efficient anticancer drug delivery system," *Mater. Sci. Eng. C Mater. Biol. Appl.*, vol. 79, pp. 280–285, Oct. 2017, doi: 10.1016/j.msec.2017.05.049.

[13] X. Wang, X. Sun, J. Lao, H. He, T. Cheng, M. Wang, S. Wang, F. Huang, "Multifunctional graphene quantum dots for simultaneous targeted cellular imaging and drug delivery," *Colloids Surf. B Biointerfaces*, vol. 122, pp. 638–644, Oct. 2014, doi: 10.1016/j.colsurfb.2014.07.043.

[14] C. Wang, C. Wu, X. Zhou, T. Han, X. Xin, J. Wu, J. Zhang, S. Guo, Enhancing Cell Nucleus Accumulation and DNA Cleavage Activity of Anti-Cancer Drug via Graphene Quantum Dots," *Sci. Rep.*, vol. 3, no. 1, Art. no. 1, Oct. 2013, doi: 10.1038/srep02852.

[15] Z. M. Markovic, B. Z. Ristic, K. M. Arsikin, D. G. Klisic, L. M. Harhaji-Trajkovic, B. M. Todorovic-Markovic, D. P. Kepic, T. K Kravic-Stevovic, S. P. Jovanovic, M. M. Milenkovic, D. D. Milivojevic, V. Z. Bumbasirevic, M. D. Dramicanin, V. S. Trajkovic, "Graphene quantum dots as autophagy-inducing photodynamic agents," *Biomaterials*, vol. 33, no. 29, pp. 7084–7092, Oct. 2012, doi: 10.1016/j.biomaterials.2012.06.060.

[16] J. Ge, M. Lan, B. Zhou, W. Liu, L. Guo, H. Wang, Q. Jia, G. Niu, X. Huang, H. Zhou, X. Meng, P. Wang, C. S. Lee, W. Zhang, X. Han, "A graphene quantum dot photodynamic therapy agent with

high singlet oxygen generation," *Nat. Commun.*, vol. 5, no. 1, p. 4596, Dec. 2014, doi: 10.1038/ncomms5596.

[17] "Modification of Structural and Luminescence Properties of Graphene Quantum Dots by Gamma Irradiation and Their Application in a Photodynamic Therapy | ACS Applied Materials & Interfaces." https://pubs.acs.org/doi/10.1021/acsami.5b08226

[18] I. J. Fidler and G. Poste, "The 'seed and soil' hypothesis revisited," *Lancet Oncol.*, vol. 9, no. 8, p. 808, Aug. 2008, doi: 10.1016/S1470-2045(08)70201-8.

[19] M. P. Lisanti, U. E. Martinez-Outschoorn, Z. Lin, S. Pavlides, D. Whitaker-Menezes, R. G. Pestell, A. Howell, F. Sotgia, "Hydrogen peroxide fuels aging, inflammation, cancer metabolism and metastasis," *Cell Cycle*, vol. 10, no. 15, pp. 2440–2449, Aug. 2011, doi: 10.4161/cc.10.15.16870.

[20] Y. Chong, C. Ge, G. Fang, X. Tian, X. Ma, T Wen, W. G. Wamer, C. Chen, Z. Chai, J. J,Yin, "Crossover between Anti- and Pro-oxidant Activities of Graphene Quantum Dots in the Absence or Presence of Light," *ACS Nano*, vol. 10, no. 9, pp. 8690–8699, Sep. 2016, doi: 10.1021/acsnano.6b04061.

[21] X. Hu, X.-Y. Ma, J. Tian, and Z. Huang, "Rapid and facile synthesis of graphene quantum dots with high antioxidant activity," *Inorg. Chem. Commun.*, vol. 122, p. 108288, Dec. 2020, doi: 10.1016/j.inoche.2020.108288.

[22] Y. Wang, W. Kong, L. Wang, J. Z. Zhang, Y. Li, X. Liu, Y. Li, "Optimizing oxygen functional groups in graphene quantum dots for improved antioxidant mechanism," *Phys. Chem. Chem. Phys.*, vol. 21, no. 3, pp. 1336–1343, Jan. 2019, doi: 10.1039/C8CP06768F.

[23] L. Zhao, Y. Wang, and Y. Li, "Antioxidant Activity of Graphene Quantum Dots Prepared in Different Electrolyte Environments," *Nanomaterials,* vol. 9, no. 12, p. 1708, Nov. 2019, doi: 10.3390/nano9121708.

[24] L. Nilewski, K. Mendoza, A.S Jalilov, V. Berka, G. Wu, W. K. A. Sikkema, A. Metzger, R. Ye, R. Zhang, D. X. Luong, T. Wang, E. McHugh, P. J. Derry, E. L. Samuel, T. A. Kent, A. L. Tsai, J. M. Tour, "Highly Oxidized Graphene Quantum Dots from Coal as

Efficient Antioxidants," *ACS Appl. Mater. Interfaces*, vol. 11, no. 18, pp. 16815–16821, May 2019, doi: 10.1021/acsami.9b01082.

[25] "Graphene Quantum Dots for Cell Proliferation, Nucleus Imaging, and Photoluminescent Sensing Applications | Scientific Reports." https://www.nature.com/articles/s41598-017-16025-w.

[26] "Multifunctional Conjugates To Prepare Nucleolar-Targeting CdS Quantum Dots | Journal of the American Chemical Society." https://pubs.acs.org/doi/10.1021/ja1002668 .

[27] "A Europium Complex That Selectively Stains Nucleoli of Cells | Journal of the American Chemical Society." https://pubs.acs.org/doi/10.1021/ja056303g

[28] H. Ding, S.-B. Yu, J.-S. Wei, and H.-M. Xiong, "Full-Color Light-Emitting Carbon Dots with a Surface-State-Controlled Luminescence Mechanism," *ACS Nano*, vol. 10, no. 1, pp. 484–491, Jan. 2016, doi: 10.1021/acsnano.5b05406.

[29] P. Zheng and N. Wu, "Fluorescence and Sensing Applications of Graphene Oxide and Graphene Quantum Dots: A Review," *Chem. – Asian J.*, vol. 12, no. 18, pp. 2343–2353, Sep. 2017, doi: 10.1002/asia.201700814.

[30] "Engineering surface states of carbon dots to achieve controllable luminescence for solid-luminescent composites and sensitive Be2+ detection | Scientific Reports." https://www.nature.com/articles/srep04976

[31] "Controlled enzymatic production of astrocytic hydrogen peroxide protects neurons from oxidative stress via an Nrf2-independent pathway | PNAS." https://www.pnas.org/doi/abs/10.1073/pnas.1003996107

[32] E. W. Miller, O. Tulyathan, E. Y. Isacoff, and C. J. Chang, "Molecular imaging of hydrogen peroxide produced for cell signaling," *Nat. Chem. Biol.*, vol. 3, no. 5, Art. no. 5, May 2007, doi: 10.1038/nchembio871.

[33] M. P. Murphy, A. Holmgren, N. G. Larsson, B. Halliwell, C. J. Chang, B. Kalyanaraman, S. G. Rhee, P. J. Thornalley, L. Partridge, D. Gems, T. Nyström, V. Belousov, P.T. Schumacker, C. C. Winterbourn, "Unraveling the Biological Roles of Reactive Oxygen

Species," *Cell Metab.*, vol. 13, no. 4, pp. 361–366, Apr. 2011, doi: 10.1016/j.cmet.2011.03.010.

[34] B. C. Dickinson and C. J. Chang, "Chemistry and biology of reactive oxygen species in signaling or stress responses," *Nat. Chem. Biol.*, vol. 7, no. 8, Art. no. 8, Aug. 2011, doi: 10.1038/nchembio.607.

[35] "A tissue-scale gradient of hydrogen peroxide mediates rapid wound detection in zebrafish | Nature." https://www.nature.com/articles/nature08119

[36] "Role of hydrogen peroxide and oxidative stress in healing responses | SpringerLink." https://link.springer.com/article/10.1007/PL00012511.

[37] "H_2O_2, a Necessary Evil for Cell Signaling | Science." https://www.science.org/doi/full/10.1126/science.1130481

[38] T. Finkel, M. Serrano, and M. A. Blasco, "The common biology of cancer and ageing," *Nature*, vol. 448, no. 7155, Art. no. 7155, Aug. 2007, doi: 10.1038/nature05985.

[39] R. G. Cutler, "Oxidative Stress and Aging: Catalase Is a Longevity Determinant Enzyme," *Rejuvenation Res.*, vol. 8, no. 3, pp. 138–140, Sep. 2005, doi: 10.1089/rej.2005.8.138.

[40] T. Finkel and N. J. Holbrook, "Oxidants, oxidative stress and the biology of ageing," *Nature*, vol. 408, no. 6809, Art. no. 6809, Nov. 2000, doi: 10.1038/35041687.

[41] "Reactive Oxygen Species as a Signal in Glucose-Stimulated Insulin Secretion | Diabetes | American Diabetes Association." https://diabetesjournals.org/diabetes/article/56/7/1783/12577/Reactive-Oxygen-Species-as-a-Signal-in-Glucose

[42] "Neurodegenerative diseases and oxidative stress | Nature Reviews Drug Discovery." https://www.nature.com/articles/nrd1330

[43] "Role of Oxidative Stress and Antioxidants in Neurodegenerative Diseases: Nutritional Neuroscience: Vol 5, No 5." https://www.tandfonline.com/doi/abs/10.1080/102841502100003376 7

[44] U. E. Martinez-Outschoorn, R. M. Balliet, D. B. Rivadeneira, B. Chiavarina, S. Pavlides, C. Wang, D. Whitaker-Menezes, K. M. Daumer, Z. Lin, A. K. Witkiewicz, N. Flomenberg, A. Howell, R.

G. Pestell, E. S. Knudsen, F. Sotgia, M. P. Lisanti, “Oxidative stress in cancer associated fibroblasts drives tumor-stroma co-evolution: A new paradigm for understanding tumor metabolism, the field effect and genomic instability in cancer cells,” *Cell Cycle Georget. Tex*, vol. 9, no. 16, pp. 3256–3276, Aug. 2010, doi: 10.4161/cc.9.16.12553.

[45] M. Thakur, M. K. Kumawat, and R. Srivastava, “Multifunctional graphene quantum dots for combined photothermal and photodynamic therapy coupled with cancer cell tracking applications,” *RSC Adv.*, vol. 7, no. 9, pp. 5251–5261, 2017, doi: 10.1039/C6RA25976F.

[46] J. Pardo, Z. Peng, and R. M. Leblanc, “Cancer Targeting and Drug Delivery Using Carbon-Based Quantum Dots and Nanotubes,” *Mol. Basel Switz.*, vol. 23, no. 2, p. 378, Feb. 2018, doi: 10.3390/molecules23020378.

[47] C. Wu, C. Wang, T. Han, X. Zhou, S. Guo, and J. Zhang, “Insight into the Cellular Internalization and Cytotoxicity of Graphene Quantum Dots,” *Adv. Healthc. Mater.*, vol. 2, no. 12, pp. 1613–1619, Dec. 2013, doi: 10.1002/adhm.201300066.

[48] “Cellular distribution and cytotoxicity of graphene quantum dots with different functional groups | Nanoscale Research Letters, vol 9, p.108, 2014, doi:10.1186/1556-276X-9-108.

CHAPTER 5

FLUORINE-RICH GRAPHENE QUANTUM DOTS FROM HYDROXY FLUOROGRAPHENE AND THEIR APPLICATION FOR SENSING OF Fe (III) IONS

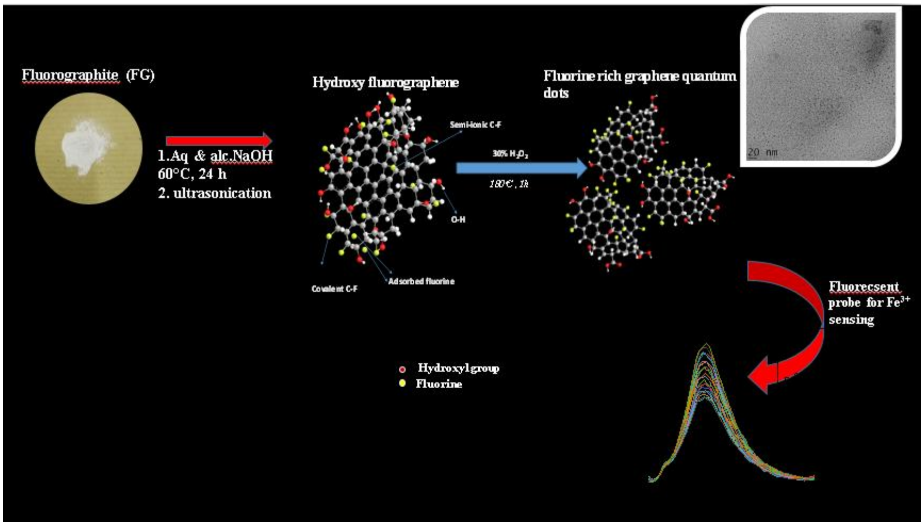

5.1 Introduction

The zero-bandgap of graphene limits most of its optoelectronic applications as a semiconductor and makes it difficult to be directly employed as a fluorescent material [1], [2]. To overcome this challenge, researchers have developed two main strategies: chemical functionalization and cutting graphene into quantum dots in order to modulate the band structure of graphene [1]-[8]. But an effective chemical functionalization of graphene under mild conditions is still a major challenge for chemists. So, the search for a two-dimensional graphene based precursor material with suitable properties which can be easily cut in to graphene quantum dots leads to fluorographite derived materials. Fluorination is an efficient method to modify the properties of carbon materials [9]-[12].

Fluorographene initially thought of as a 2D analogue of Teflon, turned out as a material with high chemical reactivity owing to the strained geometry of F adatoms in the graphene network [13]. It is reported that the highly labile F atoms in FG are susceptible to reductive defluorination [14] and nucleophilic substitution reactions [15]. Thus, fluorographene can be considered a promising precursor material for the preparation of versatile graphene derivatives such as hydroxy graphene, cyanographene, graphene acid, alkylated, arylated and alkynylated graphene [16]-[20]. Very Recently, Huang et al. [21] have reported the covalent modification of FG based on the Suzuki-Miyauara reaction of the C-F bond.

Doping of F into GQDs has gained more attention as a means to modulate their electronic and optical properties [22]-[27] essentially caused by the large electronegativity difference between carbon and fluorine as well as the possibility of covalent, ionic and semi-ionic interaction between these two atoms. Even though there are a large number of reports coming up on GQDs in the recent past, the facile synthetic strategies for fluorinated GQDs, a better understanding of the mechanism of their formation from the precursor graphene sheets by the oxidative cutting process and so on demand further investigations in this direction. Feng et al. [22] have reported the synthesis of fluorinated graphene quantum dots. Fluorographite (FG) on hydrothermal treatment resulted in fluorinated graphene quantum dots with an increase in fluorine content than FG. According to the authors, significant changes in PL properties are observed on cutting FG to FGQDs. In a work, Gong et al. [24] reported the synthesis of luminescent FGQD with tunable fluorine coverage and size from fluorinated graphite. In their other work, the authors [26] have adopted a fluorine-sacrificing strategy to synthesize FGQD from bulk fluorographite.

A simple and high-yielding method for the preparation of hydroxy graphene from fluorographite was previously reported by Rajeena et al. [28]. In this study, with ethanolic sodium hydroxide reagent, fluorographite (FG) was subjected to nucleophilic substitution reactions by hydroxyl groups. Parallel reductive defluorination were also observed and subsequent exfoliation resulted in the formation of hydroxy graphene (HG), with essentially no fluorine content. In the present study, a subtle modification of this preparation strategy is introduced for the preparation of FGQD precursor graphene sheet in which fluorine atoms are partially retained because substitution reactions dominate over reductive defluorination. The subsequent exfoliation will result in more hydroxy fluorographene (HFG) nanosheets, suited for the preparation of FGQDs. For the fine-tuning of the fluorine content as well as other parameters which are critical for their evolution as a functional material, it is essential to have a better understanding of the process of defluorination and oxidative etching used in FGQD preparation. The present study can be considered an attempt in this direction.

The prepared fluorine-rich graphene quantum dots can act as a fluorescent probe for the sensitive detection of Fe^{3+} ions in an aqueous solution. Ferric ions are among the most essential metal ions in biological systems and their deficiency as well as excess accumulation leads to several diseases including anaemia and even cancer [29], [30]. There is a high risk of leaching iron into water bodies as it is the common constructional material in drinking water pipes, automobiles, buildings, and bridges, and also as a coagulant in water treatment. Hence the constant monitoring of Fe^{3+} ions in water bodies is of vital importance. There are several recent reports on Fe^{3+} detection using GQDs [31], [32], N-GQDs [33]-[35], S-GQDs [36], B-GQDs [37], and N, S-GQDs [38]. However, the studies on the use of fluorinated GQDs as a turn-off fluorescent probe for the selective detection of ferric ions are yet to be explored more.

5.2 Experimental methods

List of chemicals used and the synthesis process of hydroxy fluorographene (HFG) and fluorine-rich graphene quantum dots (FGQDs) are detailed in chapter 2.

As discussed in 2.2.6, when fluorographite was refluxed with aqueous alcoholic NaOH at 100 ℃ for 24 h, nucleophilic substitutions of fluorine moieties on fluorographite by hydroxyl groups are carried out, in which the parallel reductive defluorinations are minimised. Mild sono-chemical exfoliation of the resulting product in water provides an aqueous dispersion of hydroxy fluorographene (HFG). Upon subsequent hydrothermal treatment with hydrogen peroxide, oxidative etching along with additional fluorinations may take place because of adsorbed fluoride ions in HFG dispersion which results in the formation of fluorescent fluorine-rich small sized graphene quantum dots (FGQDs).

5.3 Result and discussion

5.3.1 TEM analysis

Transmission electron microscopic (TEM) images reveal the morphology of synthesised HFG and FGQDs. The TEM image of the HFG (Figure 5.3.1.a) shows a good degree of exfoliation since the nucleophilic substituted hydroxyl groups on HFG are sufficiently hydrophilic and hence on sonication water molecules can easily enter into the layers resulting in spontaneous exfoliation. The TEM image of formed FGQDs and the corresponding histogram are depicted in

Figure 5.3.1.b. It is clearly evidenced from the corresponding histogram that FGQDs formed are of 1.5 nm-3 nm dimensions

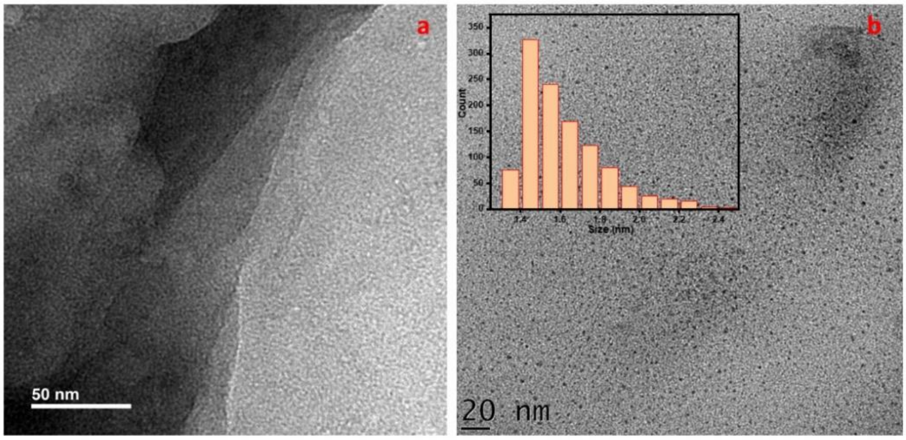

Figure 5.3.1: (a) TEM image of HFG and (b) FGQDs and the corresponding histogram (inset)

5.3.2 FTIR analysis

FTIR spectroscopy is used to characterize the chemical functional groups in HFG and FGQDs (Figure 5.3.2). The peaks at 1104 cm^{-1} (semi-ionic C-F), 1212 cm^{-1}(covalent C-F), 1589cm^{-1}(C=C), and 1640 cm^{-1} (C=O) respectively are found in the spectrum of HFG [28], [39], [40]. The strong intense peaks at 1384 cm^{-1} and 3458 cm^{-1} confirm the introduction of hydroxyl groups into the fluorographene framework.

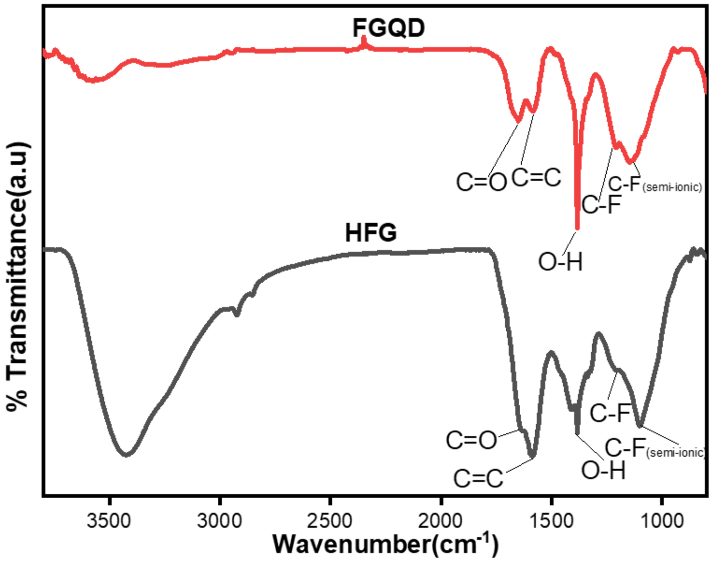

Figure 5.3.2: FTIR spectra of HFG and FGQD

Nucleophilic substitution with less reductive defluorination on the scaffold of HFG is thus well confirmed from the FTIR spectrum. In FGQDs, the relative intensities of the peak at 1146 cm^{-1} (semi-ionic C-F) and 1212 cm^{-1}(covalent C-F) are undergoing a substantial change from that of HFG indicative of more covalent C-F bonds than semi-ionic C-F in FGQDs compared to HFG. This points towards further fluorinations taking place in the presence of fluoride moieties during the hydrothermal treatment at 180℃, which results in fluorine-rich GQDs with more covalent C-F character [28], [39]- [44]. Also, the intensity of the peak at 1653 cm^{-1} (C=O) is increased in FGQDs due to the introduction of carbonyl moieties at the edges during the oxidative etching process.

5.3.3 AFM analysis

Atomic force microscopy is used to analyse the degree of exfoliation to HFG sheets. As shown in Figure 5.3.3, the thickness of HFG sheets is about 4 nm, as revealed from the height profile, which corresponds to few-layered sheets [40].

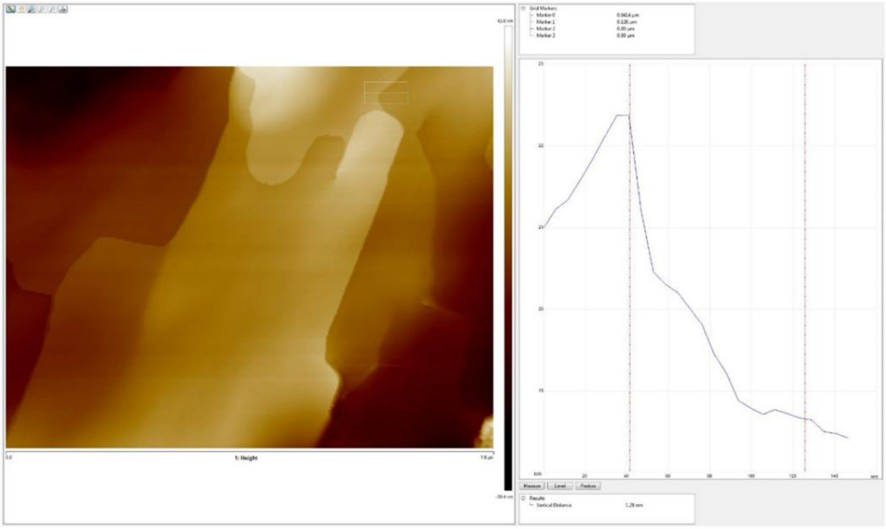

Grid Markers
Marker 0 0.0414 µm
Marker 1 0.128 µm
Marker 2 0.00 µm
Marker 2 0.00 µm

Results
Vertical Distance 1.28 nm

Figure 5.3.3.AFM image of HFG

5.3.4 Raman analysis

The Raman spectra of HFG and FGQDs are shown in Figure 5.3.4. Both HFG and FGQDs samples exhibit their disordered band or D- band (associated with the structural defects) at 1357 cm^{-1}, while the G-bands or ordered band (which arise from the in-plane stretching vibration of sp^2 domains) of HFG is at 1577 cm^{-1}, and in FGQDs it is red-shifted to 1611 cm^{-1}. The 2D bands of HFG and FGQDs at ~ 2710 cm^{-1} are strongly suppressed. The relative D band to G band intensity ratio, I_D/I_G is 0.15 for HFG and 0.99 for FGQDs. The increase in the I_D/I_G ratio of FGQDs may be attributed due to the presence of more fluorine content and increased edge defects due to the hydrothermal treatment [39].

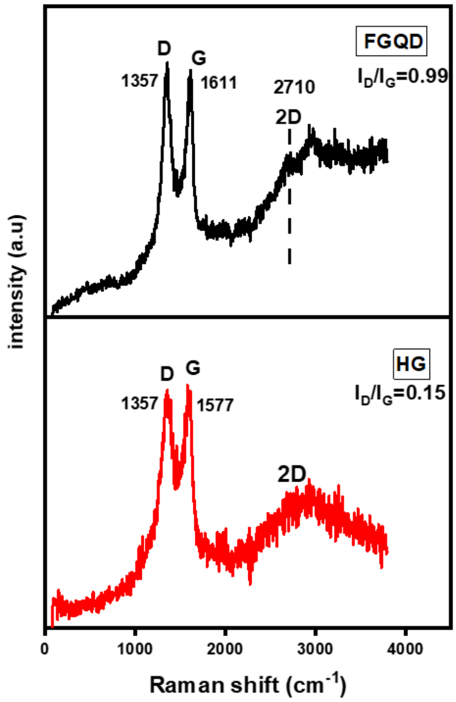

Figure 5.3.4: Raman spectra of HFG and FGQDs

5.3.5 XPS analysis

The elemental composition and chemical bonds of prepared samples were further investigated using XPS analysis. XPS survey spectra of the HFG and FGQDs (Figures 4a & b) reveal the presence of elements carbon, oxygen and fluorine. The elemental composition in HFG is found to be carbon 62.32%, oxygen 30.79%, and fluorine 6.88% while the C, O and F content in hydroxy graphene sheets prepared using alcoholic NaOH, reported by Rajeena et.al was 80.18%, 18.9%, 0.92% respectively. This result suggests that the addition of water in alcoholic sodium hydroxide reagents has triggered more substitution reactions in HFG with a lesser extent of reductive defluorination. Similarly, the C, O and F contents in FGQDs are found to be 65.27%, 16.67%, and 18.06% respectively. The decrease in oxygen content as well as an increase in fluorine content observed in FGQDs from that of HFG during the hydrothermal treatment throw light into the mechanism of oxidative cutting. In previous studies, there are reports about the chemical modifications of oxidised graphene nanosheets during the hydrothermal treatment by fluoride ions. These fluorinations take place by replacing the oxygen-containing groups and also the degree of fluorination as well as the nature of C-F bond configurations can be controlled by the reaction temperature, time and amount of F^- ions [39]-[45]. In the present work as well, hydrothermal treatment of HFG with adsorbed fluoride ions (as evident from F1s XPS spectra), some degree of fluorinations take place replacing oxygen-containing groups evident and thereby an increase in covalent C-F bonds in the formed FGQDs, as supported from the FTIR and XPS analysis.

A detailed investigation of the chemical composition of HFG and FGQDs by high-resolution C 1s XPS spectra is shown in Figure 5.3.5. The high-resolution C 1s spectra of HFG and FGQDs can be deconvoluted into 6 components. In HFG, the peaks are at 284.6 eV (C=C), 285.4 eV (C-C), 286.4 (C-O), 287.4 (C=O), and 288 eV (C-F semi-ionic), 289 eV (covalent C-F). In the corresponding spectrum of FGQDs, peaks are at 284.6 eV (C=C), 285.6 eV (C-C), 286.5 eV (C-

O), 287.1 eV (C=O), 288.8 eV (C-F semi-ionic), 290.6 eV (covalent C-F) [46]-[48]. The F1s high-resolution spectra of HFG provide 3 peaks corresponding to adsorbed F^-, C-F semi-ionic, and C-F covalent at 684.2 eV, 687.4 eV, 688.4 eV respectively, while in the spectrum of FGQDs, the corresponding values are at 683.7 eV, 687.8 eV and 688.5 eV respectively [49], [50]. The decrease in adsorbed fluorine content (Figure 4f) as well as oxygen-containing functional groups as obtained in XPS spectra of FGQDs are consistent with our suggested mechanism.

A comparison of the C-F covalent to C-F semi-ionic ratio for FG, HFG and FGQDs is summarised in Table 1 and it is clear that a drastic reduction of covalent C-F bond population is seen in the conversion of fluorographite (FG) to hydroxy fluorographene (HFG) which emphasize the nucleophilic substitution with less reductive fluorination in FG on treatment with aqueous alcoholic NaOH. However, when HFG is converted to FGQDs, the ratio is found to be slightly increasing, indicating a more covalent C-F bond population in FQDs which indicates fluorination taking place in HFG on hydrothermal treatment in presence of adsorbed fluoride ions. A schematic representation of oxidative cutting of HFG into FGQDs is shown in figure 5.3.6

Table 1: A comparison of the ratio of C-F covalent to C-F semi-ionic

	FG	**HFG**	**FGQDs**
$\frac{\textbf{C – F covalent}}{\textbf{C – F semi – ionic}}$	**5.82**	**0.71**	**0.96**

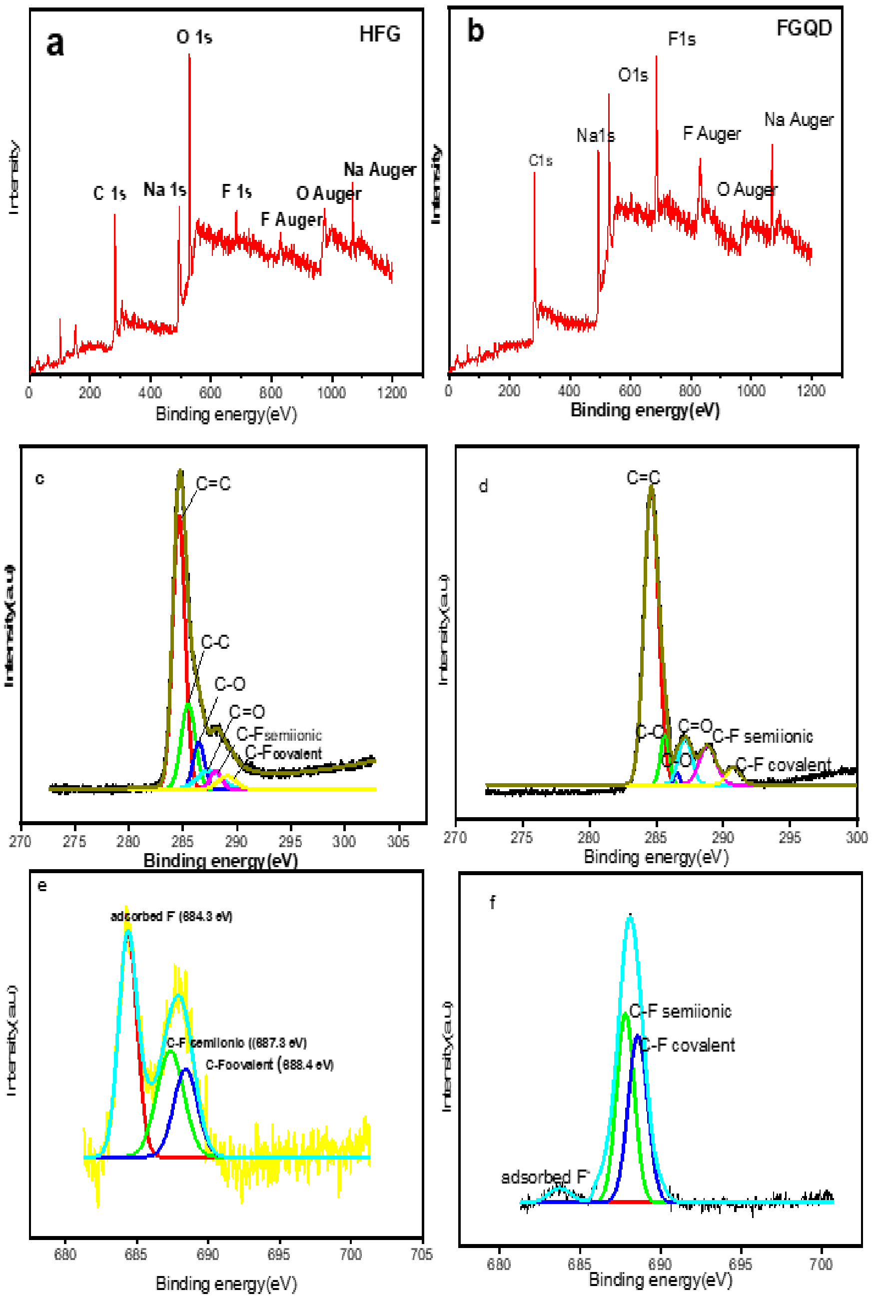

Figure 5.3.5: (a & b) survey XPS spectra, (c & d) C1s spectra and (e & f) F1s spectra of HFG and FGQDs respectively.

5.3.6 Schematic representation of the formation of FGQDs

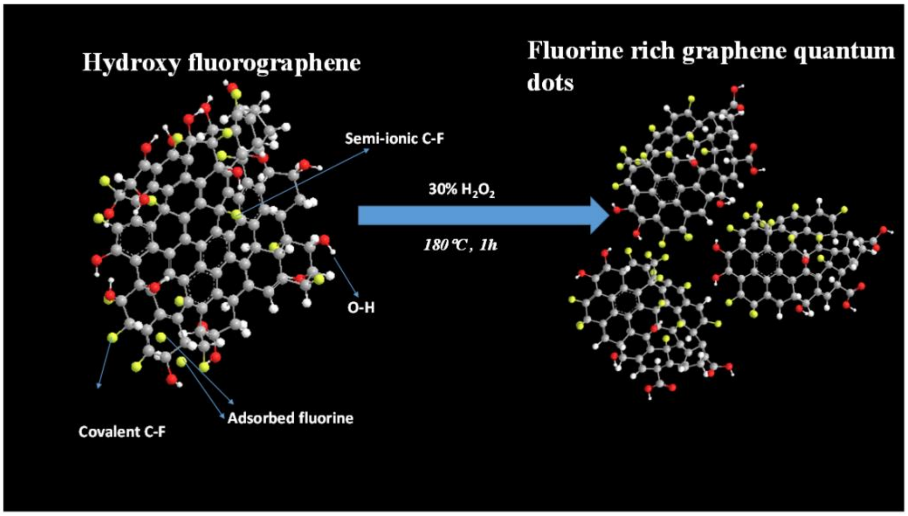

Figure 5.3.6: Schematic representation of oxidative cutting of HFG into FGQDs with H_2O_2.

5.3.7 Analysing optical properties of FGQDs

FGQDs emit blue fluorescence when irradiated with 365 nm UV light, as shown in Figure 5.3.7 (a). To further explore the optical properties of FGQDs, photoluminescence spectral measurements are carried out. It is observed that the emission wavelength of FGQDs depends on the excitation wavelengths used. As the excitation wavelength is changed from 295 to 365 nm, the PL peak also is getting shifted to longer wavelengths (Figure 5.3.7 (b)). The excitation-dependence of PL of FGQDs is thought to be resulting from the non-uniformity in sizes of the quantum dots and also due to the presence of emissive traps present in FGQDs [25]. FGQDs exhibit a strong emission peak at about 450nm when excited with 335 nm. The obtained PL and PLE spectra of FGQDs are presented in figure 5.3.7. (c). Using quinine sulphate as the standard, the PL quantum yield of FGQDs is estimated which is found to be 2.9 % (ESI).

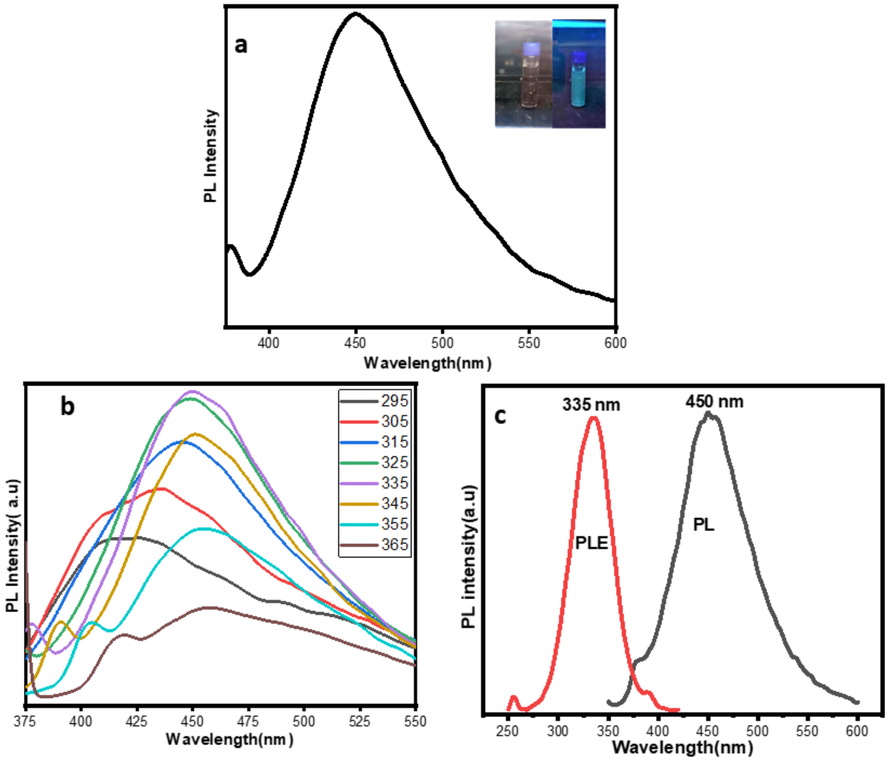

Figure 5.3.7: (a) PL spectrum of FGQDs with excitation at 365 nm. Inset is the photograph of FGQDs taken under visible and 365 nm UV light. **(b)** Fluorescence emission spectra of FGQDs solution at different excitation wavelengths. **(c)** PL and PLE spectra of FGQDs showing the maximum excitation and emission wavelengths.

5.3.8 FGQDs as a turn-off sensor for Fe^{3+}

To explore the possibility of FGQDs as a fluorescent sensor towards the detection of metallic ions, the fluorescence intensity measurement of FGQDs in the presence of various metal ions is carried out. The relative fluorescence intensities are measured after the addition of 20 µL of 0.1mM solutions of metal ions (Cd^{2+}, Hg^{2+}, Ni^{2+}, Mn^{2+}, Mg^{2+}, Cu^{2+}, Pb^{2+}, Fe^{2+}, Fe^{3+}, Al^{3+}, Ca^{2+}, Zn^{2+}, Na^{+}, K^{+}, Co^{2+}, Ag^{+}) into the FGQDs and the results are presented in figure 5.3.8 (a). Out of the 16 metal ions tested, the fluorescence intensity ratio (F/F_0) of FGQDs has lowered on the addition of Cu^{2+}, Pb^{2+}, and Fe^{2+} and only in the case of Fe^{3+} ions, an almost complete fluorescence quenching is observed. Based on the related literature reports [51]-[54], ferric ions may be getting engaged in non-specific interactions with the surface functional hydroxy /carboxy groups of FGQDs which leads to FL quenching. The sensitivity of FGQDs with different Fe^{3+} ion concentrations is analysed and it is found that the FL intensity of FGQDs is decreasing linearly with increased concentration of ferric ions. Figure 5.3.8. (b) depicts the fluorescence quenching effect on FGQDs with Fe^{3+} ion concentrations varying from 0 to 90 µM. From the Stern-Volmer plot, shown in figure 5.3.8 (c), the FL intensity ratio (F_0/F) shows a good linear response with Fe^{3+} over the concentration range 0 to 90 µM with a correlation coefficient (R^2) of 0.9993. The limit of detection (LOD) of Fe^{3+} was calculated to be 73.7 nM based on $3\sigma/m$ where σ is the standard deviation of the blank signal and m is the slope of the linear calibration plot. A comparison of other GQDs-Fe^{3+} sensor system are provided in Table 2 and Fe^{3+} ion sensing using different analytical methods are discussed in Table 3.

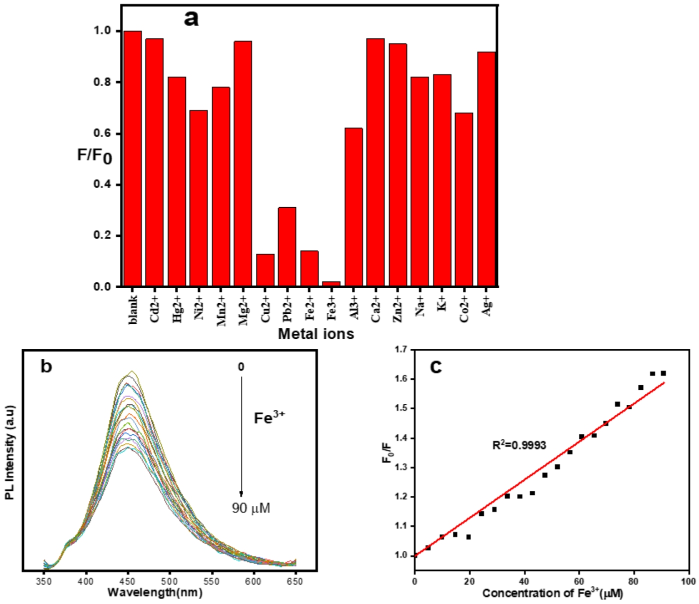

Figure 5.3.8. (a) PL response of aqueous FGQDs solution towards various metal ions. (excitation 320nm, [M^{n+}]=100μM) **(b)** Fluorescence quenching of FGQDs in the presence of a different concentration of Fe^{3+} (0-90 μM) **(c)** Stern- Volmer plot for the fluorescence quenching of FGQDs by Fe^{3+}ions.

Table 2: Comparison of GQDs-based fluorescent sensor for Fe^{3+}detection

Types of GQDs	**Linear range (μM)**	**LOD (μM)**	**Ref**
GQDs	0-80	7.22	25
CQDs	0-300	13.68	26
N-GQDs	1-500	1	27
S-GQDs	0-0.7	0.004	28
B-GQDs	0.01-100	0.005	29
N, S-GQDs	0.01-3	0.003	30
FGQDs	0-90	0.073	This work

Table 3: Comparison of Fe^{3+} sensing using different analytical methods

Method	**Linear range**	**LOD**	**Ref**
Colorimetric sensing	0-70 µM	9.5 µM	55
Atomic absorption spectrometry	0-100 µg/L	1.8 µg/L	56
Voltammetry	0.01-1 nM	1.2 nM	57
ICP-MS	-	0.085 nM	58
Fluorescent sensing	0-90 µM	73.7 nM	This work

5.3.9 Mechanism for fluorescence quenching

To understand the mechanism for fluorescence quenching, we have calculated the quenching constant (K_{sv}) from the slope of the linear fit of the Stern –Volmer plot given by equation $F_0/F=1+K_{sv}[Q]$ where F_0 and F are FL intensities of FGQDs in the presence and absence of Fe^{3+} ion at an excitation wavelength of 335 nm respectively and [Q] is the concentration of quencher. The quenching constant (K_{sv}) which denotes the binding affinity between the fluorescence molecule and quenching molecule is found to be $64.7 * 10^3 M^{-1}$. The good linearity of the Stern-Volmer plot over the measured concentration range and also the higher value of K_{sv} indicate a static quenching between FGQDs and Fe^{3+} [54], [59].

5.3.9(a) Zeta potential measurement

Zeta potential measurements are used to find the surface charge of nanoparticles which governs their stability. Studies report that nanoparticles with zeta potential in the range of -30 to 30 mV exhibit high colloidal stability [60], [61]. The surface charge measured for FGQDs is -36.8 mV due to surface-rich hydroxyl groups which impart its high stability (Figure 5.3.9.a). After the addition of Fe^{3+}, the zeta potential measurement is decreased to -30.8 mV which suggests the quenching mechanism involves the complexation of Fe^{3+}ions with the surface hydroxy/carboxy groups.

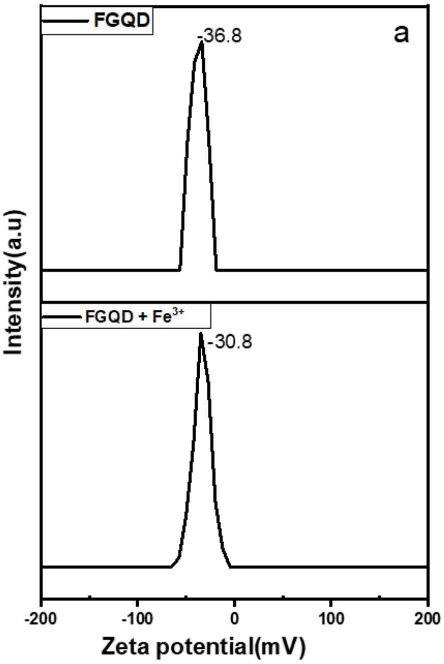

Figure 5.3.9(a) Zeta potential measurement of FGQDs and FGQDs + Fe^{3+}

5.3.9 (b) Lifetime measurement

Lifetime measurement obtained by measuring the fluorescence intensity in the absence and presence of a quencher molecule is a useful technique to distinguish static quenching from dynamic quenching [62]. Under the optimal experimental condition, before and after the addition of Fe^{3+}, the fluorescence lifetime for FGQDs remains almost constant (7.8 ns) indicating a static quenching mechanism (Figure 5.3.9.b).

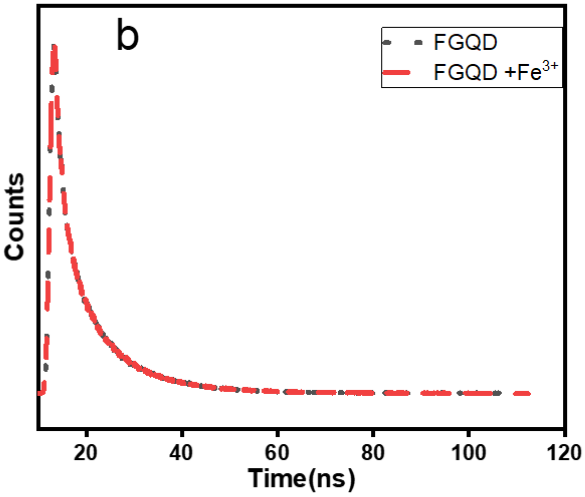

Figure 5.3.9. (b) fluorescence decay curve of FGQDs and FGQDs + Fe^{3+}

Based on the above results, we suggest that the addition of Fe^{3+} into the FGQD solution can result in the formation of a stable complex in its ground state which facilitates a non-radiative electron-hole recombination annihilation and thus triggers the quenching of fluorescence.

5.4 Conclusions

In this study, a novel method is adopted for the synthesis of hydroxylated fluorographene (HFG) from fluorographite, through nucleophilic substitution of labile fluorine atoms by hydroxyl groups, minimizing the extent of reductive defluorination in the graphene network. The hydrothermal treatment of prepared HFG dispersion with adsorbed fluoride ion resulted in additional fluorinations and oxidative etching producing fluorine-rich graphene quantum dots (FGQDs). The obtained FGQDs exhibit blue fluorescence and good water solubility. The feasibility of the prepared FGQDs to function as a label-free fluorescent probe for the selective detection of Fe^{3+} ions through a static quenching mechanism is further explored here. The sensitive response of FGQDS with Fe^{3+} concentration is found to follow a linear relationship over the range of 0-90 µM with a detection limit of 73.7 nM.

References

[1] Q. Bao and K. P. Loh, “Graphene Photonics, Plasmonics, and Broadband Optoelectronic Devices,” *ACS Nano*, vol. 6, no. 5, pp. 3677–3694, May 2012, doi: 10.1021/nn300989g.

[2] C. Galande, A. D. Mohite, A. V. Naumov, W. Gao, L. Ci, A. Ajayan, H. Gao, A. Srivastava, R. B. Weisman, P. M. Ajayan, “Quasi-molecular fluorescence from graphene oxide,” *Sci. Rep.*, vol. 1, p. 85, 2011, doi: 10.1038/srep00085.

[3] M. L. Mueller, X. Yan, J. A. McGuire, and L. Li, “Triplet States and Electronic Relaxation in Photoexcited Graphene Quantum Dots,” *Nano Lett.*, vol. 10, no. 7, pp. 2679–2682, Jul. 2010, doi: 10.1021/nl101474d.

[4] S. Kim, S. W. Hwang, M. K.Kim, D. Y. Shin, D. H. Shin, C. O. Kim, S. B. Yang, J. H. Park, E. Hwang, S. H. Choi, G. Ko, S. Sim, C.Sone, H. J. Choi, S. Bae, B. H. Hong, “Anomalous behaviors of visible luminescence from graphene quantum dots: interplay between size and shape,” *ACS Nano*, vol. 6, no. 9, pp. 8203–8208, Sep. 2012, doi: 10.1021/nn302878r.

[5] D. Pan, L. Guo, J. Zhang, C. Xi, Q. Xue, H. Huang, J. Li, Z. Zhang, W. Yu, Z. Chen, Z. Li, M. Wu, “Cutting sp2 clusters in graphene sheets into colloidal graphene quantum dots with strong green fluorescence,” J. Mater. Chem., vol. 22, no. 8, p. 3314, 2012, doi: 10.1039/c2jm16005f.

[6] S. H. Jin, D. H. Kim, G. H. Jun, S. H. Hong, and S. Jeon, “Tuning the Photoluminescence of Graphene Quantum Dots through the Charge Transfer Effect of Functional Groups,” ACS Nano, vol. 7, no. 2, pp. 1239–1245, Feb. 2013, doi: 10.1021/nn304675g.

[7] S. Zhuo, M. Shao, and S.-T. Lee, “Upconversion and Downconversion Fluorescent Graphene Quantum Dots: Ultrasonic Preparation and Photocatalysis,” ACS Nano, vol. 6, no. 2, pp. 1059–1064, Feb. 2012, doi: 10.1021/nn2040395.

[8] D. Qu, M. Zheng, L. Zhang, H. Zhao, Z. Xie, X. Jing, R. E. Haddad, H. Fan, Z. Sun, “Formation mechanism and optimization of highly luminescent N-doped graphene quantum dots,” Sci. Rep., vol. 4, p. 5294, Jun. 2014, doi: 10.1038/srep05294.

[9] J.-C. Charlier, X. Gonze, and J.-P. Michenaud, “First-principles study of graphite monofluoride (CF${)}_{\mathit{n}}$,” Phys. Rev. B, vol. 47, no. 24, pp. 16162–16168, Jun. 1993, doi: 10.1103/PhysRevB.47.16162

[10] M. Mar, Y. Ahmad, M. Dubois, K. Guérin, N. Batisse, and A. Hamwi, “Dual C F bonding in fluorinated exfoliated graphite,” J. Fluor. Chem., vol. 174, pp. 36–41, Jun. 2015, doi: 10.1016/j.jfluchem.2014.07.026

[11] X. Wang, Y. Dai, J. Gao, J. Huang, B. Li, C. Fan, J. Yang, X. Liu, ‘High-Yield Production of Highly Fluorinated Graphene by Direct Heating Fluorination of Graphene-oxide’, ACS Appl. Mater. Interfaces, vol. 5, no. 17, pp. 8294–8299, Sep. 2013, doi: 10.1021/am402958p.

[12] H. Touhara and F. Okino, ‘Property control of carbon materials by fluorination’, Carbon, vol. 38, no. 2, pp. 241–267, Jan. 2000, doi: 10.1016/S0008-6223(99)00140-2.

[13] Chronopoulos, D. D.; Bakandritsos, A.; Pykal, M.; Zbořil, R.; Otyepka, M. Chemistry, Properties, and Applications of Fluorographene. *Appl. Mater. Today* **2017**, *9*, 60–70. https://doi.org/10.1016/j.apmt.2017.05.004.

[14] Zbořil, R.; Karlický, F.; Bourlinos, A. B.; Steriotis, T. A.; Stubos, A. K.; Georgakilas, V.; Šafářová, K.; Jančík, D.; Trapalis, C.; Otyepka, M. Graphene Fluoride: A Stable Stoichiometric Graphene Derivative and Its Chemical Conversion to Graphene. *Small* **2010**, *6* (24), 2885–2891. https://doi.org/10.1002/smll.201001401

[15] Dubecký, M.; Otyepková, E.; Lazar, P.; Karlický, F.; Petr, M.; Čépe, K.; Banáš, P.; Zbořil, R.; Otyepka, M. Reactivity of Fluorographene: A Facile Way toward Graphene Derivatives. *J. Phys. Chem. Lett.* **2015**, *6* (8), 1430–1434. https://doi.org/10.1021/acs.jpclett.5b00565.

[16] Gong, P.; Wang, J.; Sun, W.; Wu, D.; Wang, Z.; Fan, Z.; Wang, H.; Han, X.; Yang, S. Tunable Photoluminescence and Spectrum Split from Fluorinated to Hydroxylated Graphene. *Nanoscale* **2014**, *6* (6), 3316–3324. https://doi.org/10.1039/C3NR05725A.

[17] Bakandritsos, A.; Pykal, M.; Błoński, P.; Jakubec, P.; Chronopoulos, D. D.; Poláková, K.; Georgakilas, V.; Čépe, K.; Tomanec, O.; Ranc, V.; Bourlinos, A. B.; Zbořil, R.; Otyepka, M. Cyanographene and

Graphene Acid: Emerging Derivatives Enabling High-Yield and Selective Functionalization of Graphene. *ACS Nano* **2017**, *11* (3), 2982–2991. https://doi.org/10.1021/acsnano.6b08449.

[18] Chronopoulos, D. D.; Bakandritsos, A.; Lazar, P.; Pykal, M.; Čépe, K.; Zbořil, R.; Otyepka, M. High-Yield Alkylation and Arylation of Graphene via Grignard Reaction with Fluorographene. *Chem. Mater.* **2017**, *29* (3), 926–930. https://doi.org/10.1021/acs.chemmater.6b05040.

[19] Lai, W.; Liu, J.; Luo, L.; Wang, X.; He, T.; Fan, K.; Liu, X. The Friedel–Crafts Reaction of Fluorinated Graphene for High-Yield Arylation of Graphene. *Chem. Commun.* **2018**, *54* (72), 10168–10171. https://doi.org/10.1039/C8CC05762A.

[20] D. Chronopoulos, D.; Medved', M.; Błoński, P.; Nováček, Z.; Jakubec, P.; Tomanec, O.; Bakandritsos, A.; Novotná, V.; Zbořil, R.; Otyepka, M. Alkynylation of Graphene via the Sonogashira C–C Cross-Coupling Reaction on Fluorographene. *Chem. Commun.* **2019**, *55* (8), 1088–1091. https://doi.org/10.1039/C8CC08492K.

[21] Huang, F.; Li, Y.; Liu, X.; Lai, W.; Fan, K.; Liu, X.; Wang, X. Suzuki–Miyaura Reaction of C–F Bonds in Fluorographene. *Chem. Commun.* **2021**, *57* (3), 351–354. https://doi.org/10.1039/D0CC07651A.

[22] Feng, Q.; Cao, Q.; Li, M.; Liu, F.; Tang, N.; Du, Y. Synthesis and Photoluminescence of Fluorinated Graphene Quantum Dots. *Appl. Phys. Lett.* **2013**, *102* (1), 013111. https://doi.org/10.1063/1.4774264.

[23] Zuo, W.; Tang, L.; Xiang, J.; Ji, R.; Luo, L.; Rogée, L.; Ping Lau, S. Functionalization of Graphene Quantum Dots by Fluorine: Preparation, Properties, Application, and Their Mechanisms. *Appl. Phys. Lett.* **2017**, *110* (22), 221901. https://doi.org/10.1063/1.4984238.

[24] Gong, P.; Hou, K.; Ye, X.; Ma, L.; Wang, J.; Yang, S. Synthesis of Highly Luminescent Fluorinated Graphene Quantum Dots with Tunable Fluorine Coverage and Size. *Mater. Lett.* **2015**, *143*, 112–115. https://doi.org/10.1016/j.matlet.2014.12.058.

[25] Gong, P.; Yang, Z.; Hong, W.; Wang, Z.; Hou, K.; Wang, J.; Yang, S. To Lose Is to Gain: Effective Synthesis of Water-Soluble Graphene Fluoroxide Quantum Dots by Sacrificing Certain Fluorine

Atoms from Exfoliated Fluorinated Graphene. *Carbon* **2015**, *83*, 152–161. https://doi.org/10.1016/j.carbon.2014.11.027.

[26] Gong, P.; Wang, J.; Hou, K.; Yang, Z.; Wang, Z.; Liu, Z.; Han, X.; Yang, S. Small but Strong: The Influence of Fluorine Atoms on Formation and Performance of Graphene Quantum Dots Using a Gradient F-Sacrifice Strategy. *Carbon* **2017**, *112*, 63–71. https://doi.org/10.1016/j.carbon.2016.10.091.

[27] Li, Z.; Wang, D.; Xu, M.; Wang, J.; Hu, X.; Anwar, S.; Tedesco, A. C.; Morais, P. C.; Bi, H. Fluorine-Containing Graphene Quantum Dots with a High Singlet Oxygen Generation Applied for Photodynamic Therapy. *J. Mater. Chem. B* **2020**, *8* (13), 2598–2606. https://doi.org/10.1039/C9TB02529D.

[28] Rajeena, U.; Akbar, M.; Raveendran, P.; Ramakrishnan, R. M. Fluorographite to Hydroxy Graphene to Graphene: A Simple Wet Chemical Approach for Good Quality Graphene. *New J. Chem.* **2018**, *42* (12), 9658–9665. https://doi.org/10.1039/C8NJ01392F\

[29] Beard, J. L. Iron Biology in Immune Function, Muscle Metabolism and Neuronal Functioning. *J. Nutr.* **2001**, *131* (2), 568S-580S. https://doi.org/10.1093/jn/131.2.568S.

[30] Emerit, J.; Beaumont, C.; Trivin, F. Iron Metabolism, Free Radicals, and Oxidative Injury. *Biomed. Pharmacother.* **2001**, *55* (6), 333–339. https://doi.org/10.1016/S0753-3322(01)00068-3.

[31] Ananthanarayanan, A.; Wang, X.; Routh, P.; Sana, B.; Lim, S.; Kim, D.-H.; Lim, K.-H.; Li, J.; Chen, P. Facile Synthesis of Graphene Quantum Dots from 3D Graphene and Their Application for Fe $^{3+}$ Sensing. *Adv. Funct. Mater.* **2014**, *24* (20), 3021–3026. https://doi.org/10.1002/adfm.201303441.

[32] Xu, F.; Shi, H.; He, X.; Wang, K.; He, D.;Yan,L.; Ye, X.; Tang ,J.; Shangguan, J.; Luo, L. Masking agent-free and channel-switch-mode simultaneous sensing of $Fe^{3+}$and Hg^{2+}using dual-excitation graphene quantum dots.. *Analyst* **2015**, *140*, 3925-3928.

[33] Tam, T. V.; Trung, N. B.; Kim, H. R.; Chung, J. S.; Choi, W. M. One-Pot Synthesis of N-Doped Graphene Quantum Dots as a Fluorescent Sensing Platform for Fe3+ Ions Detection. *Sens. Actuators B Chem.* **2014**, *202*, 568–573. https://doi.org/10.1016/j.snb.2014.05.045.

[34] Ju, J.; Chen, W. Synthesis of Highly Fluorescent Nitrogen-Doped Graphene Quantum Dots for Sensitive, Label-Free Detection of Fe (III) in Aqueous Media. *Biosens. Bioelectron.* **2014**, *58*, 219–225. https://doi.org/10.1016/j.bios.2014.02.061.

[35] Xu, H.; Zhou, S.; Xiao, L.; Wang, H.; Li, S.; Yuan, Q. Fabrication of Nitrogen-Doped Graphene Quantum Dot from MOFs- Derived Porous Carbon and Its Application for Highly Selective Fluorescent Detection of Fe3+. *J. Mater. Chem. C* 9.

[36] Li, S.; Li, Y.; Cao, J.; Zhu, J.; Fan, L.; Li, X. Sulfur-Doped Graphene Quantum Dots as a Novel Fluorescent Probe for Highly Selective and Sensitive Detection of Fe^{3+}. *Anal. Chem.* **2014**, *86* (20), 10201–10207. https://doi.org/10.1021/ac503183y.

[37] Chen, L.; Wu, C.; Du, P.; Feng, X.; Wu, P.; Cai, C. Electrolyzing Synthesis of Boron-Doped Graphene Quantum Dots for Fluorescence Determination of Fe^{3+} Ions in Water Samples. *Talanta* **2017**, *164*, 100–109. https://doi.org/10.1016/j.talanta.2016.11.019.

[38] Xia, C.; Hai, X.; Chen, X.W.; Wang, J.H.Simultaneously fabrication of free and solidified N,S-doped graphene quantum dots via a facile solvent-free synthesis route for fluorescent detection. *Talanta* **2017**, 168, 269–278.

[39] An, H.; li, yu; Long, P.; Gao, Y.; Qin, C.; Cao, C.; Feng, Y.; Feng, W. Hydrothermal Preparation of Fluorinated Graphene Hydrogel for High-Performance Supercapacitors. *J. Power Sources* **2016**, *312*, 146–155. https://doi.org/10.1016/j.jpowsour.2016.02.057.

[40] Lee, J.-W.; Jeong, S.-P.; You, N.-H.; Moon, S.-Y. Tunable Synthesis of Predominant Semi-Ionic and Covalent Fluorine Bonding States on a Graphene Surface. *Nanomater. Basel Switz.* **2021**, *11* (4), 942. https://doi.org/10.3390/nano11040942.

[41] Feng, W.; Long, P.; Feng, Y.; Li, Y. Two-Dimensional Fluorinated Graphene: Synthesis, Structures, Properties and Applications. *Adv. Sci.* **2016**, *3* (7), 1500413. https://doi.org/10.1002/advs.201500413.

[42] Samanta, K.; Some, S.; Kim, Y.; Yoon, Y.; Min, M.; Lee, S. M.; Park, Y.; Lee, H. Highly Hydrophilic and Insulating Fluorinated Reduced Graphene Oxide. *Chem. Commun.* **2013**, *49* (79), 891. https://doi.org/10.1039/c3cc45376f.

[43] Wang, Z.; Wang, J.; Li, Z.; Gong, P.; Liu, X.; Zhang, L.; Ren, J.; Wang, H.; Yang, S.Synthesis of Fluorinated Graphene with Tunable Degree of Fluorination. *Carbon* **2012**, *50* (15), 5403–5410. https://doi.org/10.1016/j.carbon.2012.07.026.

[44] Bon, S. B.; Valentini, L.; Verdejo, R.; Garcia Fierro, J. L.; Peponi, L.; Lopez-Manchado, M. A.; Kenny, J. M. Plasma Fluorination of Chemically Derived Graphene Sheets and Subsequent Modification With Butylamine. *Chem. Mater.* **2009**, *21* (14), 3433–3438. https://doi.org/10.1021/cm901039j.

[45] Kim, Y. H.; Park, J. S.; Choi, Y.-R.; Park, S. Y.; Lee, S. Y.; Sohn, W.; Shim, Y.-S.; Lee, J.-H.; Park, C. R.; Choi, Y. S.; Hong, B. H.; Lee, J. H.; Lee, W. H.; Lee, D.; Jang, H. W. Chemically Fluorinated Graphene Oxide for Room Temperature Ammonia Detection at Ppb Levels. *J. Mater. Chem. A* **2017**, *5* (36), 19116–19125. https://doi.org/10.1039/C7TA05766K.

[46] Wang, X.; Dai, Y.; Gao, J.; Huang, J.; Li, B.; Fan, C.; Yang, J.; Liu, X. High-Yield Production of Highly Fluorinated Graphene by Direct Heating Fluorination of Graphene-Oxide. *ACS Appl. Mater. Interfaces* **2013**, *5* (17), 8294–8299. https://doi.org/10.1021/am402958p.

[47] Sun, C.; Feng, Y.; Li, Y.; Qin, C.; Zhang, Q.; Feng, W. Solvothermally Exfoliated Fluorographene for High-Performance Lithium Primary Batteries. *Nanoscale* **2014**, *6* (5), 2634–2641. https://doi.org/10.1039/C3NR04609E.

[48] Ren, M.; Wang, X.; Dong, C.; Li, B.; Liu, Y.; Chen, T.; Wu, P.; Cheng, Z.; Liu, X. Reduction and Transformation of Fluorinated Graphene Induced by Ultraviolet Irradiation. *Phys. Chem. Chem. Phys.* **2015**, *17* (37), 24056–24062. https://doi.org/10.1039/C5CP03473F.

[49] Ding, H.; Xu, J.; Jiang, L.; Dong, C.; Meng, Q.; Rehman, S. ur; Wang, J.; Ge, Z.; Osipov, V. Yu.; Bi, H. Fluorine-Defects Induced Solid-State Red Emission of Carbon Dots with an Excellent Thermosensitivity. *Chin. Chem. Lett.* **2021**, *32* (11), 3646–3651. https://doi.org/10.1016/j.cclet.2021.04.033.

[50] Thiruppathi, A. R.; Sidhureddy, B.; Keeler, W.; Chen, A. Facile One-Pot Synthesis of Fluorinated Graphene Oxide for Electrochemical

Sensing of Heavy Metal Ions. *Electrochem. Commun.* **2017**, *76*, 42–46. https://doi.org/10.1016/j.elecom.2017.01.015.

[51] Abbas, A.; Tabish, T. A.; Bull, S. J.; Lim, T. M.; Phan, A. N. High Yield Synthesis of Graphene Quantum Dots from Biomass Waste as a Highly Selective Probe for Fe^{3+} Sensing. *Sci. Rep.* **2020**, *10* (1), 1–16. https://doi.org/10.1038/s41598-020-78070-2.

[52] Nair, R. V.; Thomas, R. T.; Sankar, V.; Muhammad, H.; Dong, M.; Pillai, S. Rapid, Acid-Free Synthesis of High-Quality Graphene Quantum Dots for Aggregation Induced Sensing of Metal Ions and Bioimaging. *ACS Omega* **2017**, *2* (11), 8051–8061. https://doi.org/10.1021/acsomega.7b01262.

[53] Raveendran, V.; Babu, A. R. S.; Renuka N. K. Mint Leaf Derived Carbon Dots for Dual Analyte Detection of Fe(III) and Ascorbic Acid. *RSC Adv.* **2019**, *9* (21), 12070–12077. https://doi.org/10.1039/C9RA02120E.

[54] Singh, V.; Mishra, A. K. Green and Cost-Effective Fluorescent Carbon Nanoparticles for the Selective and Sensitive Detection of Iron (III) Ions in Aqueous Solution: Mechanistic Insights and Cell Line Imaging Studies. *Sens. ActuatorsBChem.***2016**,*227*, 467–474. https://doi.org/10.1016/j.snb.2015.12.071.

[55] Narayanaswamy, N.; Govindaraju, T. Aldazine-Based Colorimetric Sensors for Cu^{2+} and $Fe3^{+}$. *Sens. Actuators B Chem.* **2012**, *161* (1), 304–310. https://doi.org/10.1016/j.snb.2011.10.036.

[56] Andersen, J. E. T. A Novel Method for the Filterless Preconcentration of Iron. *The Analyst* **2005**, *130* (3), 385. https://doi.org/10.1039/b412061b.

[57] Zhu, Y.; Hu, X.; Pan, D.; Han, H.; Lin, M.; Lu, Y.; Wang, C.; Zhu, R. Speciation Determination of Iron and Its Spatial and Seasonal Distribution in Coastal River. *Sci. Rep.* **2018**, *8* (1), 2576. https://doi.org/10.1038/s41598-018-20991-0.

[58] Wu, J.; Boyle, E. A. Determination of Iron in Seawater by High-Resolution Isotope Dilution Inductively Coupled Plasma Mass Spectrometry after $Mg(OH)_2$ Coprecipitation. *Anal. Chim. Acta* **1998**, *367* (1–3), 183–191. https://doi.org/10.1016/S0003-2670(98)00145-7.

[59] Xie, Z.; Sun, X.; Jiao, J.; Xin, X. Ionic Liquid-Functionalized Carbon Quantum Dots as Fluorescent Probes for Sensitive and Selective Detection of Iron Ion and Ascorbic Acid. *Colloids Surf. Physicochem. Eng. Asp.* **2017**, *529,* 38–44. https://doi.org/10.1016/j.colsurfa.2017.05.069

[60] He, P.; Sun, J.; Tian, S.; Yang, S.; Ding, S.; Ding, G.; Xie, X.; Jiang, M. Processable Aqueous Dispersions of Graphene Stabilized by Graphene Quantum Dots. *Chem. Mater.* **2015**, *27* (1), 218–226. https://doi.org/10.1021/cm503782p.

[61] Joseph, E.; Singhvi, G. Multifunctional Nanocrystals for Cancer Therapy: A Potential Nanocarrier. In *Nanomaterials for Drug Delivery and Therapy*; Elsevier, 2019; pp 91–116. https://doi.org/10.1016/B978-0-12-816505-8.00007-2.

[62] Wang, Z.; Chen, D.; Gu, B.; Gao, B.; Liu, Z.; Yang, Y.; Guo, Q.; Zheng, X.; Wang, G. Yellow Emissive Nitrogen-Doped Graphene Quantum Dots as a Label- Free Fluorescent Probe for Fe^{3+} Sensing and Bioimaging. *Diam. Relat. Mater.* **2020**, *104*, 107749. https://doi.org/10.1016/j.diamond.2020.107749

CHAPTER 6

HYDROTHERMAL CONVERSION OF GRAPHENE OXIDE TO CARBON NANO ONIONS FOR METAL SENSING AND BIOLOGICAL APPLICATIONS

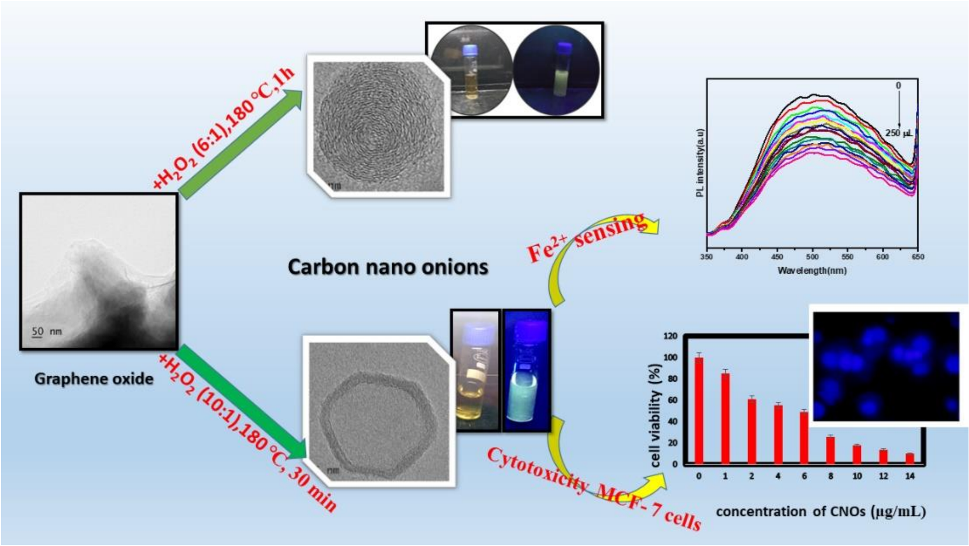

6.1 Introduction

Carbon-based nanomaterials with fascinating shapes, sizes and uniqueness in their properties continued to generate enormous interest in recent scientific research. Among them, Carbon nano-onions (CNOs) or multi-layered fullerene gained significant attention with their exciting properties. CNOs are members of the fullerene family consisting of quasi-spherical and polyhedral-shaped concentric graphitic layers made up of hexagonal and pentagonal carbon rings with delocalized electron clouds [1], [2]. The number of carbon atoms in each graphitic layer will be $60n^2$, where n is the corresponding layer number [3], and the d-spacing in CNOs will be around 0.335 nm, similar to graphite [1]. The fascinating properties like high surface to volume ratio, thermal stability and electrical conductivity [4]-[7], makes CNOs a desirable candidate in the field of supercapacitors, gas and energy storage, catalysis, hyper lubricants, electromagnetic shielding, biological imaging, sensing and water treatment [7]-[23].

Even after its accidental discovery in 1980 by Iijima [24], the promising nanomaterials, CNOs, remained unnoticed until Daniel Ugarte in 1992 marked its synthesis by irradiating carbon soot with high energy electron beam [25]. Following this, several methods including annealing of ultra-dispersed nanodiamonds (NDs) [26], arc-discharge [27], pyrolysis [28], ion implantation [29], chemical vapour deposition [30], electron-beam irradiation [31], laser irradiation [32], ball-milling [33], solvothermal reduction and hydrothermal treatment with mild conditions [3] are reported for the synthesis of CNOs. The structural morphology of the formed CNOs (big or small sized, spherical or polyhedral shaped, dense or hollow core) depends mostly on the reaction condition and precursor used for the synthesis [1] and the chemical reactivity is higher for small sized CNOs with high surface strain [34].

Since pristine CNOs exhibit poor solubility in polar and non-polar solvents, their applications are limited or hindered by this fact. Hence a facile and easy method for the synthesis of water soluble CNOs gains huge research interest. Chemical functionalization on CNO surfaces can improve its solubility and physicochemical properties. Both covalent and non–covalent functionalization of CNOs are reported so far which include oxidation [35], [36], 1,3-dipolar cycloaddition [37], amidation [38], [2+1] cycloaddition [39], nucleophilic substitution [40], and radical polymerization [41].

Recently, researches have explored the possibility of chemically modified CNOs containing bioactive molecules and fluorophores as an ideal candidates for drug delivery, tissue engineering, cellular imaging and cancer therapy [42]-[47]. The functionalized CNOs exhibit weak inflammatory and less cytotoxicity both in-vivo and in-vitro mode. This opens up the tremendous possibility of their potential use as an efficient biosafety theranostic agents [48]. The toxicity of CNOs was first investigated by Ding et al. on human skin fibroblast and found that compared to multi-walled carbon nanotubes, CNOs induced less stress on the cells at low dosage [49]. Studies on human umbilical vein endothelial cells by Xu et al.

revealed that CNOs exhibited a dose-dependent inhibitory concentration effect on cell growth and induced apoptosis and DNA damage due to reactive oxygen species generation [50]. Water-soluble fluorescent CNOs reported by Ghosh et al. were used for the life cycle imaging of Drosophila Melanogaster without any toxicity to its the normal life activity [51]. According to Kang et al. spherical shape of CNOs make them a better drug delivery platform compared to multi-walled carbon nano tubes [52].

Herein, we report a novel, easy and quick strategy for the preparation of good quality water soluble CNOs from graphene oxide, employing facile hydrothermal method. Due to faster detection with high selectivity and sensitivity, sensing of metal ions with fluorescent sensors received much attention. The optical properties of prepared CNOs were investigated and its fluorescent sensing property for the selective and sensitive detection of ferrous ion was examined.

In the present study, the anti-cancer activity of CNOs is investigated. Among the widespread reports of cancer deaths, female breast cancer remains to be the second cause of cancer deaths even though the death rate had declined overtime. Therefore, an attempt to discover the ability of synthesized CNOs in the growth inhibition of human breast cancer cell line MCF-7 was carried out. The cell viability of CNOs against normal breast cell HBL-100 was also studied. The morphology of MCF-7 cells treated with CNOs were analysed by an inverted light microscopy. DAPI staining was used to study the nuclear morphology of treated cell and to assess the apoptosis.

6.2 Experimental methods

The chemicals used and the synthetic procedure adapted for the preparation of spherical as well as hollow CNOs are discussed in chapter 2.

Graphene oxide (GO) dispersion obtained by modified Hummer's method (discussed in 2.2.1) when hydrothermally treated at 180 ℃ with hydrogen peroxide by varying the GO - H_2O_2 ratio as well as reaction time resulted in CNOs with different morphology ie spherical and hollow CNOs , as detailed in 2.2.5.

6.3 Results and discussion

6.3.1 TEM images

HRTEM images (Figure 6.3.1(ⅰ)(a-b) and 6.3.1(ⅱ)(a-c)) reveals the formation of CNOs. When graphene oxide was hydrothermally treated with 30% hydrogen peroxide in 16:1 ratio at a temperature of 180 °C for 1 h, resulted in solid spherical CNOs with concentric graphitic shells. But the hydrothermal treatment of graphene oxide with 30% hydrogen peroxide in 10: 1 ratio at 180 °C for 30 min produced hollow CNOs with lesser number of graphitic shells. Thus, varying the time for the hydrothermal treatment as well as the graphene oxide with hydrogen peroxide ratio successful production of CNOs with two different morphologies were achieved. This is consistent with the earlier reports that depending on reaction conditions, formed CNO differs in size, shape and surface area [53].

Figure 6.3.1(ⅰ)(a-b) shows the TEM image of solid spherical CNOs with concentric graphitic multi-shells architecture, with an average size of ~ 20 nm. The interlayer spacing of graphitic shells was found to be ~ 0.354 nm, slightly greater the d spacing in graphite which is consistent with the previous reports [54]. Figure 6.3.1(ⅱ)(a-c) depicts the TEM image of CNOs with hollow core and lesser number of graphitic shells.

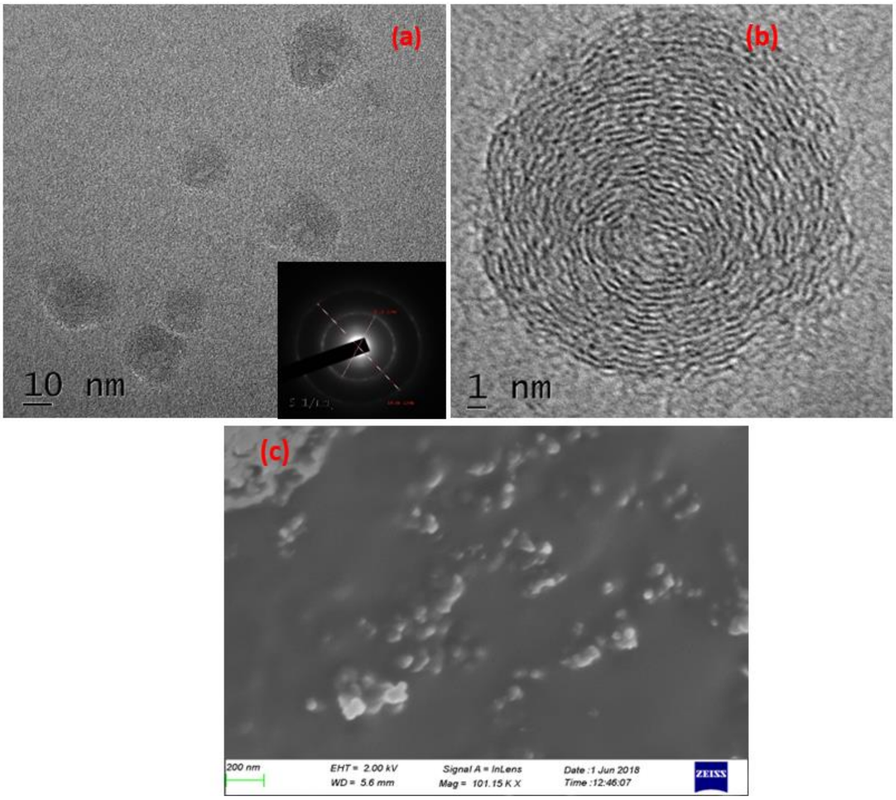

Figure 6.3.1(ⅰ):(a-b) HR-TEM images of spherical CNOs (inset is the SAED pattern) and (c) FESEM image of spherical CNOs

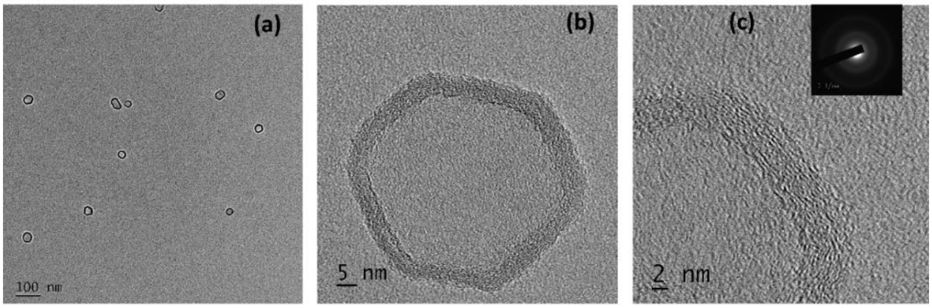

Figure 6.3.1(ⅱ)(a-c): HR-TEM images of hollow CNOs (inset is the SAED pattern)

6.3.2 FTIR and Raman Analysis

The functionalization of CNOs were confirmed with FTIR analysis. FTIR spectrum of spherical CNOs, as shown in figure 6.3.2(ⅰ)(a) exhibited sharp bands at 1095 cm^{-1} (C-O stretching vibration), 1435 cm^{-1} (O-H bending vibration) 1633 cm^{1}(symmetric COO^{-} stretching vibration), 2927 cm^{-1} (C-H stretching vibration), 3420 cm^{-1} (O-H stretching vibration). These results indicate the presence of carboxy and hydroxy groups on CNO surface which imparts to its high solubility [55]. The Raman spectrum of spherical CNOs, (figure 6.3.2 (ⅰ) (b)) exhibit D band at ~1347 cm^{-1} for disordered carbon and G band at ~ 1596 cm^{-1} corresponding to graphitic carbon along with second order peaks with a 2D band at ~2692 cm^{-1} and G+D band at ~ 2945 cm^{-1} [56]. The I_D/I_G ratio is calculated and the obtain value of 1.3 further confirms the presence of defects arisen due to surface functionalisation. In hollow CNOs, the FTIR spectrum gives peaks at 1096, 1404, 1632, 1727 cm^{-1} corresponding to C-O, O-H, C=C and C=O vibrations respectively which implies the presence of oxygen surface functionalities as depicted in Figure 6.3.2.(ⅱ)(a). The Raman spectrum of hollow CNOs show D band 1352 cm^{-1} and G band at 1604 cm^{-1} with an I_D/I_G value of 1.2, (figure 6.3.2(ⅱ)(b) which again points towards heavy surface functionalization.

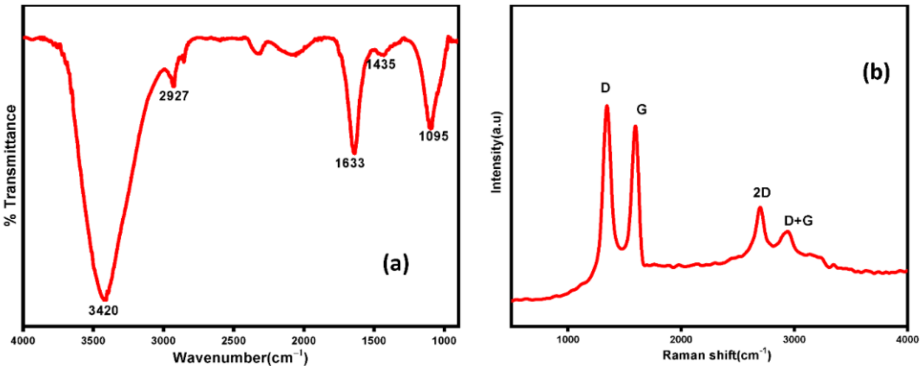

Figure 6.3.2 (ⅰ):(a) FTIR spectrum (b) Raman spectrum of Spherical CNOs

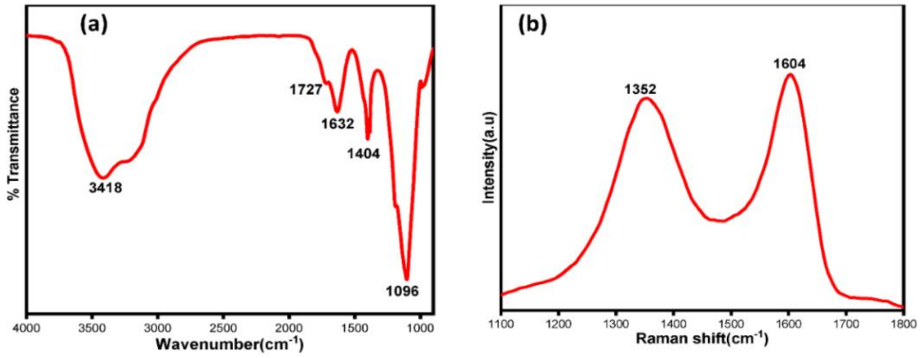

Figure 6.3.2 (ⅱ):(a) FTIR spectrum and(b) Raman spectrum of hollow CNOs

6.3.3. Curling and closure- CNO formation

The curling and closure of graphitic layers occur in CNOs in order to reduce the strain and surface energy due to dangling bonds and pentagonal carbon rings, resulting in amorphous or crystalline CNOs [1], [25], [57], [58]. Consistent with the above reports, a probable mechanism is proposed here on the formation of CNOs from GO as shown in figure 6.3.3. In a drastic hydrothermal condition assisted by the oxidative etching by hydrogen peroxide, edge defects arise in GO sheets, caused by the formation of dangling bonds and holes which will act as the driving force for the curling and closure of GO nanosheets ultimately resulting in the formation of CNOs.

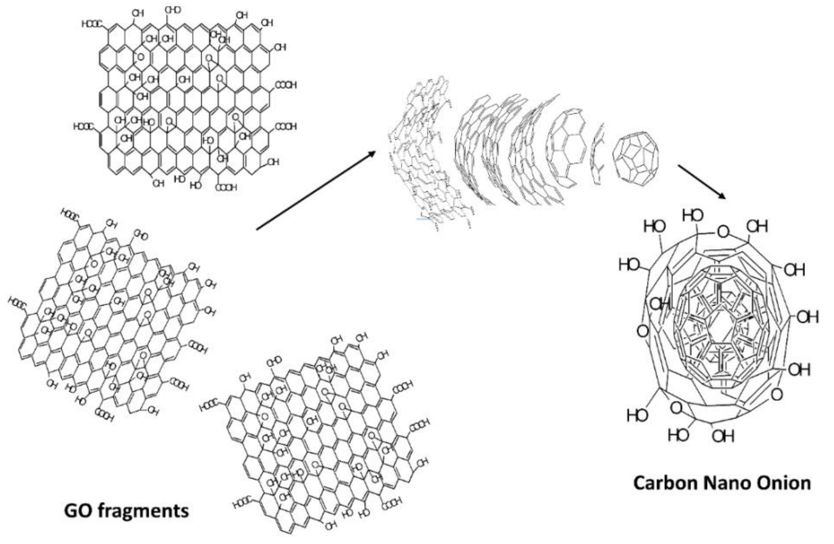

Figure 6.3.3: proposed mechanism for the formation of carbon nano onion from graphene oxide.

6.3.4 PL spectroscopic analysis

When irradiated with 365 nm UV light, a strong greenish yellow fluorescence was observed with an emission peak showing a λ_{max} at 512 nm for spherical CNOs and 523 nm for hollow CNOs as shown in figure 6.3.4.(a) & (b) respectively. Photoluminescence is a characteristic of zero-dimensional carbon materials such as quantum dots, carbon dots, carbon nano onions. Some of the major factors which contribute to photoluminescence are the optical selectivity of different size (quantum effect), emissive traps on the surface including defects, surface groups, and surface states.

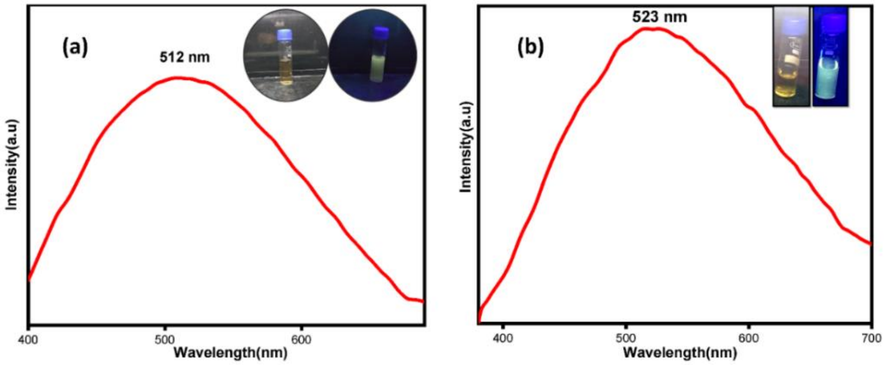

Figure 6.3.4: (a) Emission spectrum of (a) spherical CNOs showing a λ_{max} at 512 nm (b) hollow CNOs showing λ_{max} at 523 nm when excited at 365 nm (inset shows the photograph of CNO without and with UV illumination at 365 nm)

6.3.5 Exploring the optical properties of hollow CNOs

Since strong fluorescence was exhibited by hollow CNOs than spherical CNOs, the optical properties of hollow CNOs were further explored with fluorescence studies. Figure 6.3.5 (a) shows the variation of emission fluorescence intensity of CNOs with different excitation wavelengths ranging from 300 nm to 380 nm and it is found that the CNOs exhibited an excitation dependent PL behaviour with highest fluorescence intensity on excitation wavelength of 330 nm. The fluorescence excitation and emission spectra of CNOs are presented in figure 6.3.5(b). The dependence of fluorescence intensity of CNOs with different concentration of NaCl solution (0-50 µM) was estimated and is shown in figure 6.3.5(c)

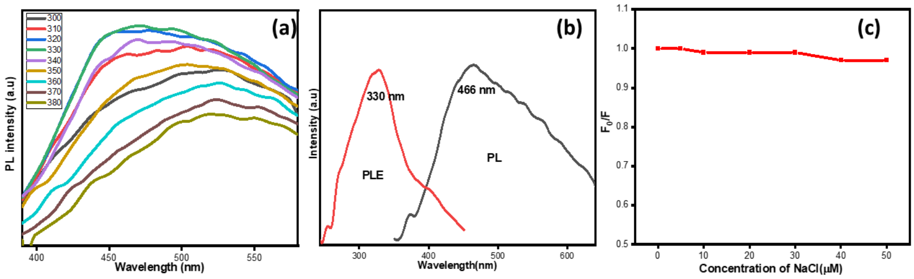

Figure 6.3.5: (a) Excitation dependent fluorescence spectra of CNOs (b) Fluorescence excitation and emission spectrum of CNOs (c) Variation of fluorescence intensity of CNOs with different concentration of NaCl

6.3.6. Fluorescent detection of Fe^{2+} ions

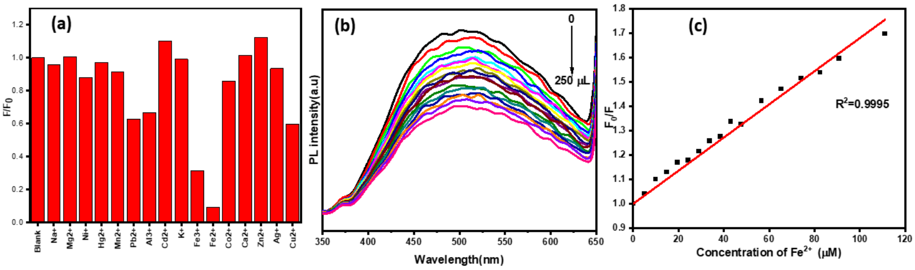

Figure 6.3.6: (a) Relative fluorescence intensity of CNOs in the presence of different metal ions. (b)Fluorescence spectra of CNOs with increasing concentration of Fe^{2+} ions (0-250 µL) (c) Relative fluorescence response of CNOs as a function of Fe^{2+} concentration.

The feasibility of using hollow CNOs as a label–free fluorescent probe for the detection of metal ions was examined by measuring the fluorescence intensity of CNOs in the presence of different metal ions. As shown in figure 6.3.6 (a), among the various metal ions (including Na^+, Mn^{2+}, Ca^{2+}, Hg^{2+}, Fe^{3+}, K^+, Fe^{2+}, Mg^{2+}, Zn^{2+}, Cu^{2+}, Al^{3+}, Cr^{3+}, Cd^{2+}, Co^{2+}, Ni^{2+}, Pb^{2+}, Ag^+) the relative fluorescence intensity of aqueous solution of CNOs was almost completely quenched in the presence Fe^{2+} ions. In order to evaluate the sensitivity of the prepared system, the fluorescence intensity of the CNOs was constantly measured after the addition of different concentration of Fe^{2+}. It was found that the fluorescence intensity of the CNOs decreased apparently with an increase in the concentration of Fe^{2+}. Figure 6.3.6 (b) depicts the gradual decrease in fluorescence intensity upon addition ferrous ion solution from 0 to 250 µL.

The fluorescence quenching mechanism of CNO- Fe^{2+} sensor system follows the Stern-Volmer equation, $F_0/F= 1+K_{sv}[Q]$, where F_0 and F are fluorescence intensities in the absence and presence of Fe^{2+}, Ksv is the Stern-Volmer quenching constant, [Q] is the analyte concentration. The Stern-Volmer plot, shown in figure 6.3.6 (c), exhibit a good linear response between the fluorescence intensity ratio and Fe^{2+} over 0 to 111 µM concentration range with a correlation coefficient (R^2) of 0.9995. The limit of detection calculated from the standard deviation (σ) and the slope (m) of S-V plot using equation 3σ/m was found to be 44.8 nM which is lower than the threshold level for ferrous ion (1780 nM) in drinking water according to World health organisation guideline [59]. The higher value of association constant, K_{sv} ($6.81 * 10^4\ M^{-1}$) obtained describes an efficient interaction of ferrous ion with oxygen moieties on CNOs surface resulting in charge transfer quenching. This further confirms the fact that the mechanism involved here must be static quenching.

6.3.7 Investigating the anti-cancer activity of CNOs on MCF-7 cell line

6.3.7.1 MTT assay

The effects of hollow CNOs on the cell response of the human breast cancer (MCF-7) cell line as well as normal human breast epithelial cell line (HBL-100) were examined by using the MTT assay (figure 6.3.7.1.(a & b)) and it was found that CNOs exhibited dose-dependent in- vitro cytotoxicity towards the MCF-7 cells, while no significant cytotoxicity was observed for normal HBL-100 cells even after 48 h of exposure, safeguarding the in-vitro usage of as-synthesized CNOs for anticancer studies.

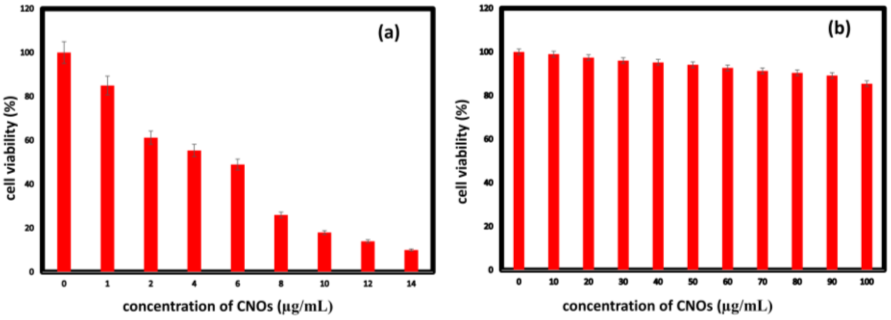

Figure 6.3.7.1: Dose- dependent in- vitro cytotoxicity of CNOs towards (a) human breast cancer (MCF-7) cells (b) normal human breast epithelial (HBL-100) cells

Figure 6.3.7.1 (a) shows the dose-reliant in-vitro cytotoxicity activity of CNOs at different concentrations (0, 1, 2, 4, 6, 8, 10, 12, 14 µg/mL) over MCF-7 cell line. The experimental results demonstrate that CNOs can inhibit cell proliferation of MCF-7 cells in a dose dependent manner. On increasing the dosage of CNOs from 0 to 14 µg/mL, cell death was almost 90%. The half maximal inhibitory concentration (IC_{50}) value of CNOs against MCF-7 cells was found to be 6 µg/ml.

The high specificity of CNOs towards the cancerous cell over normal cell is related to the overexpression of H_2O_2 in cancerous cells [60], [61]. H_2O_2 generally produced by the normal cells (<20 nM concentration) play an active role in a series of physiological process. Normal cells have metabolic system that remove H_2O_2. Glutathione peroxidase and catalase are the three main antioxidant enzymes responsible for the elimination of H_2O_2 [62]–[64]. Since the intrinsic level of antioxidant enzymes are low in most malignancy cells, the concentration of H_2O_2 in malignant tumour cells may reach up to 100 µM [65]–[67]. Since our prepared CNOs are rich in surface hydroxyl and carboxyl groups, they generate reactive oxygen species (ROS) in cancerous cells and thereby inhibiting further cell proliferation by cell apoptosis.

6.3.7.2 MCF-7 cell morphology analysis

The structural morphology of the MCF-7 cell line in the presence and absence of CNOs were also studied using inverted phase contrast microscopy. The cells treated with different concentration of CNOs are shown in Figure 6.3.7.2 (a-h). Cells in the control were tightly packed, multinucleated with spindle shaped as shown in 6.3.7.2 (a & e). Nevertheless, cell growth appeared inhibited in cells treated with CNOs, and cell membranes were crooked and more blebby in the cells, signifying the apoptotic activation [68] as evident from 6.3.7.2 (b & f, c & g, d & h).

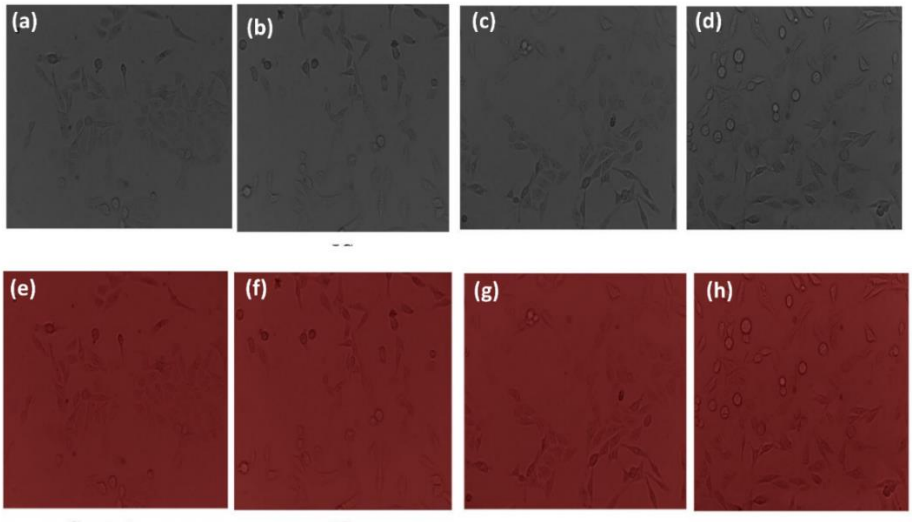

Figure 6.3.7.2: Morphology of MCF-7 cells treated with (a & e) control, (b & f) CNOs at IC_{25} concentration, (c & g) CNOs at IC_{50} concentration and (d & h) CNOs at IC_{75} concentration.

6.3.7.3 DAPI staining-to study nuclear morphology

Chromatin changes phase from an active network to an inactive condensed state during apoptosis. This condensed chromatin is digested by the nucleases generating DNA ladders. So, chromatin compression and DNA shattering are the hallmarks of late apoptosis

[69]–[71]. DAPI (4, 6-diamidino-2-phenylindole) staining was used to visualize the nuclear morphology of the cells as it binds strongly to adenine –thymine regions of DNA resulting in the emission of blue fluorescence when excited with UV radiation. Apoptotic cells with compacted chromatin will be brighter than chromatin from non-apoptotic cell [71]. As seen from the images in Figure 6.3.7.3 (a), spherical nuclei with intact normal morphology and a faint blue fluorescence were present in untreated control. Furthermore, CNO-treated cells (Figure 6.3.7.3 (b–d)) displayed enhanced chromatin condensation, smaller nuclei, and nuclear fragmentation in addition to their vivid blue colour emission. Hence the present study suggested that CNOs could induce cell apoptosis in MCF-7 cells.

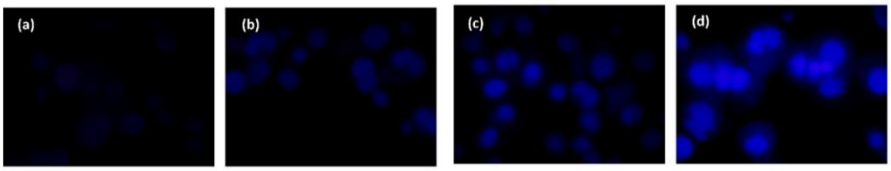

Figure 6.3.7.3: Fluorescent images of MCF-7 cells treated with (a) control (b) 2 (C) 6 (d) 10 µg/mL of CNOs. Cells are stained with 1 mg/mL of DAPI.

6.4 Conclusions

Thus, in brief, we report a facile, straight forward synthesis of spherical dense core as well as polygonal hollow core carbon nano-onions from graphene oxide employing hydrothermal methods by effectively tuning the parameters like the ratio of oxidising agent and time of reaction. The obtained CNOs were characterised using TEM, SEM, FTIR and Raman analysis. The optical properties of prepared CNOs were investigated and its fluorescent quenching property for the selective and sensitive detection of ferrous ion were studied. The synthesised hollow polygonal CNOs can act as effective fluorescent sensor for the detection of ferrous ion over a linear range of 0 µM to 111 µM Fe^{2+} concentration with a detection limit of 44.8 nM. Furthermore, the cell viability of CNOs against human breast cancer (MCF-7) cells and normal HBL-100 cells were investigated and found that CNOs can inhibit the cell proliferation of MCF-7 cells in a dose-dependent manner without affecting the normal cell activity. The half maximal inhibitory concentration (IC_{50}) value of 6 µg/mL was calculated from the MTT assay. The morphology studies from inverted light microscopic images and DAPI staining images of treated cells confirms the CNOs-induced cell apoptosis in MCF-7 cells. The high water-solubility, stable photoluminescence, low cytotoxicity with anti-cancer activity makes the prepared CNOs a promising fluorescent probe and an efficient theragnostic agent.

References

[1] O. Mykhailiv, H. Zubyk, and M. E. Plonska-Brzezinska, “Carbon nano-onions: Unique carbon nanostructures with fascinating properties and their potential applications,” *Inorganica Chim. Acta*, vol. 468, pp. 49–66, Nov. 2017, doi: 10.1016/j.ica.2017.07.021.

[2] J. Bartelmess and S. Giordani, “Carbon nano-onions (multi-layer fullerenes): chemistry and applications,” *Beilstein J. Nanotechnol.*, vol. 5, pp. 1980–1998, Nov. 2014, doi: 10.3762/bjnano.5.207.

[3] A. Guo, K. Bao, S. Sang, X. Zhang, B. Shao, C. Zhang, Y. Wang, F. Cui, X. Yang, “Soft-chemistry synthesis, solubility and interlayer spacing of carbon nano-onions,” *RSC Adv.*, vol. 11, no. 12, pp. 6850–6858, Feb. 2021, doi: 10.1039/D0RA09410B.

[4] M. Zeiger, N. Jäckel, M. Aslan, D. Weingarth, and V. Presser, “Understanding structure and porosity of nanodiamond-derived carbon onions,” *Carbon*, vol. 84, pp. 584–598, Apr. 2015, doi: 10.1016/j.carbon.2014.12.050.

[5] C. Portet, G. Yushin, and Y. Gogotsi, “Electrochemical performance of carbon onions, nanodiamonds, carbon black and multiwalled nanotubes in electrical double layer capacitors,” *Carbon*, vol. 45, no. 13, pp. 2511–2518, Nov. 2007, doi: 10.1016/j.carbon.2007.08.024.

[6] V. Kuznetsov, S. Moseenkov, A. Ischenko, A. Romanenko, T. Buryakov, O. Anikeeva, S. Maksimenko, P. Kuzhir, D. Bychanok, A. Gusinski, O. Ruhavets, O. Shenderova, P. Lambin,“Controllable electromagnetic response of onion-like carbon based materials,” *Phys. Status Solidi B*, vol. 245, no. 10, pp. 2051–2054, 2008, doi: 10.1002/pssb.200879603.

[7] D. Pech, M. Brunet, H. Durou, P. Huang, V. Mochalin, Y. Gogotsi, P. L. Taberna, P. Simon, “Ultrahigh-power micrometre-sized supercapacitors based on onion-like carbon,” *Nat. Nanotechnol.*, vol. 5, no. 9, Art. no. 9, Sep. 2010, doi: 10.1038/nnano.2010.162.

[8] G. Moussa, C. Matei Ghimbeu, P.-L. Taberna, P. Simon, and C. Vix-Guterl, “Relationship between the carbon nano-onions (CNOs) surface chemistry/defects and their capacitance in aqueous and organic electrolytes,” *Carbon*, vol. 105, pp. 628–637, Aug. 2016, doi: 10.1016/j.carbon.2016.05.010.

[9] K. L. Van Aken, K. Maleski, T. S. Mathis, J. P. Breslin, and Y. Gogotsi, “Processing of Onion-like Carbon for Electrochemical Capacitors,” *ECS J. Solid State Sci. Technol.*, vol. 6, no. 6, pp. M3103–M3108, 2017, doi: 10.1149/2.0181706jss.

[10] R. Borgohain, J. Li, J. P. Selegue, and Y.-T. Cheng, “Electrochemical Study of Functionalized Carbon Nano-Onions for High-Performance Supercapacitor Electrodes,” *J. Phys. Chem. C*, vol. 116, no. 28, pp. 15068–15075, Jul. 2012, doi: 10.1021/jp301642s.

[11] M. Zeiger, N. Jäckel, V. N. Mochalin, and V. Presser, “Review: carbon onions for electrochemical energy storage,” *J. Mater. Chem. A*, vol. 4, no. 9, pp. 3172–3196, 2016, doi: 10.1039/C5TA08295A.

[12] A. V. Raghu, K. K. Karuppanan, and B. Pullithadathil, “Highly Surface Active Phosphorus-Doped Onion-Like Carbon Nanostructures: Ultrasensitive, Fully Reversible, and Portable NH_3 Gas Sensors,” *ACS Appl. Electron. Mater.*, vol. 1, no. 11, pp. 2208–2219, Nov. 2019, doi: 10.1021/acsaelm.9b00412.

[13] K. M. Tripathi, T. S. Tran, Y. J. Kim, and T. Kim, “Green Fluorescent Onion-like Carbon Nanoparticles From Flaxseed Oil for Visible Light-Induced Photocatalytic Applications and Label-Free Detection of Al(III) Ions,” p. 28.

[14] M. B. Seymour, C. Su, Y. Gao, Y. Lu, and Y. Li, “Characterization of carbon nano-onions for heavy metal ion remediation,” *J. Nanoparticle Res.*, vol. 14, no. 9, p. 1087, Sep. 2012, doi: 10.1007/s11051-012-1087-y.

[15] S. Lettieri, M. d’Amora, A. Camisasca, A. Diaspro, and S. Giordani, “Carbon nano-onions as fluorescent on/off modulated nanoprobes for diagnostics,” *Beilstein J. Nanotechnol.*, vol. 8, pp. 1878–1888, Sep. 2017, doi: 10.3762/bjnano.8.188.

[16] L. Joly-Pottuz, B. Vacher, N. Ohmae, J. M. Martin, and T. Epicier, “Anti-wear and Friction Reducing Mechanisms of Carbon Nano-onions as Lubricant Additives,” *Tribol. Lett.*, vol. 30, no. 1, pp. 69–80, Apr. 2008, doi: 10.1007/s11249-008-9316-3.

[17] J. Xu, X. Chen, P. Grützmacher, A. Rosenkranz, J. Li, J. Jin, C. Zhang, J. Luo, “Tribochemical Behaviors of Onion-Like Carbon

Films as High-Performance Solid Lubricants with Variable Interfacial Nanostructures," p. 5.

[18] A. F. Hassan, "Synthesis of carbon nano-onion embedded metal–organic frameworks as an efficient adsorbent for cadmium ions: kinetic and thermodynamic studies," *Environ. Sci. Pollut. Res.*, vol. 26, no. 23, pp. 24099–24111, Aug. 2019, doi: 10.1007/s11356-019-05581-5.

[19] P. P. Kuzhir, D. S. Bychanok, S. A. Maksimenko, A. V. Gusinski, O. V. Ruhavets, V. L. Kuznetsov, S. I. Moseenkov, C. Jones, O. Shenderova, Ph. Lambin, "Onion-like carbon based polymer composite films in microwaves," *Solid State Sci.*, vol. 11, no. 10, pp. 1762–1767, Oct. 2009, doi: 10.1016/j.solidstatesciences.2008.12.003.

[20] S. K. Sonkar, M. Roy, D. G. Babar, and S. Sarkar, "Water soluble carbon nano-onions from wood wool as growth promoters for gram plants," *Nanoscale*, vol. 4, no. 24, p. 7670, 2012, doi: 10.1039/c2nr32408c.

[21] N. Keller, N. I. Maksimova, V. V. Roddatis, M. Schur, G. Mestl, Y. V. Butenko, V. L. Kuznetsov, R. Schlögl, "The catalytic use of onion-like carbon materials for styrene synthesis by oxidative dehydrogenation of ethylbenzene," *Angew. Chem. Int. Ed Engl.*, vol. 41, no. 11, pp. 1885–1888, Jun. 2002, doi: 10.1002/1521-3773(20020603)41:11<1885::aid-anie1885>3.0.co;2-5.

[22] D. Su, N. Maksimova, G. Mestl, V. Kuznetsov, V. Keller, R. Schlögl, N. Keller, "Oxidative dehydrogenation of ethylbenzene to styrene over ultra-dispersed diamond and onion-like carbon," *Carbon*, vol. 45, pp. 2145–2151, Oct. 2007, doi: 10.1016/j.carbon.2007.07.005.

[23] S. Giordani, J. Bartelmess, M. Frasconi, I. Biondi, S. Cheung, M. Grossi, D. Wu, L. Echegoyen, D. F. O'Shea, "NIR fluorescence labelled carbon nano-onions: synthesis, analysis and cellular imaging," *J Mater Chem B*, vol. 2, no. 42, pp. 7459–7463, 2014, doi: 10.1039/C4TB01087F.

[24] S. Iijima, "Direct observation of the tetrahedral bonding in graphitized carbon black by high resolution electron microscopy," *J. Cryst. Growth*, vol. 50, no. 3, pp. 675–683, Nov. 1980, doi: 10.1016/0022-0248(80)90013-5.

[25] D. Ugarte, "Curling and closure of graphitic networks under electron-beam irradiation," *Nature*, vol. 359, no. 6397, Art. no. 6397, Oct. 1992, doi: 10.1038/359707a0.

[26] V. Kuznetsov, A. Chuvilin, Y. V. Butenko, I. Mal'kov, and V. Titov, "Onion-like carbon from ultra-disperse diamond," 1994, doi: 10.1016/0009-2614(94)87072-1.

[27] N. Sano, H. Wang, M. Chhowalla, I. Alexandrou, and G. A. Amaratunga, "Synthesis of carbon 'onions' in water," *Nature*, vol. 414, no. 6863, pp. 506–507, Nov. 2001, doi: 10.1038/35107141.

[28] M. Choucair and J. A. Stride, "The gram-scale synthesis of carbon onions," *Carbon*, vol. 50, no. 3, pp. 1109–1115, Mar. 2012, doi: 10.1016/j.carbon.2011.10.023.

[29] T. Cabioc'h, M. Jaouen, E. Thune, P. Guérin, C. Fayoux, and M. F. Denanot, "Carbon onions formation by high-dose carbon ion implantation into copper and silver," *Surf. Coat. Technol.*, no. 128–129, pp. 43–50, 2000.

[30] X. Chen, F. Deng, J. Wang, H. Yang, G. Wu, X. Zhang, J. Peng, W. Li, "New method of carbon onion growth by radio-frequency plasma-enhanced chemical vapor deposition," *Chem. Phys. Lett. - CHEM PHYS LETT*, vol. 336, pp. 201–204, Mar. 2001, doi: 10.1016/S0009-2614(01)00085-9.

[31] M. Choi, I. S. Altman, Y. J. Kim, P. V. Pikhitsa, S. Lee, G. S. Park, T. Jeong, J. B Yoo,. "Formation of Shell-Shaped Carbon Nanoparticles Above a Critical Laser Power in Irradiated Acetylene," *Adv. Mater.*, vol. 16, no. 19, pp. 1721–1725, 2004, doi: 10.1002/adma.200400179.

[32] T. Gorelik, S. Urban, F. Falk, U. Kaiser, and U. Glatzel, "Carbon onions produced by laser irradiation of amorphous silicon carbide," *Chem. Phys. Lett.*, vol. 373, pp. 642–645, May 2003, doi: 10.1016/S0009-2614(03)00677-8.

[33] X. H. Chen, H. S. Yang, G. T. Wu, M. Wang, F. M. Deng, X. B. Zhang, J. C. Peng, W. Z. Li, "Generation of curved or closed-shell carbon nanostructures by ball-milling of graphite," *J. Cryst. Growth*, vol. 218, no. 1, pp. 57–61, Sep. 2000, doi: 10.1016/S0022-0248(00)00486-3.

[34] A. Palkar, F. Melin, C. M. Cardona, B. Elliott, A. K. Naskar, D. D. Edie, A. Kumbhar, L. Echegoyen, “Reactivity Differences between Carbon Nano Onions (CNOs) Prepared by Different Methods,” *Chem. – Asian J.*, vol. 2, no. 5, pp. 625–633, May 2007, doi: 10.1002/asia.200600426.

[35] M. E. Plonska-Brzezinska, A. Palkar, K. Winkler, and L. Echegoyen, “Electrochemical Properties of Small Carbon Nano-Onion Films,” *Electrochem. Solid-State Lett.*, vol. 13, no. 4, p. K35, 2010, doi: 10.1149/1.3299252.

[36] M. E. Plonska-Brzezinska, A. Lapinski, A. Z.Wilczewska, A. T. Dubis, A. Villalta-Cerdas, K. Winkler, L. Echegoyen, “The synthesis and characterization of carbon nano-onions produced by solution ozonolysis,” *Carbon*, vol. 49, no. 15, pp. 5079–5089, Dec. 2011, doi: 10.1016/j.carbon.2011.07.027.

[37] V. Georgakilas, D. M. Guldi, R. Signorini, R. Bozio, and M. Prato, “Organic functionalization and optical properties of carbon onions,” *J. Am. Chem. Soc.*, vol. 125, no. 47, pp. 14268–14269, Nov. 2003, doi: 10.1021/ja0342805.

[38] “Pyridyl-Functionalized and Water-Soluble Carbon Nano Onions: First Supramolecular Complexes of Carbon Nano Onions | Chemistry of Materials.” https://pubs.acs.org/doi/10.1021/cm7035508

[39] L. Zhou, C. Gao, D. Zhu, W. Xu, F. F. Chen, A. Palkar, L. Echegoyen, E. S. W. Kong, “Facile Functionalization of Multilayer Fullerenes (Carbon Nano-Onions) by Nitrene Chemistry and ‘Grafting from’ Strategy,” *Chem. – Eur. J.*, vol. 15, no. 6, pp. 1389–1396, 2009, doi: 10.1002/chem.200801642.

[40] A. Molina-Ontoria, M. N. Chaur, M. E. Plonska-Brzezinska, and L. Echegoyen, “Preparation and characterization of soluble carbon nano-onions by covalent functionalization, employing a Na–K alloy,” *Chem. Commun.*, vol. 49, no. 24, pp. 2406–2408, Feb. 2013, doi: 10.1039/C3CC39077B.

[41] A. S. Rettenbacher, M. W. Perpall, L. Echegoyen, J. Hudson, and D. W. Smith, “Radical Addition of a Conjugated Polymer to Multilayer Fullerenes (Carbon Nano-onions),” *Chem. Mater.*, vol. 19, no. 6, pp. 1411–1417, Mar. 2007, doi: 10.1021/cm0626132.

[42] A. Camisasca and S. Giordani, “Carbon Nano-onions for Bioimaging and Cancer Therapy Applications,” in *Nanooncology: Engineering nanomaterials for cancer therapy and diagnosis*, G. Gonçalves and G. Tobias, Eds. Cham: Springer International Publishing, 2018, pp. 417–455. doi: 10.1007/978-3-319-89878-0_13.

[43] J. Ahlawat, S. M. Asil, G. G. Barroso, M. Nurunnabi, and M. Narayan, “Application of carbon nano onions in the biomedical field: recent advances and challenges,” *Biomater. Sci.*, vol. 9, no. 3, pp. 626–644, Feb. 2021, doi: 10.1039/D0BM01476A.

[44] N. Mamidi, J. Villela Castrejón, and A. González-Ortiz, “Rational design and engineering of carbon nano-onions reinforced natural protein nanocomposite hydrogels for biomedical applications,” *J. Mech. Behav. Biomed. Mater.*, vol. 104, p. 103696, Apr. 2020, doi: 10.1016/j.jmbbm.2020.103696.

[45] C. D. Grande Tovar “Preparation of Chitosan/Poly(Vinyl Alcohol) Nanocomposite Films Incorporated with Oxidized Carbon Nano-Onions (Multi-Layer Fullerenes) for Tissue-Engineering Applications,” *Biomolecules*, vol. 9, no. 11, Art. no. 11, Nov. 2019, doi: 10.3390/biom9110684.

[46] V. Revuri, K. Cherukula, M. Nafiujjaman, K. Cho, I.-K. Park, and Y.-K. Lee, “White-Light-Emitting Carbon Nano-Onions: A Tunable Multichannel Fluorescent Nanoprobe for Glutathione-Responsive Bioimaging,” *ACS Appl. Nano Mater.*, vol. 1, Dec. 2017, doi: 10.1021/acsanm.7b00143.

[47] W. Sun, X. Zhang, H. R. Jia, Y. X. Zhu, Y. Xuo, G. Gao, Y. H. Li, F. G. Wu,“Water-Dispersible Candle Soot-Derived Carbon Nano-Onion Clusters for Imaging-Guided Photothermal Cancer Therapy,” *Small Weinh. Bergstr. Ger.*, vol. 15, no. 11, p. e1804575, Mar. 2019, doi: 10.1002/smll.201804575.

[48] A. Camisasca and S. Giordani, “Carbon nano-onions in biomedical applications: Promising theranostic agents,” *Inorganica Chim. Acta*, vol. 468, pp. 67–76, Nov. 2017, doi: 10.1016/j.ica.2017.06.009.

[49] L. Ding, J. Stilwell, T. Zhang, O. Elboudwarej, H. Jiang, J. P. Selegue, P. A. Cooke, J. W. Gray, F. F. Chen, “Molecular characterization of the cytotoxic mechanism of multiwall carbon nanotubes and nano-onions on human skin fibroblast,” *Nano Lett.*, vol. 5, no. 12, pp. 2448–2464, Dec. 2005, doi: 10.1021/nl051748o.

[50] Y. Xu, S. Y. Wang, J. Yang, X. Gu, J. Zhang, Y. F. Zheng, J. Yang, L. Xu, X. Q. Zhu,"Multiwall carbon nano-onions induce DNA damage and apoptosis in human umbilical vein endothelial cells," *Environ. Toxicol.*, vol. 28, no. 8, pp. 442–450, Aug. 2013, doi: 10.1002/tox.20736.

[51] M. Ghosh, S. K. Sonkar, M. Saxena, and S. Sarkar, "Carbon Nano-onions for Imaging the Life Cycle of Drosophila Melanogaster," *Small*, vol. 7, no. 22, pp. 3170–3177, Nov. 2011, doi: 10.1002/smll.201101158.

[52] S. Kang, J. E. Kim, D. Kim, C. G. Woo, P. V. Pikhitsa, M. H. Cho, M. Choi, "Comparison of cellular toxicity between multi-walled carbon nanotubes and onion-like shell-shaped carbon nanoparticles," *J. Nanoparticle Res.*, vol. 17, p. 378, Sep. 2015, doi: 10.1007/s11051-015-3181-4.

[53] O. Mykhailiv, A. Lapinski, A. Molina-Ontoria, E. Regulska, L. Echegoyen, A. T. Dubis, M. E. Plonska-Brzezinska,"Influence of the Synthetic Conditions on the Structural and Electrochemical Properties of Carbon Nano-Onions," *ChemPhysChem*, vol. 16, no. 10, pp. 2182–2191, 2015, doi: 10.1002/cphc.201500061.

[54] S. Y. Sawant, R. S. Somani, A. B. Panda, and H. C. Bajaj, "Formation and characterization of onions shaped carbon soot from plastic wastes," *Mater. Lett.*, vol. 94, pp. 132–135, Mar. 2013, doi: 10.1016/j.matlet.2012.12.035.

[55] G. H. G. Ahmed, R. B. Laíño, J. A. G. Calzón, and M. E. D. García, "Facile synthesis of water-soluble carbon nano-onions under alkaline conditions," *Beilstein J. Nanotechnol.*, vol. 7, pp. 758–766, May 2016, doi: 10.3762/bjnano.7.67.

[56] J. K. McDonough and Y. Gogotsi, "Carbon Onions: Synthesis and Electrochemical Applications," *Interface Mag.*, vol. 22, no. 3, pp. 61–66, Jan. 2013, doi: 10.1149/2.F05133if.

[57] A. Chuvilin, U. Kaiser, E. Bichoutskaia, N. A. Besley, and A. N. Khlobystov, "Direct transformation of graphene to fullerene," *Nat. Chem.*, vol. 2, no. 6, Art. no. 6, Jun. 2010, doi: 10.1038/nchem.644.

[58] J. Li, R. Cui, Y. Chang, H. Huang, X. Guo, J. Wang, R. Liu, K. Chen, J. Kong, G. Xing, B. Sun, "Preparing dangling bonds by nanoholes on graphene oxide nanosheets and their enhanced

magnetism," *RSC Adv.*, vol. 10, no. 60, pp. 36378–36385, 2020, doi: 10.1039/D0RA05945E.

[59] G. Liu, B. Li, Y. Liu, Y. Feng, D. Jia, and Y. Zhou, "Rapid and high yield synthesis of carbon dots with chelating ability derived from acrylamide/chitosan for selective detection of ferrous ions," *Appl. Surf. Sci.*, vol. 487, pp. 1167–1175, Sep. 2019, doi: 10.1016/j.apsusc.2019.05.069.

[60] P. T. Varsha Raveendran and N. K. Renuka, "Hydrothermal synthesis of biomass-derived carbon nanodots: Characterization and applications," *Mater. Chem. Phys.*, vol. 288, p. 126236, Sep. 2022, doi: 10.1016/j.matchemphys.2022.126236.

[61] C. M. Doskey, V. Buranasudja, B. A. Wagner, J. G. Wilkes, J. Du, J. J. Cullen, G. R. Buettner, "Tumor cells have decreased ability to metabolize H2O2: Implications for pharmacological ascorbate in cancer therapy," *Redox Biol.*, vol. 10, pp. 274–284, Dec. 2016, doi: 10.1016/j.redox.2016.10.010.

[62] C.S. Cho, S. Lee, G. T. Lee, H. A. Woo, E.-J. Choi, and S. G. Rhee, "Irreversible Inactivation of Glutathione Peroxidase 1 and Reversible Inactivation of Peroxiredoxin II by H_2O_2 in Red Blood Cells," *Antioxid. Redox Signal.*, vol. 12, no. 11, pp. 1235–1246, Jun. 2010, doi: 10.1089/ars.2009.2701.

[63] "Ascorbic acid: Chemistry, biology and the treatment of cancer | Elsevier Enhanced Reader." https://reader.elsevier.com/reader/sd/pii/S0304419X12000509?token=CFE31E741B921DEC2750920EDC1FC54CA03F5548EF8BA0232EC5F7902DFD82EE7263A75C8B8EF1D71CC44587A59F886F&originRegion=eu-west-1&originCreation=20221105073751

[64] R. Benfeitas, G. Selvaggio, F. Antunes, P. M. B. M. Coelho, and A. Salvador, "Hydrogen peroxide metabolism and sensing in human erythrocytes: A validated kinetic model and reappraisal of the role of peroxiredoxin II," *Free Radic. Biol. Med.*, vol. 74, pp. 35–49, Sep. 2014, doi: 10.1016/j.freeradbiomed.2014.06.007.

[65] S. L. Marklund, N. G. Westman, E. Lundgren, and G. Roos, "Copper- and zinc-containing superoxide dismutase, manganese-containing superoxide dismutase, catalase, and glutathione peroxidase in normal and neoplastic human cell lines and normal

human tissues," *Cancer Res.*, vol. 42, no. 5, pp. 1955–1961, May 1982.

[66] T. D. Oberley and L. W. Oberley, "Antioxidant enzyme levels in cancer," *Histol. Histopathol.*, vol. 12, no. 2, pp. 525–535, Apr. 1997.

[67] M. Valko, C. J. Rhodes, J. Moncol, M. Izakovic, and M. Mazur, "Free radicals, metals and antioxidants in oxidative stress-induced cancer," *Chem. Biol. Interact.*, vol. 160, no. 1, pp. 1–40, Mar. 2006, doi: 10.1016/j.cbi.2005.12.009.

[68] S. S. E. Puthumana and B. Damodaran, "ICT-Based Blue-Emitting Dual-Functional Probe (Ugi EML BLUE) for Bio-Imaging and Cytotoxic Activities on HeLa Cells," *ChemistrySelect*, vol. 4, no. 18, pp. 5366–5374, May 2019, doi: 10.1002/slct.201900474.

[69] "Chromatin Condensation - an overview | ScienceDirect Topics." https://www.sciencedirect.com/topics/biochemistry-genetics-and-molecular-biology/chromatin-condensation

[70] F. A. Oberhammer, K. Hochegger, G. Fröschl, R. Tiefenbacher, and M. Pavelka, "Chromatin condensation during apoptosis is accompanied by degradation of lamin A+B, without enhanced activation of cdc2 kinase," *J. Cell Biol.*, vol. 126, no. 4, pp. 827–837, Aug. 1994, doi: 10.1083/jcb.126.4.827.

[71] "Nuclear condensation & DNA fragmentation in apoptosis." https://www.abcam.com/kits/nuclear-condensation-dna-fragmentation-and-membrane-disruption-during-apoptosis

CHAPTER 7

SUMMARY AND CONCLUSIONS

7.1 Overall conclusions

In the present thesis, investigations on the preparation, characterisation and applications of zero-dimensional carbon nanomaterials such as graphene quantum dots, two different types of nitrogen-doped graphene quantum dots, dense carbon nano onions, hollow polygonal carbon nano onions, fluorine-rich carbon quantum dots are presented. A brief summary of the major findings in each chapter is provided here.

Chapter 1 consolidates a general introduction and literature review of the zero-dimensional nanomaterials included in the present research work. The properties and applications of these nanomaterials were also briefly summarised.

In Chapter 2, the experimental methods for the synthesis and the analytical techniques adopted for the characterisation of carbon nanomaterials as well as applications carried out are included. All the zero-dimensional nanomaterials included in this thesis were prepared through simple and facile methods. This chapter also provides the details of the materials used in the study.

Chapter 3 summarises investigations on GQDs and two different types of nitrogen-doped GQDs prepared by following hydrothermal strategies and their nanocomposites with TiO_2 photocatalysts in two different methods. The formation of GQDs and NGQDs was inferred from the TEM analysis and the incorporation of NGQDs over TiO_2 was further confirmed from the XRD, FTIR, and

UV-DRS analysis. The performance of the TiO_2-GQDs, TiO_2-NGQDs and P25TiO_2-NGQDs hybrid catalysts was evaluated using hydrogen generation via photocatalytic water-splitting and compared with that of pristine titania photocatalysts. The NGQD-sensitized TiO_2 photocatalysts were found to be superior to the bare sol-gel titania catalysts in their photocatalytic performances. GQDs and NGQDs are anticipated to have an exciting future as green sensitizers in various semiconductor-based catalytic systems for their performance enhancement in visible light harvesting. The high performance of NGQDs-sensitized photocatalysts can be attributed to the unique optical and physical properties of NGQDs which enable them to be a promising material for commercial photocatalytic applications in the near future.

In chapter 4, we reported the successful synthesis of graphene quantum dots with small size, high water solubility and strong fluorescence through a simple and rapid hydrothermal method employing graphene oxide and H_2O_2 at a temperature of 180 °C for 1.5 h reaction time. The prepared GQDs were characterised with the help of TEM, FTIR, Raman and PL analysis. TEM images reveal the formation of 1-3 nm-sized GQDs. FTIR and Raman spectroscopic studies further confirm the surface oxygen functionalisation in GQDs which provides them with excellent water solubility. The strong and excitation-dependent fluorescence properties of the prepared GQDs were analysed using PL spectroscopy. Since GQDs are non-toxic, small-sized, highly water soluble and exhibit strong fluorescence, they could find immense potential applications in the biological and medicinal fields. We tried to explore such possibilities. The cytotoxicity assay of GQDs was carried out in normal human breast cells (HBL-100 cell line) and human breast cancer cells (MCF-7 cell line). The synthesised GQDs exhibited excellent anti-cancer properties and MTT assays revealed a concentration-dependent cell growth inhibition of human breast cancer cells treated with GQDs in in-vitro conditions. Only negligible cytotoxicity was observed towards normal breast cells. The IC_{50} value of GQDs calculated was 9 µg/mL. Further, the anti-oxidant property of GQDs was evaluated and confirmed from the H_2O_2 scavenging assay. GQDs also exhibited cell penetration into the nucleus and multi-colour fluorescence emission in HBL-100 cells which suggests their application in cell imaging.

In Chapter 5, nucleophilic substitutions of fluorine moieties on fluorographite by hydroxyl groups were carried out by a strategy in which the parallel reductive defluorination was minimised. Mild sonochemical exfoliation of the resulting product in water provided an aqueous dispersion of hydroxylated fluorographene (HFG) in which C-F bonds are largely semi-ionic in character. Upon subsequent hydrothermal treatment with hydrogen peroxide, additional fluorinations were taken place because of adsorbed fluoride ions. Further, oxidative etching resulted in the formation of blue fluorescent fluorine-rich small-sized (1.5-3 nm) graphene quantum dots (FGQDs) with excellent solubility and high stability. A schematic representation of the suggested mechanism was also included in the chapter. The results from the FTIR and XPS analysis also confirmed our findings. The size of the prepared FGQDs in the 1.5-3 nm was analysed using TEM images and the corresponding histogram. AFM analysis of HFG confirmed good exfoliation. Raman analysis of FGQDs revealed the surface defects, the source of its strong fluorescence. The optical properties suggested that FGQDs can act as a good sensing platform for the detection of metal ions. Detailed analysis showed that the fluorescence of FGQDs was completely quenched in the presence of Fe^{3+} ions in an aqueous solution. Thus, FGQDs could act as fluorescent turn-off sensors for the detection of Fe^{3+} ions. A good linear response was obtained for Fe^{3+} concentrations over a range of 0-90 µM with a limit of detection of 73.7 nM.

In chapter 6, investigations leading to a simple and straightforward synthesis of highly water-soluble, fluorescent carbon nano-onions (spherical dense core as well as polygonal hollow core carbon nano-onion) from graphene oxide employing hydrothermal methods by varying the ratio of oxidising agent and time of reaction are presented. The morphology and functionalization of CNOs were characterised using TEM, SEM, FTIR, Raman and PL spectral analysis. The synthesised hollow polygonal CNOs can act as an effective fluorescent sensor for the detection of ferrous ions over a linear range of 0 to 111 µM Fe^{2+} concentration with a detection limit of 44.8 nM. Also, it could inhibit the cell proliferation of human breast cancer (MCF-7) cells in a dose-dependent manner with a half maximal inhibitory concentration (IC_{50}) value of 6 µg/mL, while providing no significant cytotoxicity towards normal breast (HBL-100) cells. The morphology studies using inverted light microscopy of treated cells and DAPI staining of nucleus confirmed that the CNOs could induce cell apoptosis in MCF-7 cells.

CHAPTER 8

FUTURE OUTLOOK

7.1 Future outlook

The work presented in this dissertation involves simple, cost-effective and facile hydrothermal methods which can be performed in a short reaction time, for the development of a variety of exciting zero-dimensional carbon nanomaterials known to possess promising applications, as demonstrated here. Since the 0-D nanomaterials are considered as next-generation materials, their straightforward preparation methods gain special attention.

As discussed in chapter 3, GQDs and NGQDs are anticipated to have an exciting future as green sensitizers in various semiconductor-based catalytic systems for their performance enhancement in visible light harvesting. The high performance of NGQDs-sensitized photocatalysts can be attributed to the unique optical and physical properties of NGQDs, enabling them to be a promising material for commercial photocatalytic applications in the near future.

The small-sized GQDs developed in this work is demonstrated to be highly promising as potential candidates in the field of cancer therapy. Its small size, excellent water solubility, strong fluorescence, biocompatibility, and ease of functionalisation make these GQDs a suitable material for theragnostic applications. The high surface area to volume ratio of GQDs and π-conjugation enable efficient drug loading. Hence, the research offers promising future directions in this aspect.

In chapter 5, we have reported a novel reaction method for carrying the nucleophilic substitution, minimizing the rate of reductive defluorination. Hydroxy fluorographene (HFG) with a more semi-ionic character can find more applications in the field of electrochemical sensing. Fluorine-rich GQDs prepared from HFG with more covalent character can also find more applications in the field of sensing and as a dual-modal agent for MRI and ^{19}F MRI.

Another fascinating 0-D carbon nanomaterial developed is carbon nano-onions which are presented in chapter 6. Pristine CNOs offer immense potential applications in the field of energy storage and their cost-effective synthetic strategies can lead to many investigations in future. Lack of water solubility hinders the application of pristine CNOs in many other fields. We successfully synthesised highly water-soluble CNOs with strong fluorescence. The biological applications they exhibited are promising and open up the scope for further research to be carried out in this direction.

PUBLICATIONS

1. Sreeja, K.; Usha, M.; Rajeena, U.; Raveendran, P.; Ramakrishnan, R. M. Fluorine-Rich Graphene Quantum Dots by Selective Oxidative Cutting of Hydroxy Fluorographene and Their Application for Sensing of Fe (III) Ions. *J. Fluor. Chem.* **2023**, *268*, 110130. https://doi.org/10.1016/j.jfluchem.2023.110130

2. Usha, M.; Sreeja, K.; Rajeena, U.; Chakkingal Parambil, P.; Raveendran, P.; Ramakrishnan, R. M. Preparation of Mesoporous Poly(Fullerene Oxide) Framework by Thermal [3 + 2] Cycloadditions and Its Application as a Semiconductor Photocatalyst. *Fuller. Nanotub. Carbon Nanostructures* **2022**, *0* (0), 1–10. https://doi.org/10.1080/1536383X.2022.2152440

PAPERS COMMUNICATED

1. Kalapparambil Sreeja[a], Poovathinthodiyil Raveendran, Resmi M. Ramakrishnan[a]* “Preparation, characterizations and biological applications of small sized fluorescent graphene quantum dots”

2. Kalapparambil Sreeja[a], Poovathinthodiyil Raveendran, Resmi M. Ramakrishnan[a]* “Hydrothermal conversion of graphene oxide to carbon nano onions for sensing and biological applications”

PAPERS PRESENTED IN SEMINAR / CONFERENCE

1. SREEJA K., MOHAMMED AKBAR, SRUTHI K.S., RESMI M.R : “Effective utilization of nitrogen doped graphene quantum dots (N-GQD) from oxidation debris as green photo-sensitizers in titania based photocatalyst for water splitting” ,National seminar on Emerging trends in nanoscience and technology (ETNST 2017) at SNGS college Pattambi on December(19-20), 2017

2. SREEJA K., SWATHY K.J., AMRUTHA K., RAJEENA U. AND RESMI M. RAMAKRISHNAN “The selective oxidation of cyclohexene over g-C3N4/rGO metal free catalysts” International conference chemistry and physics of materials, St. Thomas college. Trissur, Kerala, December 19-21, 2018. (Isbn:978-81-935818-1-9)

3. SREEJA K. AND RESMI M.R. “Nitrogen doped graphene quantum dots (N-GQDs) as attractive fluorophores for detection of Pb 2+ and Al 3+ ions.” Chemistry past present future (CPPF), National seminar, Sree Neelakanta Govt. Sanskrit college, Pattambi, Kerala, November, 21-22, 2019